Decoding Coordinated Hand Movement in Human Primary Motor Cortex Using High Resolution Electrocorticography

Timothy Blakely

A dissertation

submitted in partial fulfillment of the

requirements for the degree of

Doctor of Philosophy

University of Washington

2013

Reading Committee:

Dr. Rajesh Rao, Chair

Dr. Jeffrey Ojemann

Dr. Jay Rubinstein

Program Authorized to Offer Degree:

Bioengineering

University of Washington

Abstract

Decoding Coordinated Hand Movement in Human Primary Motor Cortex Using High Resolution Electrocorticography

Timothy Blakely

Chair of the Supervisory Committee:
Dr. Rajesh Rao
Bioengineering and Computer Science

Electrophysiology studies of the brain allow us to study the dynamics of the cortex as subjects perform tasks and experiment. Of particular interest in human studies is the activity that occurs in motor related areas of the brain that occur during precise, dexterous movements of the hand – a unique property among primates. Previous studies of the central and peripheral motor nervous systems suggest the presence of synergistic activations of musculoskeletal groups during coordinated movement, and that these "motor primitives" may be present at the level of the spinal column and possibly in higher levels of CNS. In this thesis we explore the presence of these synergistic movements of individual digit joints during coordinated object grasping by leveraging high-resolution electrocorticographic (ECoG) recordings and the subsequent viability of this type of dimensionality reduction as a possible model of prosthetic control. We demonstrate that ECoG recordings are a stable and viable tool to investigate the underlying neural physiology, and explore the spatial distribution of activity during dexterous hand movement in medium (5mm-spacing) and high resolution (3mm) ECoG grids. High gamma (75-200Hz) activity in primary motor cortex shows high spatial preference for individual digit movements during overt finger flexions. In contrast, the average spatial activity during object grasping appears to show little unique spatial organization relative to the grasps performed. However, by applying a Kalman filter to predict the hand pose, we are able to accurately reconstruct the position of the hand in real-time. The Kalman filter coefficients suggest that a plausible model for motor movement may be the initiation of a common kinematic grasping motion by the first dimensional component, allowing the brain to modify this trajectory in real time as the hand approaches the object by modulating spatial networks associated with subsequent dimensions.

Table of Contents

Acknowledgements

The author would like to thank his advisors Dr. Rajesh P.N. Rao and Dr. Jeffrey Ojemann, as well as committee members Dr. Jay Rubinstein, Dr. Joan Sanders and Dr. Eberhardt Fetz, for their guidance during his studies.

In addition, the author would like to acknowledge the help and support of the GRID neuroscience lab whose members are a constant source of support and insight. The mentoring and advising of all the members of the lab were critical in the creation and direction of this document.

Dedication

This document is dedicated to my family, without whom I would never be where I am today. Thank you for your support and love all these years.

1 Chapter 1 – The Neural Basis of Dexterous Movement

1.1 Prologue: Brains are complex

The "holy grail" of sorts of the entire neuroscientific community would be to discover that brains - and neuron-based systems in general - operate on some common underlying code. This code would describe ideas, concepts and thoughts as trains of pulses of neurons, providing a consistent pattern across different people for similar concepts. If such a code were to exist, it means that even second or third order metrics - such as local field potentials, ECoG and EEG - would be built up of common neural building blocks and thus be possibly decoded into its basic neural coding parts.

However, even in theory this concept has its problems. Consider the following example: imagine the sport of football. The theory of the "neural code" would suggest that this concept would be built up of one or more firing patterns, and that these firing patterns would have similarities between person. Upon hearing the word "football", one person may imagine the sport of football and produce a series of neural spikes that encoding the concept of a sport played with helmets, pigskins, quarterbacks and wide receivers. However, another person may hear the word "football" and, though thinking about the similar concept of sporting, imagine a completely different scenario with a round ball, goalies, shinguards and goals. It is hard to imagine any type of higher level "code" that would be descriptive enough to encode the concept of football but flexible enough to accommodate multiple different interpretations. That isn't to say that the brain doesn't rely on some sort of underlying building block or coding scheme, but the current state of understanding of nervous systems - that it's an organic, procedural system highly reliant on remote input - means that analysis of these systems is not straightforward.

Complicating the issue of truly understanding how the brain works is compounded by its sheer size. The average human brain has roughly 87 billion cells, though most of it in the cerebellum; the telencephalon – or cortex – only contains 12-15 billion neurons[1–4]. If we were to attempt to encode and record this information with the most minimal amount of information possible - a single bit, 1 or 0, whether the neuron is firing or not - it would require over 80GB of memory alone to store the state of the entire brain. On top of that, it does not take into account how the system changes over time (how one neuron affects another). The best case naive scenario would be that the brain could be described with a single mathematical equation relating X neurons to Y neurons (xt = Axt-1), though it is almost universally agreed that this is not in fact the case[5–8].

And even bigger issue than the count of 87 billion cells is the number of interconnections called synapses between them. While the exact number varies from cell to cell, a broad estimate puts the

number of cells that a single neuron synapses on at roughly 10,000[9]. Combining these metrics, we arrive at a staggering number of 870 trillion interconnections in the brain; a number hard to conceive much less represent in a mathematical model. It is impossible to enumerate all the possible connections between these cells, as the number of combinatorial possibilities is far greater than the number of atoms in the universe[10]. Spatial culling can decimate this number significantly with upwards of 90% of these connections local in nature (usually within the local neighborhood of the neurons' branching connection tree, or "dendritic tree"), but up to 10% project far beyond the local area of the cell[11]. We have yet to discover how to reliably describe the way a single cell begins to make these connections much less the brain as a whole, though recent studies by have begun to shed some light on some possible single-cell models[12–14].

Luckily the brain is not the chaotic interconnecting mess that it could be; scientists have identified some forms of organization that the brain adheres to. By simply visual inspection one can see that the brain has a form of spatial organization. Two hemispheres are divided amongst a number of lobes. The cortex is divided up into two main types of cells: gray matter, associated with neural computation, and white matter, neural wiring that connects remote areas of the brain. The gray matter is known be organized into six distinct layers on the outside of the cortex, with recent theories being presented that these layers are organized into tightly packed, highly repeated 'columns' of cells15,16. The "wrinkles" in a brain serve the purpose of increasing the surface area of the brain; increased surface area from the sulci (valleys) and gyri (ridges) of the brain allow more gray matter to be packed onto the surface17–19.

In order to study such systems however, we have to rely on second- or third-order metrics. There is currently no way of recording the activity of all the cells in the cortex, much less any way to identify and enumerate all the synaptic connections in their entirety. Indeed, these synaptic connections have been known to change, grow and decay over time. Such changes in the wiring are thought to be the basis of the way our brains adapt and learn. In spite of this neural re-wiring, there are areas of the brain that show very highly correlated increases in neural activity with certain actions. For example, should a normal, healthy human decide to shake their right leg, an area on the medial (middle) surface of the left hemisphere would likely engage. This pattern of activity is common and robust across many studies and many different methods of recording neural firing. And though the precise position within the cortex may vary and the exact networks are almost certainly unique from individual to individual, the shared ability to move, talk, and thing alike suggests there may be some underlying building blocks encoded within these networks.

The studies and experiments described in this document describe our attempts at making sense of these complex networks and attempts to shed light on the way networks within primary motor cortex – the area of the brain that has been implicated in volitional movement – begins and executes coordinated, complex movements of the hand. Our cumulative results provide evidence that these complex networks may direct coordinated not by operating at the joint angle level, but by leveraging a set of lower dimensional, synergistic movements that can be added up to create nearly any hand pose.

Hypothesis

Great strides have been made since the study of the human brain began and our understanding of its organization is more detailed than ever. Advances in clinical neurology, signal analysis and high-speed recording equipment, coupled with cutting edge technology have introduced new recording and imaging techniques such as functional magnetic resonance imaging (fMRI) and electroencephalography (EEG), allowing us to probe the inner workings of the brain even further. However, only recently have these technologies been combined to explore the possibility of a direct biological interface with the cortex. Neural activity recorded directly from the cortical surface in real time can be quantified, classified and mapped to actions on a computer using electrocorticography (ECoG), resulting in a true brain-computer interface (BCI). These interfaces allow subjects to control actions on a computer by modulating activity in specific areas of the cortex. BCI systems offer the hope of greatly improving the quality of life for paralyzed and locked-in patients by allowing rapid communication and can introduce dramatically new ways to control dexterous prosthetic devices.

Though the idea of mapping neural activity directly from the cortical surface to the operation of a prosthetic limb is enticing – allowing the circumvention of physiological absences or defects that may exist lower in the motor system – it is not a straightforward issue. How cortical neurons interact between themselves and the peripheral nervous system to generate coordinated, multijoint movements of the arm, wrist and hand is not well understood. Current ECoG BCI paradigms are insufficient to probe these complex interactions in primary motor cortex, an area of the brain likely involved in proximal and distal joint movement. **In order to identify the specific role that primary motor cortex plays in the generation and synchronization of multijoint movements, we propose to combine high dimensional motion capture with a novel high-spatial-resolution ECoG electrode design to identify the neurophysiological method used to encode high dimensional dexterous movement.**

Aim 1: **Establish that micro-ECoG grid recordings can provide physiologically relevant biokinematic correlates** – Electrocorticography studies involve epileptic patients whose brains have had electrodes implanted for the purposes of seizure foci mapping. Current clinical protocols dictate the use

of grids of electrodes that are 3mm in diameter and spaced at 1cm apart. Because this undersamples the area of cortex dedicated to hand motor control, this study investigates the use of miniature ECoG grids exclusively for the purposes of identifying activity correlated with hand motor cortex, ensuring both the stability of cortical signals recorded with grids and that cortical potentials recorded using microgrids show similar spectral features to standard grids.

Aim 2: **Validate micro-ECoG as a means of identifying spatially distributed cortical activity and establish synergistic components of grip** – Our hypothesis that the underlying motor control signals generated by primary motor cortex may be spatially distributed, we need to demonstrate that micro-ECoG devices can identify spatially distributed activity. In addition, research into the control mechanisms behind dexterous hand motions has shown that the cortex may be encoding motion at a higher level than that of individual distal positions joint angles. We will attempt to validate these findings initially in a healthy subject population using synergies derived from joint angles to use as a control for further simultaneous micro-ECoG study.

Aim 3: **Reconstruction of multi-dimensional hand postures using spatially distributed cortical activity patterns –** Cortical activity will be recorded using micro-ECoG as subjects manipulate objects and perform freeform movement. Identification of linearly independent spatial and temporal patterns of neural activity will be performed. Patterns that are highly correlated to individual or groups of elemental hand synergies could demonstrate that individual muscle activation is not controlled at the cortical level, but instead are formed in later levels of the central and peripheral nervous system. Time-course measurements of cortical activity patterns associated with the identified muscle synergies will be used to investigate the viability of complex pose reproduction derived directly from motor cortex.

1.2 Background

1.2.1 Brain-machine interfaces

Humans are able to express themselves and manipulate the world around them through a complex network of neurons whose output induces motion via force production from skeletal muscles. The central nervous system directs goal-oriented cognition and relays the outputs from cerebral gray matter and down through the spinal column. The spinal column translates these directions into commands for the motor neurons in the peripheral nervous system. Damage or incapacitation of any stage of the information processing pathway can severely limit the ability of the person to interact with

many aspects of daily life. Though recent innovations in cellular and tissue therapies show promise of restoring lost functionality to the nervous system, there is no near-term solution for those who are currently affected. Recent technological advances have brought to light an alternative to repairing the damaged pathways: creating artificial pathways that can re-route the blocked information around the damaged tissue. Brain-machine interfaces are systems designed to read activity from the earliest stages of the information pathway in an effort to bypass all damaged or missing biological elements.

1.2.2 Bypassing the peripheral and central nervous system

Brain-computer interfaces (BCI) systems can be extremely important to patients with debilitating diseases that effectively shut down the body's ability to perform motion while leaving the nervous system intact. Individuals with syndromes such as amyotrophic lateral sclerosis (ALS) and cerebral palsy experience a disconnect in the continuity between the brain and the rest of the body. These patients retain full mental capability, and can only communicate through extremely limited means such as blinking eyelids. A testament to the fact that these patients retain full mental capacity is illustrated by Jean-Dominique Bauby, who experienced locked-in syndrome due to a brain stem stroke. He was able to write an entire book despite his locked-in state, though his only form of communication was by assisted eye blinks. After composing paragraphs in his head, his assistant painstakingly recited a frequency-ordered alphabet until Bauby blinked, indicating the desired letter. While it proved that his mental capacity was retained in his locked-in state, the wearisome communication process proved frustrating. By reading neural activity from the cerebral cortex before the point of communication breakdown, BCIs offer the ability to provide a much higher bandwidth of communication.

By recording at the earliest possible stage in cognition, BCIs remove any possibility of interference from damaged later stages. However this shortcutting also removes many important processing stages further down in the central nervous system. Any translation between cortical commands and afferent axonal output will not be present in BCI systems that are missing these post-processing stages. Previous brain-computer interface studies have chosen to ignore the processing that goes on in the later stages of the central nervous system, showing that it is possible both to control a computer program and to stimulate paralyzed muscles by clever mapping of raw cortical activity. Any computation and behaviors done subcortically are thus forced on the cortex, requiring that it perform functions previously delegated to the spinal cord. Limitations imposed by the spatial resolution and complex inter-neuron synaptic circuits have constrained these activities to just a two degrees of freedom. Though enough to control simple tasks, emulation of the neural circuitry present in the spinal

cord could provide a much more natural method of controlling devices functioning to translate the higher level control signals into multidimensional control.

1.2.3 Primate model research and limitations

Few animal models can provide a good basis for exploring the complex cortical activity required for performing dexterous movements of proximal and distal limbs. Though their dexterity is not quite human level and the substantial differences in hand morphology between macaques and humans are the subject of current scientific debate, it is pertinent to compare the practice of grasping objects in humans and monkeys because of the ability to look for homologous activity between the species' brains[6-8]. Primate models additionally offer a larger subject population subject to fewer ethical problems than studies of cortical activity using human subjects.

Through stimulation of the cervical spinal cord, Moritz et al. have demonstrated that forelimb movements and coordinated muscle responses can be evoked via microstimulation in sedated monkeys[9]. This study demonstrating that the stimulation of multiple muscles in a coordinated fashion can be achieved from stimulation of the central nervous system in primates provides significant insights into the understanding of spinal synergistic circuitry and their application to neuroprosthesis. A further study by Moritz, Perlmutter and Fetz sought to circumvent descending control signals around a blocked peripheral nervous system pathway by recording directly from the cortical surface of a macaque monkey and using FES to induce movement of the primate's hand[10]. They found that decoding local populations of neurons by using firing rates allowed the monkey to regain movement even after a complete nerve block, regardless of any previous association to movement; a finding that greatly expands the pool of possible control signals.

Vargas-Irwin *et al*. recently published a paper investigating how the activity of populations of cortical neurons generates coordinated multijoint movements of both proximal and distal upper limbs in primates[11]. The study combined an implanted multi-electrode array over primary motor cortex with a full-arm, 25-marker motion capture system to relate the recorded neural activity to the kinematics and dynamics of arm, wrist and hand posture during grasping movements. They showed that single neurons were kinematically coupled to multiple joints and that local ensembles of motor neurons in primary motor cortex contained sufficient information to decode 25 measured joint angles. The results also suggested that decoding high-dimensional reach and grasp motions was plausible using miniature intracortical neuroprosthetic devices.

While these primate studies offer support to the theory that these types of circuits are present in higher primates (i.e. humans), there are significant limitations in experimental design. Vargas-Irwin

noted that while they were able to record from primary motor cortex and train the monkey to grasp the swinging object presented to it, individual distal joint angles tended to be highly correlated with each other due to the monkey's strategy of moving all fingers in concert during grasping. It is not possible to train or instruct primates to perform highly dexterous tasks, limiting experiments to ones that do not require a high degree of dexterity. Additional neuroanatomy differences between humans and lower primates also confound any neural encoding that may be present in animal models.

1.2.4 Evidence of synergistic musculoskeletal control

The motor systems present in the spinal cord have long been known to be capable of producing a wide range of motor behaviors when isolated from the rest of the central nervous system. Evidence of complex muscle synergies residing the vertebrate spinal column has been proposed given recent experiments in frogs and cats. Bizzi *et al.* investigated the role of the spinal cord in lower limb kick production in decerebrate frogs and found that stimulation of specific spinal interneuron sites produced robust, reproducible activations of leg muscles[12]. Depending on the initial position, the direction of motion of the leg could be predicted by a vector field. Different stimulation sites produced unique vector fields. Giszter et al. proceeded to show that these force fields are not due to random activation of motor neurons, afferent stimulation, or direct stimulation of descending systems in the spinal cord[13].

Though these initial findings might imply that every action performed is contained within a certain special area and generated by a unique circuit of spinal interneurons, the presence of only a few units of motor output is impractical based on the wide range of motor behaviors exhibited. Subsequent work into spinal interneuron systems indicates that the vertebrate nervous system might combine these modules to produce a range of unique movements. Mussa-Ivaldi et al. found that when two sites of the frog spinal cord were stimulated, their unique force vector fields produced by individual stimulation generated a new vector field nearly an exact linear summation of the two unique vector fields[14]. Extension of this principle implies that a few individual spinal units can be multiplexed to produce a wide range of motor responses in a computationally simple manner.

It is important to demonstrate that these systems can be volitionally controlled via supraspinal structures of the central nervous system and are not reflexes produced by solely afferent input. d'Avella and Bizzi examined the force fields evoked by vestibular stimulation in frogs, a neural pathway that exists above the brain stem. By applying principal component analysis to the resulting fields, they found that the dimensionality of the vector fields produced was surprisingly low[15]. This work, combined with much of the recent spinal cord research, indicates that the spinal cord plays a key role in contributing to

the neural production of movement instead of acting as a simple relay between supraspinal systems and the peripheral nervous system.

In recording directly from the cortical surface, neural recording systems miss a significant portion of the neural computation that goes into the production of movement. In order to produce movements approaching the dexterity of those able to be performed by the human upper body – particularly the complex and precise movement of the hand – cortical signals need to be augmented by a system that can emulate the synergistic movement primitives encoded in later stages of the motor pathway. Little is known about these types of muscle synergies in higher mammals and humans in particular. Furthermore, the role the cortex plays during synergy generation is currently unknown. Our proposal will complement and extend these promising studies in frogs and illuminate cortical activity during muscle synergy generation.

1.3 Electrocorticography (ECoG)

1.3.1 Recording cortical electrical activity

A range of technologies have been developed that allow exploration of activity in the human brain by detecting the minute electric fields given off by neurons firing action potentials. Each method contains its own unique set of trade-offs between invasiveness, signal fidelity, temporal and spatial resolution that must be considered when choosing what technique to investigate the desired neural activity.

Electroencephalography (EEG) was among the first non-invasive methods of physiological measure of cerebral function[16]. It consists of placing electrodes on the surface of the scalp in a regular pattern and measuring the electrical fields generated by cortical neural activity. While these systems have allowed the exploration of cortical dynamics in healthy subjects without exposing them to the risk of cranial surgery, it is hampered by a low signal-to-noise ratio and by distance from the surface of the brain. EEG source analysis involves triangulation of dipole current location. Due to the extremely small dipoles generated by neural firing, this triangulation can prove difficult due to the introduction of noise from both physiological noise due to skull conductivity and hemodynamic activity and external artificial amplifier and line noise[17]. In addition, because EEG observes dipole currents, an electric field generated by a neuron falls off as $1/r^3$. This dramatic loss of signal with distance implies that even at the surface of the scalp, the distance between the electrodes and the surface of the brain is large enough that any signals that are detected have been spatially smeared. These limitations imply that cortical activity that produces synchronized rhythmic firing over a large area of cortex can be identified (such as the classical

alpha, theta and beta rhythms), but any unique local network activity that occurs asynchronously from these rhythms would be lost. As such, it is not viable to investigate local spatial organization of the cortex.

Recent advances in computing and engineering has allowed the development of functional magnetic resonance imaging (f77), a non-invasive tool capable of measuring three dimensional hemodynamic responses associated with neural activity[18]. However, while the metric used to measure hemodynamic activity – blood oxygen level dependent or BOLD – is correlated with neural activity, the underlying physiological mechanism that causes changes in the BOLD signal are still not well understood[19]. Changes in the BOLD signal are hypothesized to be linked to the increase in metabolic activity that is present between 1-6 seconds after an area of cortex has increased in neural activity[20]. In spite of its non-invasiveness and high spatial resolution – especially with newer 1.5 and 3 Tesla fMRI machines – the lack of temporal accuracy and limitations in blood oxygen diffusion are not conducive to investigating the intricacies of hand motor cortex during dynamic movement.

To increase control speed and recording accuracy, many researchers have begun utilizing invasive recording methods. Arrays of electrodes were designed to be implanted beneath the skull and the dura – a tough protective membrane between the brain and skull – directly on the surface of the brain. Each electrode would be inserted into the neocortex and record the electrical potentials of neighboring neurons as they fired action potentials. As far back as the 1970s, Fetz and Finocchio were able to implant single-unit electrodes by performing cranial surgery on macaque monkeys. These initial trials allowed the monkeys to volitionally control an external device driven solely by recorded neural activity[21]. Promising results spurred the first human trials of these devices to drive a brain-computer interface[22]. Extending the basic proof-of-concept single unit neuroscience research allowed several groups to develop real-time, closed-loop, BCI systems capable of controlling multiple degrees of freedom in both monkeys and humans[23-25].

In order to record single unit activity, microwires 20 um in diameter are implanted within gray cortical matter a few millimeters down into the parenchyma and usually anchored to the skull. Layer V pyramidal cells in primary motor cortex have classically been the targets for BCI studies, given their characteristic activation and relatively large amplitude extracellular potentials. Because of their small size, their lateral recording volume does not detect more than 200 um in radius. Any migration of the cells or small movement of the soft brain matter can change the area the microwires record, potentially causing stability issues during long-term recording[26-28]. In addition, several studies have noted that implanting these single units directly into cortical matter causes local vasculature and neural damage.

1.3.2 Electrocorticographical recordings

ECoG offers the best hope of a long-term BCI implant by providing a better signal-to-noise ratio and spatial specificity than EEG, higher temporal response than fMRI, and less chance of tissue damage and better biocompatibility than single unit recordings. ECoG achieves better resolution than EEG by placing electrode arrays onto the arachnoid mater surrounding the brain, below the skull and dura. Since most large cortical neurons are oriented vertically through the cortex (i.e. perpendicular to the cortical surface with dendrites on top and axons descending below), correlated electric potentials within the cortical column sum constructively. The optimal location to record this correlated activity is at the surface of the brain, directly above the cortical column of interest. Electrical potentials recorded by ECoG are generally five times higher than those recorded via EEG (±100 μV vs. ±20 μV)[29]. Typical grid implants are 8x8 grids of 2-3mm diameter platinum electrodes with 1cm center-to-center spacing embedded into polydimethylsiloxane (PDMS)[30], allowing low-impedance recording by using an intracranial reference electrode. Grids are implanted by cutting a flap in the scalp and excising a section of skull to provide a window for implantation[31]. An incision is made in the dura, which is pulled back exposing the brain and arachnoid mater. Grids and strips of electrodes are placed over specific anatomic regions. Microwires containing leads that connect to the electrodes are combined into thin macrowires within the PDMS and exit the skull via a small hole left after replacement of the skull window. The macrowires are then connected to electrode ribbons which feed into biosignal amplifiers.

1.3.3 Characteristic neural activity changes observed in ECoG

We have previously shown that during active movement, the electrical potentials measured over motor cortex exhibit consistent modulation containing two distinct processes within the power spectrum[32]. At low frequencies generally below 40 Hz, narrow-band power decreases occur during movement over a spatially large area of cortex indicating the cessation of a synchronous process, known as event-related desynchronization (ERD) or the Beta frequency band. Higher frequencies exhibit a power-law like broad band increase in power, known as the chi-shift, over a focal area of motor cortex, analogous to an increase in a noise-like process. These high-frequency increases have previously been understood to show synchronous processes within local cortical networks, but our recent work has showed that they reflect broad-band spectral changes across the entire spectrum that are obscured in the lower bands by a synchronous low-frequency process. Using principal component analysis (PCA) on the power spectra, we have been able to separate the broad spectral, spatially focal process from the low frequency rhythm decrease [33]. This provides a theory to bridge the gap between the action potentials recorded by single units and the continuous potentials recorded by ECoG.

The shifts in the power law are estimated to be based on the physiological changes that occur during changes in neural activity. The beta band has been suggested as a rhythmic thalamocortical reset circuit, causing large numbers of neurons to fire synchronously and become too exhausted to begin communicating in local circuits. When the thalamocortical connection ceases, neurons become free to communicate in independent local circuits across the cortex, temporally spreading out the spiking activity in noise-like process. Superposition of these two proposed processes can explain the spectral shifts seen during ECoG recordings: a low-frequency, spatially distributed decrease in low frequency power and a broad power increase in a high frequency band (HFB, 75-200Hz).

These broadband high frequency spectral changes may provide evidence for a macroscale correlate of population firing rate[34]. Models of the broadband spectral changes in potentials recorded via ECoG imply a correlation with the action potential rate at the single-unit local field potential scale, a possible generic representation of mean firing rate of the population of neurons generating the electrical field. A recent study has provided evidence for this model, showing that in order to increase HFB activity in ECoG, a subject can either increase the firing rate in the population of neurons being recorded by the electrode or increase the coherence in spiking neurons [35].

Constraints of current ECoG technology

ECoG provides a semi-invasive method to control computational devices by using real-time classification of neural signals, requiring very little training time[36]. Further discoveries are limited with current ECoG technologies and signal classifications. Due to the wide 1cm spacing of electrodes currently used in clinical studies, large populations of up to $5x10^5$ neurons are recorded under each electrode site. While this can provide evidence of activity in specific areas of the brain, the identification and classification of local spatially distributed neural networks is impossible at current resolutions. Developing electrode arrays with smaller inter-electrode distances could provide the resolution needed, though research into the minimum spacing needs to be done to ensure neighboring electrodes are sensing unique information and are not compromised by a salt bridge being formed by ions within the cerebrospinal fluid surrounding the brain.

Current BCI paradigms screen for gross high frequency activity during certain modalities of movement. Electrodes showing activity correlated with periods of movement have their changes in high frequency mapped to a control signal; increasing spectral power beyond a linear threshold triggers the control signal output. This technique, while viable for simple control mappings, provides only a binary output of a positive or negative result. Each electrode can provide only one control signal, meaning multiple degrees of freedom require multiplexing the identified control features. This leads to

complications when controlling two or three degrees of freedom from two or three control features and the near impossibility of controlling high-dimensional systems. Controlling modern prosthetics in this way would be an effort in futility, as some manipulators precisely mimic more than 20 degrees of freedom present in the human hand[37].

Even if a creative mapping solution were applied, merging multiple control feature modalities would be un-intuitive. Consider hand and tongue features identified and mapped to control of a 24 degree of freedom robotic hand. The subject's hand movement could be applied to cycling through the currently controlled joint with tongue motion controlling the direction of joint movement. Performing even the simplest of tasks with this unintuitive mapping would be extremely difficult. Though the human central nervous system has shown an amazing ability to adapt, applying unintuitive mappings of control w ould require long time periods to learn and may not ever approach the level of dexterity required for even the simplest tasks.

Our proposal involves addressing all of these shortcomings of current ECoG tasks. We will investigate a mapping of activity in the hand motor that does not require identification of each joint velocity or muscle force in the human hand, and apply this mapping of cortical activity to the dexterous control of a highly articulated prosthesis.

1.4 Hypothesis

In the remainder of this document we aim to show that, given evidence the musculoskeletal system is driven synergistically by descending cortical commands, we propose that **high dimensional hand dynamics are encoded in low-dimensional, spatially distributed networks within primary motor cortex.**

We present our study of this hypothesis in using the following organization:

Aim 1: Establish that micro-ECoG grid recordings can provide physiologically relevant biokinematic correlates

- **Chapter 2 – ECoG as a stable form of cortical measurement**. Should the signals we record during our ECoG studies change and shift on short order, that would suggest that any mappings and encodings we find may only be temporary and not a true basis for musculoskeletal locomotion. It is critical to show that the signals we record are stable over time, and we do so by investigating the ability of subjects to elicit robust, volitional modulation of local areas of cortex using a brain-computer interface as a form of experimental control

- **Chapter 3 – Evaluating the returns of increasing ECoG resolution.** Before designing and manufacturing a micro-ECoG array, it is prudent to investigate the return on increasing the density of ECoG electrodes. Should we discover that there is a spacing or resolution limit where ECoG recordings would provide diminishing or no returns, there is no use in developing a micro-ECoG grid smaller than this theoretical limit.

Aim 2: Validate micro-ECoG as a means of identifying spatially distributed cortical activity and establish synergistic components of grip

- **Chapter 4 – Using micro-ECoG to identify phoneme generation.** To establish that micro-ECoG can identify unique spatial activity patterns, we studied the patterns generated during speech phoneme generation. Previous studies have shown that parts of auditory cortex are arranged tonotopically. These tonotopic maps can provide a good target to see if micro-ECoG can discriminate these spatially arranged networks of neurons and their corresponding patterns of activity.
- **Chapter 5 – Identifying grip synergies using joint angles in healthy populations.** Our experimental setup for mapping micro-ECoG signals to hand poses requires that we establish the presence of the hand synergies at the musculoskeletal level. This chapter addresses two aspects of synergy generation: first, that synergies exist not only in end-effector space as measured in Cartesian coordinates but also in joint-angle space; and second, that these synergies, should they exist, are present in healthy populations to discount the possibility that synergies identified in the epileptic subjects are not products of their unique pathology.

Aim 3: Reconstruction of multi-dimensional hand postures using spatially distributed cortical activity patterns

- **Chapter 6 – Recorded dynamics of primary hand motor cortex during simple tasks.** Based on our previous ECoG studies with macro, mini and micro-ECoG, we design a high resolution ECoG grid for intraoperative subdural cortical recording. In this chapter we explore brain activity during rest, gross hand motor movement, and highly stereotyped, simple finger flexion as a basis for examining more dynamic, dexterous movements.
- **Chapter 7 – Identifying and mapping cortical activity patterns to synergies.** Expanding on the previous chapter, we explore in depth cortical activity that occurs during highly stereotyped yet dexterous hand motion in the form of object grasping. By building a mapping of cortical activity

recorded during grasping to muscle synergies identified during the recording, we can begin to reconstruct the estimated hand pose based solely on primary motor cortex activity and compare our estimates to the ground truth. In addition, we explore the ability of this mapping to predict hand motion during non-stereotyped, freeform volitional motion.

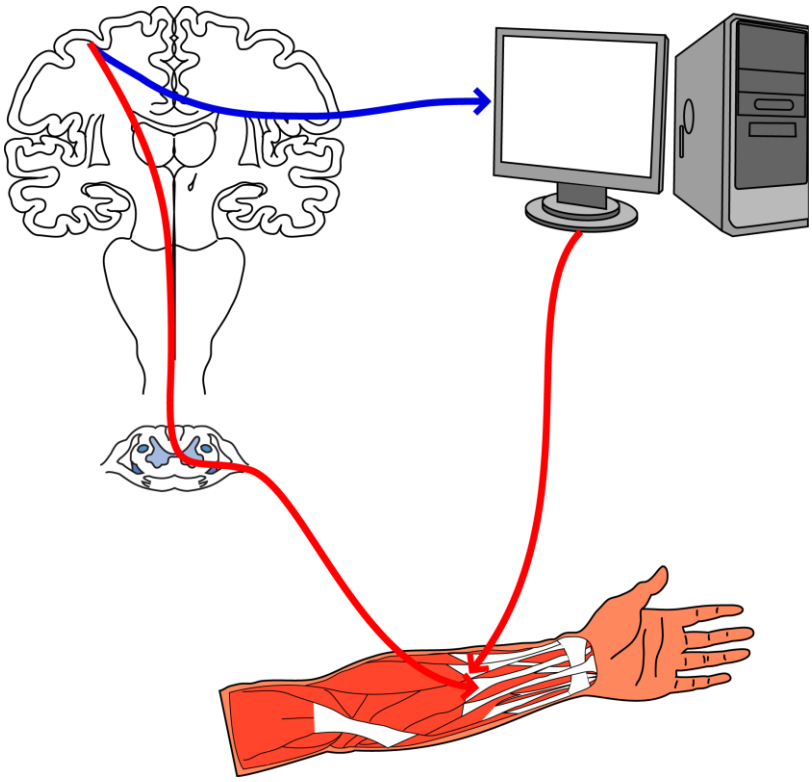

Figure 1 – Brain-computer interfaces attempt to decode natural neural activity in the cortex. Should a descending motor pathway become damaged or dysfunctional, it is possible that an artificial pathway can be created by decoding intent at the cortical level and bypass the biological system

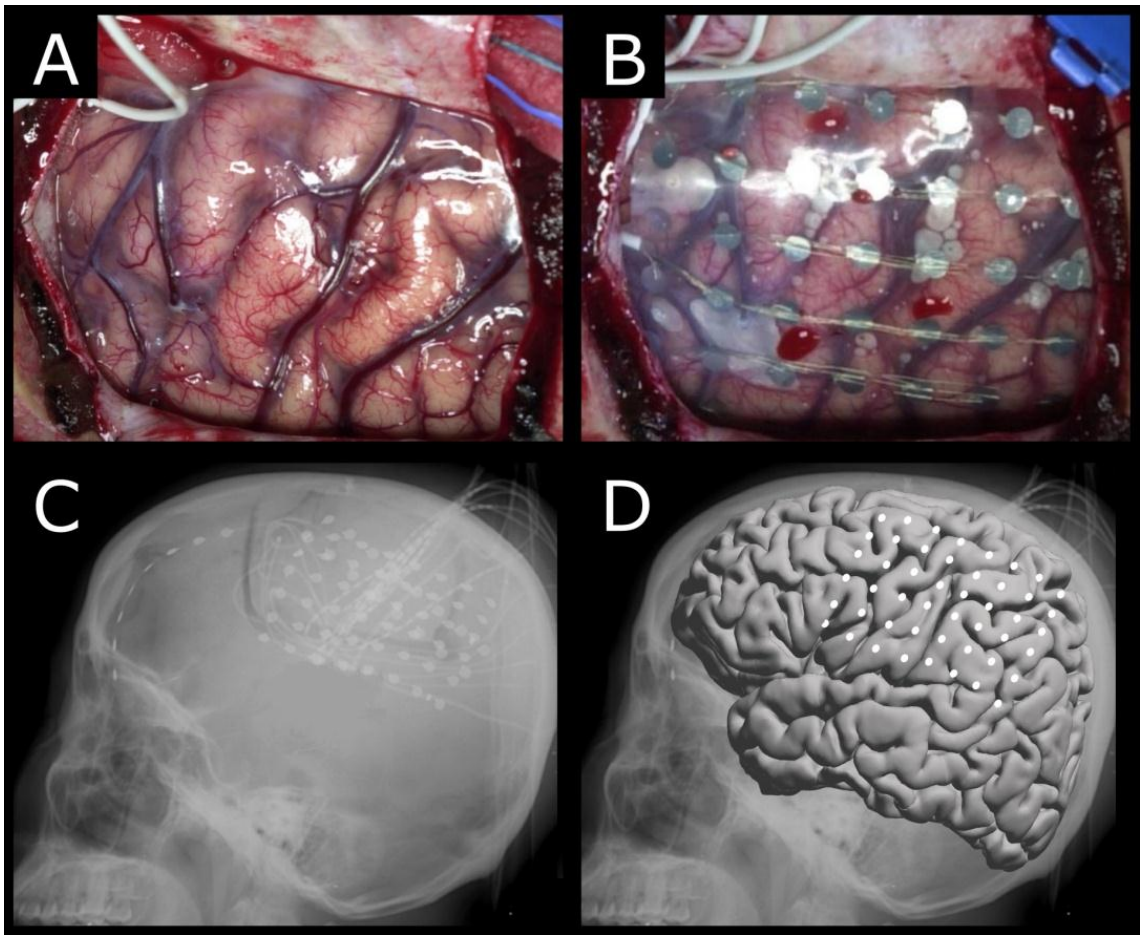

Figure 2 – Example of electrocorticography (ECoG) mapping. A) Craniotomy window is removed and dural flap opened, revealing the cortical surface. B) Implantation of platinum electrode grid embedded in PDMS, placed directly on the cortical surface. C) Post-implant x-ray showing the craniotomy window, electrode grid and strips. D) Estimated location of electrodes based on x-ray localization. *Original image by K. Miller, 2007*.

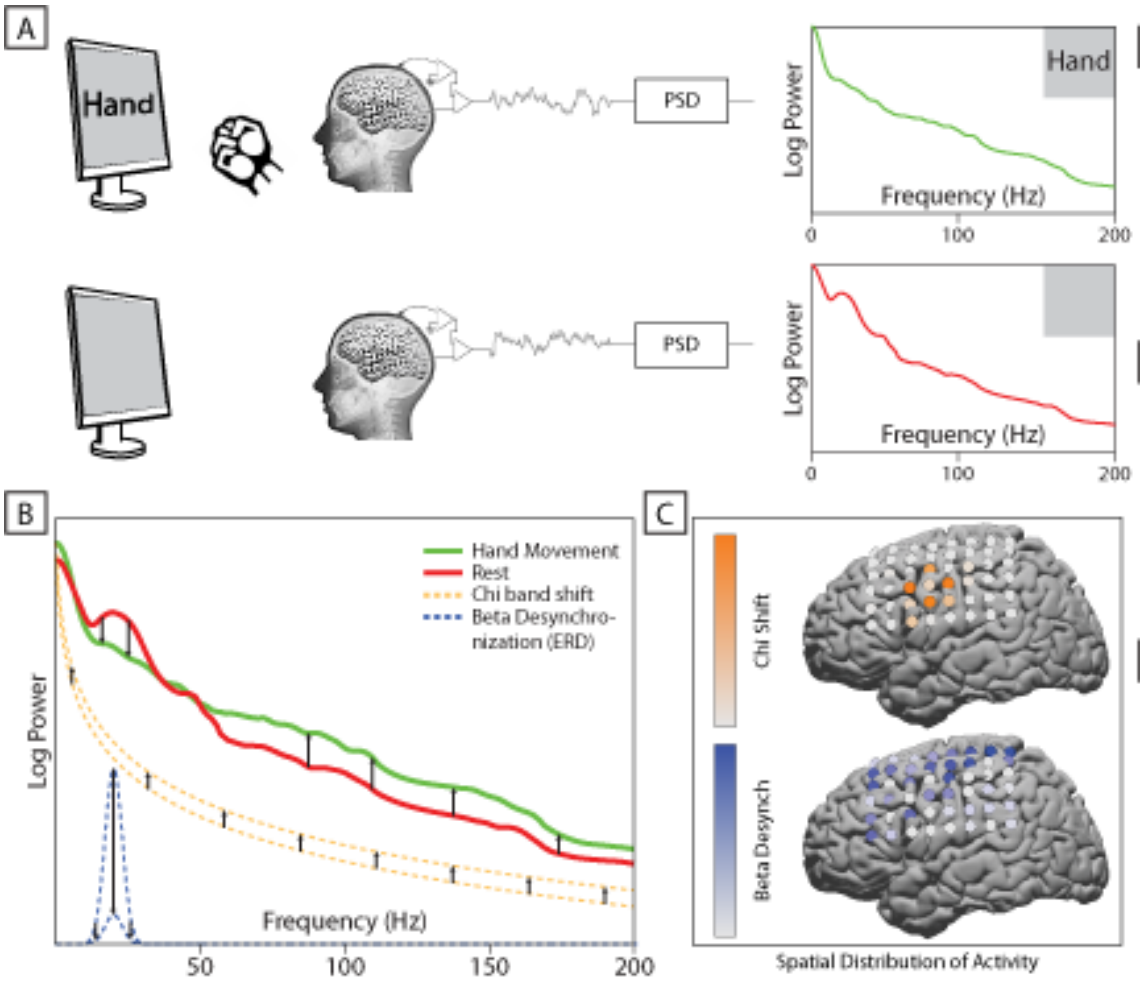

Figure 3 – Overview of basic electrocorticographic (ECoG) screening. A) When presented with a cue, subjects perform an overt or imagined movement. Cortical signals are recorded by subdural platinum electrodes and the power spectral density is calculated. When the cue disappears, the subject ceases movement and the power spectra is calculated. B) The characteristic changes in power spectra between rest (red) and movement (green) can be seen as the superposition of two phenomena: a low large decrease in power in low frequencies (beta range, 15-35 Hz, blue), and a broadband increase across all frequencies (orange). C) Beta desynchronization appears over a large area of cortex, while the broad-band high frequency changes occur in spatially focal areas.

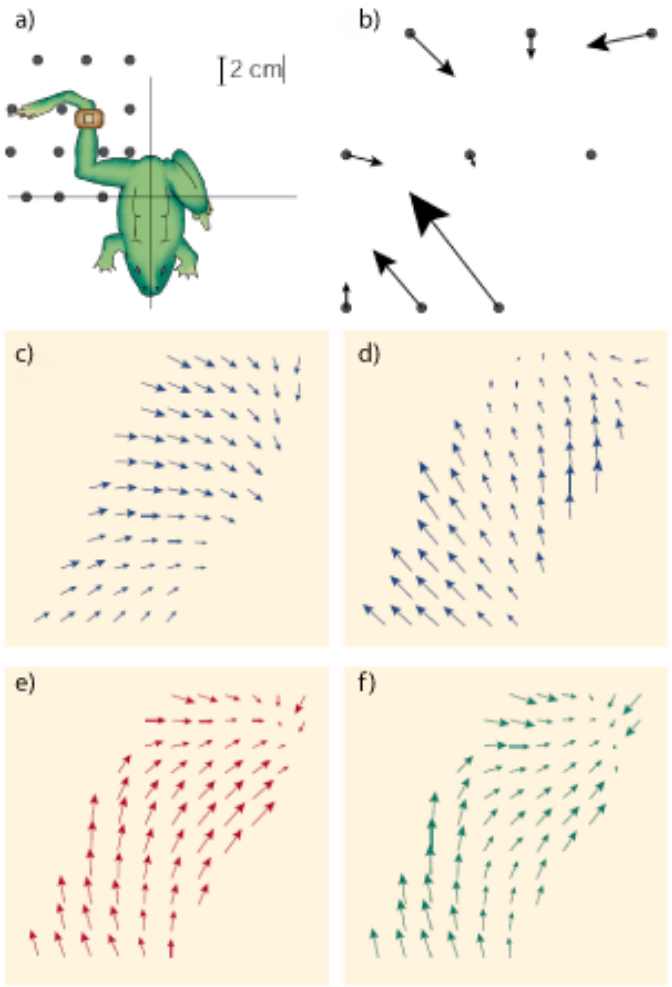

Figure 4 – Evidence of muscle synergies discovered by Bizzi *et al.* in frog spinal cord. A) Force sensing and positional information was recorded from decerebrate frogs. B) Stimulation of spinal interneurons produced forces describable by a robust, reproducible fector field. C and D) Two vector fields produced by separate interneuron stimulation sites. E) A model of the linear vector field sum of C and D. F) Experimental results of costimulation, closely matching the linear model in E. *Image adapted from Bizzi et al, 1991.*

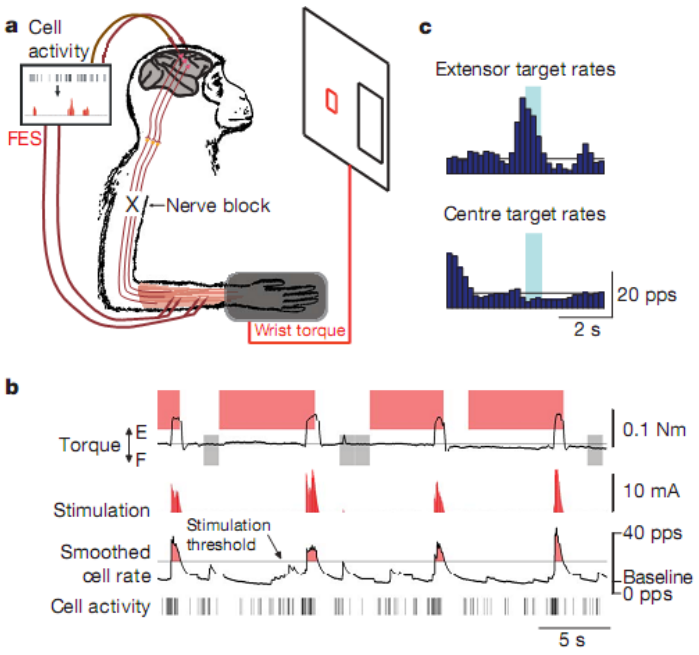

Figure 5 - Schematic adapted from Moritz *et al.* demonstrating their study recording from primary motor cortex in macaque monkeys that underwent a chemically induced peripheral nerve block. Neural firing rates in M1 were decoded and linked to intra-muscular simulation, allowing the monkey to volitionally control wrist torques that it was physiologically incapable of generating due to the block. *Adapted from Moritz et al 2007*

2 Chapter 2 – Electrocorticography as a Viable Neural Platform

2.1 Motivation

In order to identify the spatial distribution of activity in motor cortex during active movement, the underlying signals must be stable between recording sessions. In addition, any future application of cortical synergies identified in this research proposal must remain unchanging and stable over time if they are to be used to drive a prosthetic device. However, studying ECoG signals recorded is problematic in that the brain is simultaneously processing and acting upon large amounts of sensory input. It is an understatement to say that the brain is complex. It is capable of processing huge amounts of data, encoding it, and executing complex coordinated motions all simultaneously. Trying to study how the brain accomplishes this can prove difficult due to the asynchronous, parallel nature of neural networks. The fields of psychology and philosophy have been struggling with these types of problems for a long time. Given a novel scenario, how does one "learn" to solve or approach a problem? How does the brain plan and encode motor movement? Is the brain capable of producing unique, volitional patterns of activity? It becomes nearly impossible to design a non-invasive experiment that can have enough scientific controls to begin to investigate these types of questions.

By their very nature, current studies that use BCIs are simple, tightly controlled experiments. Scientists are required to design paradigms in such a way as to remove confounding factors that may interfere with the operation of the BCI. The control signal that drives the BCI is likewise usually very simple: a single control electrode, a certain ICA component, a single frequency band, etc. It is precisely these types of limitations that can show the true value of BCIs as a tool for investigating the stability of ECoG recordings. BCIs have very clearly established control signals, priors, and parameters (the decoding model) that can be directly correlated to a known, measureable output (the BCI output). Changes in the input control feature are inherently linked with both the output feedback the subject receives and the conscious and subconscious changes the subject makes to optimize their use of the BCI. In this way, BCIs offer a unique, compelling and controlled way of studying the stability of the neural signals generated by the cortex and recorded via electrocorticography.

All previous multiple-day brain computer interface experiments have dynamically adjusted the parameterization between the signals measured from the brain, and the features used to control the interface. In this paper we present the results of a multiple day electrocorticographic (ECoG) brain computer interface (BCI) experiment. After an initial screening and feature selection on the first day, five consecutive days of cursor based feedback were performed with a fixed parameterization. Control

of the interface was robust throughout all days, demonstrating that ECoG-based BCIs can be implemented for multiple-day control without the necessity for sophisticated re-training and adaptation.

2.2 Background

Human neocortical activity is dependent upon a wide variety of interdependent parameters. Across different spatial and temporal scales, this has been associated with a non-stationary neural signature in experimental recording. Attempts to capture and translate this neural activity as a control signal in a brain-computer interface have, to date, all relied upon dynamic decoding algorithms which either adapt continuously or are re-calibrated between experimental runs.

Brain-computer interfaces (BCI) translate cortical signals for device control, bypassing the peripheral nervous system and motor pathways, and directly coupling neural activity in the central nervous system to a computational device for communication or manipulation of virtual and physical devices. Some common recording methods that researchers have used to capture neural activity have been to record the electric potential from extra-cranial electroencephalography (EEG), cortical surface electrocorticography (ECoG), and single-unit electrode recording using penetrating electrodes[20]. Regardless of recording technique, devices that replace natural control pathways will have to be robust over very long timescales.

In order to detect and localize a specific control signal for the purposes of a BCI, a neural feature which is correlated with intent, and which can be volitionally modified, must be identified. The translation of the brain signal to a reliable control feature is characterized by some parameterization. An appropriate set of parameter values are typically learned during a controlled behavioral screening, and updated using continual adaptation or repeated screening. Wolpaw *et al* proposed the idea of two levels of training and adaptation of a BCI system[21]. The first level has the BCI system initially adjust to the user and then remains fixed for the duration of control. Unfortunately, many cortical recording techniques have been found to show large variation both within and across experimental sessions[22–26]. Wolpaw suggested a second level of adaptation was required that contained multiple online adjustments to account for and adjust to variation within a single experimental session. Other researchers have performed long-term experiments where the translation parameters were not adjusted during the online experimental period, but parameterization values were re-learned prior to each online experimental session[27–29].

EEG, the acquisition of cortical potentials from the surface of the scalp, allows long-term data acquisition of human cortical signals at the expense of spatial resolution. Guger *et al* proposed that an appropriate method for an EEG-based BCI is an adaptive autoregressive approach to parameter estimation[30], based upon changes in spectral power, and many EEG brain-computer interface research groups employ this autoregressive estimation in order to isolate features for acceptable control of EEG systems[31–33]. This approach was used by Shenoy, *et al*, who performed closed-loop control of an EEG system with control parameters found using training data. Because of the intrinsic discrepancy between training and online data, they found that an adaptive control algorithm was necessary for accurate classification[34].

"Single-unit" recordings use penetrating intra-cortical electrodes to record spike events from one or a few neurons adjacent to the electrode tip. They have been used successfully to extract features for feedback in primates[35–37] and humans[29] but, in all cases, the parameterization required adaptive algorithms that modified the control parameters in real-time. In primate studies, Donoghue *et al* used coadaptive constant-parameter prediction[35] while Fetz *et al* and Wessberg *et al* used artificial neural networks that adapted to changes in spike rates during online control[38,39] to attain viable levels of classification. Furthermore, both cases required novel control parameter selection prior to each experimental session. The long-term single-unit BCI experiments in humans performed by Hochberg *et al*., over a 9 month period, required re-learning of control parameters before each of 57 consecutive recording sessions[29].

Schwartz *et al* have recently demonstrated the ability to record neural spikes from an intracortical microelectrode array implanted in the proximal arm region of monkey primary motor cortex and use these recordings to control a prosthetic arm in three dimensions for the purpose of self-feeding[40]. Though the monkey was able to gain control over the arm, a training period consisting of four iterations of control parameter calibration was required at the beginning of each daily session. Control parameters from the final training estimation were used by the expectation-maximization algorithm used for control throughout the remainder of the day.

ECoG, in turn, requires invasive placement of an electrode array subdurally to record cortical potentials at a higher spatial resolution, and thus a more local neuronal population, than EEG. ECoG arrays have been successfully used to control a BCI device in one dimension[24,25] and recently in two dimensions[32]. Both control paradigms have employed adaptive algorithms that updated control parameters during closed-loop control. The short duration of these trials, due to the clinical needs of

the subjects enrolled in these studies, has prevented investigation of the day-by-day variability of the classification parameters.

We demonstrate that, using anatomically intuitive feature localization and a robust high frequency signal from the electrocorticogram, continuous control using fixed parameters is possible without re-training, re-learning of parameters or continuous parameter adaptation over five consecutive days of robust control of a brain-computer interface.

2.3 Methods

2.3.1 Patient availability

The subject in our ECoG study was a 32 year old male patient at Harborview Hospital at the University of Washington (UW) with intractable epilepsy, refractory to medical therapy. The patient underwent implantation of a subdural electrode array above the right fronto-temporal cortex to localize the seizure focus during a 7 day monitoring period. The post-operative x-ray was used to determine the electrode grid locations[41]. Informed consent was given by the subject in accordance with University of Washington Institutional Review Board protocol.

2.3.2 Signal Acquisition

The implanted electrocorticography array contained platinum electrodes in an 8x6 rectangular formation. Electrode contacts were circular (4mm in diameter, 2.3mm exposed) and embedded in silastic with a face-center spacing of 1cm. After leaving the head, the signals are split into two paths: one into the clinical monitoring system and the other into a Synamp2 [Neuroscan, El Paso, TX] recording system. The amplified signals were passed to the general-purpose BCI2000 software suite. Samples were taken at 1000Hz and band pass filtered from 0.3Hz to 200Hz. Since the sampling rate and filtering settings were much greater than the range used for control in this trial (80-100Hz), the Nyquist frequency considerations did not impact the findings and filtering artifacts were not present. The BCI2000 software suite [21] was used for stimulus presentation, data acquisition, and real-time processing.

2.3.3 Tasks

The study consisted of an initial screening for control features, and then a five-day repeated BCI feedback experiment. The initial screening was a simple cue-based movement task to identify an appropriate electrode-frequency band combination for cursor control. In this task, a 3 second visual word cue was given to move either the tongue (the word “tongue” displayed on the screen) or the hand (“hand”). During the cue presentation, the subject would repeatedly open and close his left hand 3-4

times or protrude and retract his tongue 3-4 times. Thirty cues of each type were interleaved in random order, with 3 second rest periods (blank screen) between each cue. An appropriate frequency range – electrode combination for feedback (80-100 Hz, in two electrodes, at Talairach locations <58, 13, 28> and <58, 4, 33>) was chosen by comparing the distributions of power at each frequency, in each electrode, during "tongue" cues with the corresponding distribution from rest cues (quantified using the squared cross-correlation, r^2, associated with the comparison). The power in this frequency range – electrode combination was then coupled to the movement of a cursor in a cursor based brain computer interface experiment [2,8,9,11,19,28]. The velocity of the cursor, $\dot{y}$, was determined by the relation $\dot{y} = g\,(P(t) - P_0)$, where $P(t)$ denotes the power between 80-100 Hz in the electrode at Talairach locations <58, 13, 28> and <58, 4, 33> (Figure 6B). P_0 denotes a "mean" value (Figure 6C), above which the cursor moved up, and below which, the cursor moved down. The gain, g, was chosen so that the cursor would move in a reasonable range. The parameters P_0 and g were not changed throughout the task. For each target trial during the BCI experimental runs, the subject was presented with a cursor in the center of the screen and a target at either the top or bottom of the screen (Figure 6A). When the patient imagined moving or actually moved his tongue, the cursor would be driven upwards and when the patient was at rest, the cursor would move downwards (according to the relation above). If the cursor was successfully directed to the target or 7 seconds elapsed without cursor/target collision, the trial was reset and a new target was presented. Target locations at the top or bottom of the screen were presented in randomized order, but in roughly equal number during each experimental trial. A set of 40 consecutive, randomized target presentations ("trials") were performed during an experimental run. Specific instructions were given to imagine the kinematics of the movement ("kinesthetic imagery"[42]). Sublingual differential EMG was used to verify that there was no muscle movement during the imagery-based experimental runs.

2.3.4 Offline Analysis

The signal was re-referenced to the common average potential across all electrodes at each sample. The data was then segmented into blocks from three types of periods: when the upper target was presented, when the lower target was presented, and when no target was presented. The power spectral density (PSD) for each block was calculated using Welch's averaged periodogram method with the fast fourier transform (FFT) and a Hann windowing function. The length of data for the FFT was a 1000 sample window, and windows were overlapped by 900ms. The spectra from each block were normalized by dividing through by the mean power across all blocks (of all types combined) at each

frequency (effectively whitening the spectra), and then the log of the summed values across the 80-100Hz range were determined as shown in the figures.

2.3.5 Online Control

For each electrode in the grid, we continuously calculated the voltage PSD using an autoregressive technique[43] for frequencies between 0 and 200 Hz (binned at 2Hz) for each trial and for the rest periods in-between trials. The PSD was calculated from the previous 280ms of data, every 40 ms. Cursor velocity was calculated by comparing the power between 80-100Hz in electrodes at Taliarach location <58, 13, 28> and <58, 4, 33>. The position was then updated according to $\dot{y} = g\,(P(t) - P_0)$, as described above.

2.4 Results

After the initial learning trial (difference in power within the control band was significant at $p<0.01$), every subsequent overt trial had a significance of $p<0.001$ (bootstrap 10^5 iterations, comparing mean power between movement/imagery targets versus rest targets). During all but one overt trial, target accuracy was 100% with the remaining trial at 97.5%. Once control was demonstrated with overt control, imagery tasks were performed. Due to the nature of the imagery task, it is not possible to ensure that every run or trial is performed in the exact same manner for each run. The final run of imagery based feedback for each day during imagery (Figure 7) showed significant ($p<0.001$, bootstrap 10^5 iterations) control, with accuracies of 20/2 (hits/misses), 19/0, 19/5, 14/4, and 17/2, compared with a randzom chance accuracy of 50/50.

2.5 Discussion

All previous brain-computer interface studies have used some form of adaptive algorithm. In this study, however, we have demonstrated that extended control of a simple ECoG-based BCI is possible with fixed parameters for a five day period, without recalibration, adaptation, or re-training. This suggests that the high-frequency ECoG signal is robust across several days. Previous ECoG studies [20,24,25,44,45] were not able to explore this because of the limited time with this subject population. This finding suggests that ECoG-based BCIs can be implemented in an impaired subject population (paralysis, stroke, ALS, etc) for the purpose of prosthesis development. Furthermore, recent studies[32] have demonstrated the potential to extract several simultaneous control signals from an ECoG array.

For any long-term brain-computer interface applications such as prosthetic limbs, it is important that the neural signals used for control be robust and remain spatially and frequency-range stable over a long period of time. Re-learning control parameters before every use of BCI applications may not be realistic

or feasible, thus a signal that is robust and stable over long periods of time would be an ideal candidate for a control feature.

We have shown that it is possible to select a control feature in the high gamma range that is stable and robust over a long period of time. This is an important result for future studies; studies that identify high frequency changes that are highly correlated with an experimental metric should not be instantly assumed to be spurious, transient activity patterns. In the context of identifying the underlying patterns of cortical activity during dexterous movement, this suggests that if patterns of activity are discovered to be correlated with some type of muscle synergies

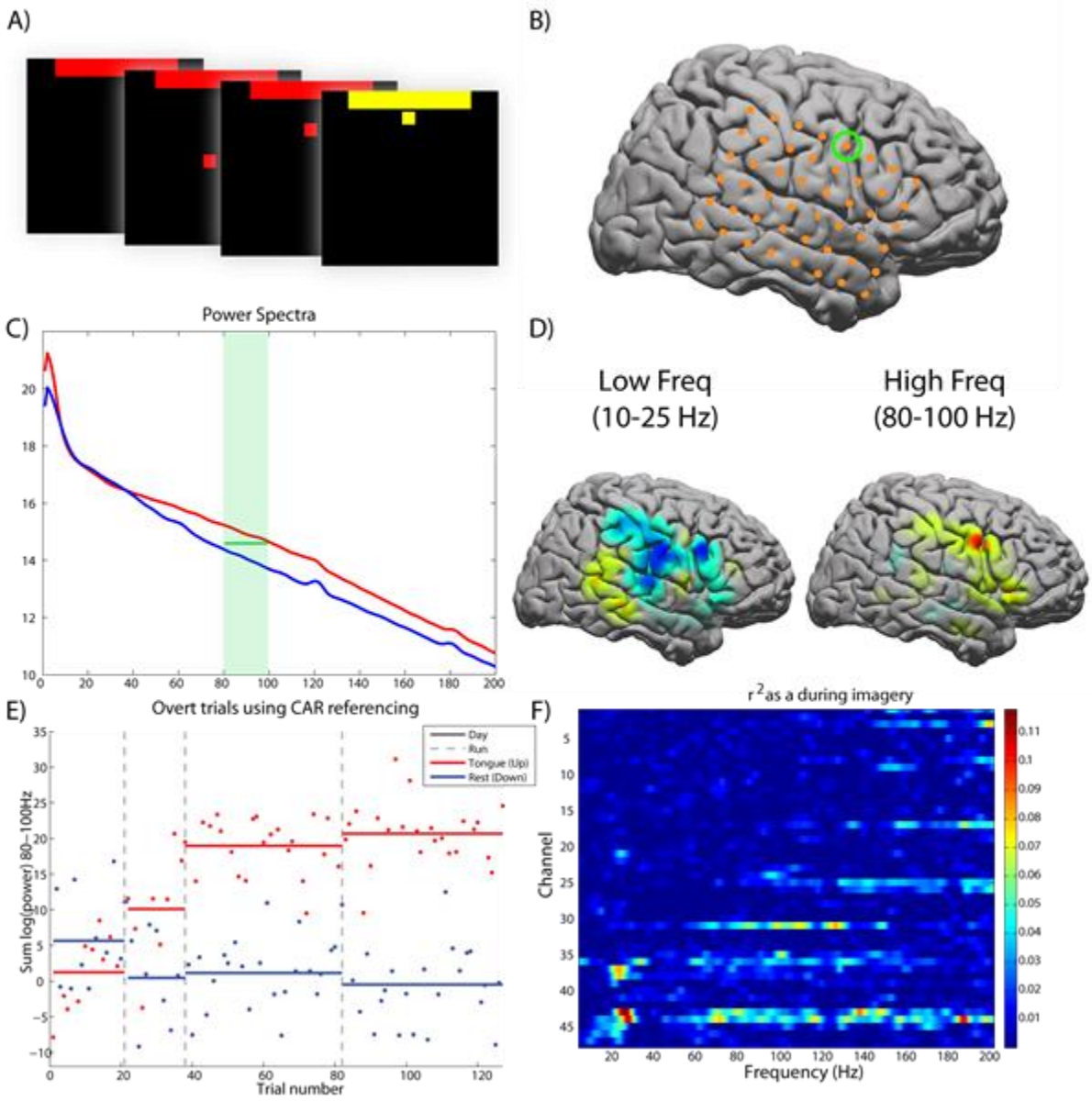

Figure 6 - A) Cursor control task – sequence of a successful trial B) electrode location on standardized brain; electrode used for control is highlighted C) Linear feature found during screening for electrode 44 (see B). Blue trace is the power spectral density during rest; red shows the movement spectra. The green line within 80-100Hz is the threshold set on the first day, was not modified during the 5 day recording session. Note that the broad spectral shift within the chi band (75-150 Hz) D) cortical plot of low and high frequency power, showing a broad decrease in power at low frequencies and a localized increase in high frequency power E) Four overt cursor control runs, showing the learning curve during the first day. The second run was significant at $p < 0.05$ and the final two runs at $p < 0.001$ f) r^2 correlation for a single imagery trial. P-value for trial was $p < 0.001$. F) r^2 plot of frequency vs channel for an imagined control trial. High frequency band activity can be seen from 60-200Hz on a number of channels, including the control channel 44.

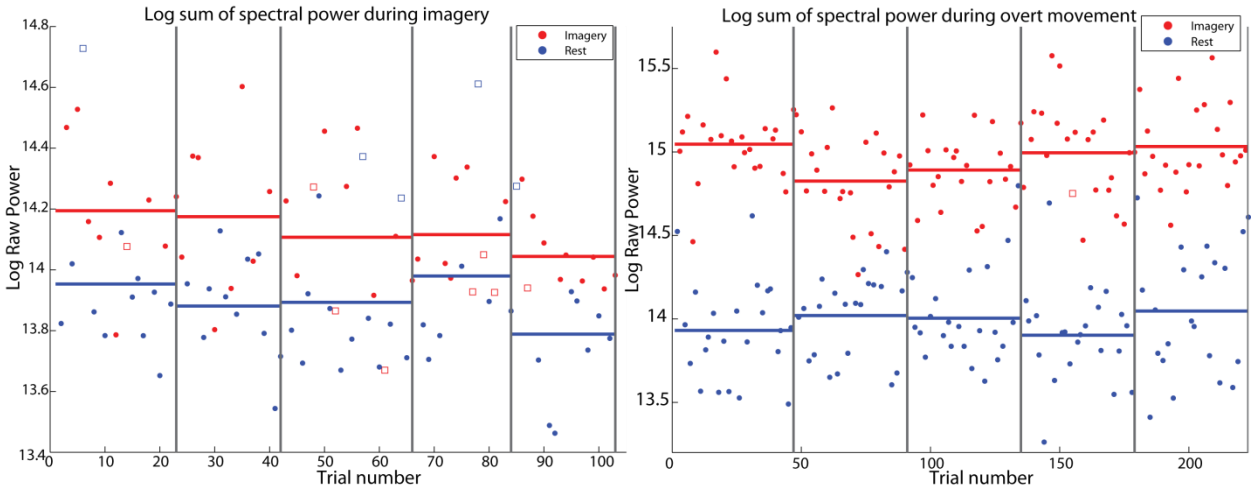

Figure 7 - Final control trials for imagery and overt movement – Points represent total power within the control band for each individual run during the final trial across five days. Vertical bars separate each day; horizontal bars represent the geometric mean for all runs each day. Failed runs (where the target was not reached by the cursor) are shown as squares. During movement and imagery (red), and increase in power can be seen for all runs in comparison to rest runs (blue). All trials were significant at $p < 0.001$ (bootstrap 10^5 iterations, comparing mean power between movement/imagery target trials versus rest target trials).

3 Chapter 3 – Exploring the Returns on Miniaturization

3.1 Motivation

Higher density ECoG grids with the same number of electrodes as those used clinical are restricted in the amount of cortex that is covered by each implant. It is critical to show that the new microgrid design will be sufficient to cover the entirety of primary hand motor cortex. Miller *et al.* and Scherer *et al.* have demonstrated that HFB activity observed during digit flexion is usually on 3-4 electrodes on standard 1cm ECoG implants, with up to 4 showing preferential activity for individual digits[46,47]. In all instances, electrodes showing characteristic activation for individual digits were proximal in grid space, with the largest end-to-end Euclidean distance of 1.73cm, and largest area covered of approximately $2cm^2$. Current grid designs used in clinical settings are usually 8x8 electrodes spaced at 3mm, or 2.1mm on a side. It is possible that by adding additional electrode contacts over this $2cm^2$ surface, much more robust and accurate classification could be performed.

In September 2010, a pediatric patient was admitted to Seattle Children's Hospital to undergo electrode implantation for the purpose of epileptic seizure foci localization. Though this standard surgical protocol has been regularly used in adults and recently with increased frequency in pediatric patients, at 2.5 years old this subject was unique in that he was significantly younger than the standard pediatric patient population. In spite of recurrent generalized tonic-clonic seizures, physiological and musculoskeletal development was normal for a child his age.

The clinical protocol for localization of epileptogenic tissue is to implant an array of electrodes covering a large area of cortex that is suspected of initiating seizure activity. However, due to this subject's pathology – the seizures were suspected to be coming from an area of cortex in close proximity to primary motor cortex – the standard resolution clinical grids were insufficient. Instead of the standard 3mm diameter electrode grid spaced at 10cm center-to-center, a grid of electrodes spaced at 5mm center-to-center was implanted. This presented the unique opportunity to study the neural dynamics of motor cortex at a higher spatial resolution than previous studies we had performed.

In this chapter we present a unique case study that serves as the basis for our future work into investigating unique spatially distributed patterns of cortical activity across primary hand motor cortex using higher resolution, non-standard ECoG arrays.

3.2 Methods

3.2.1 Subject

The subject was a 2.5 year old right handed male admitted to Seattle Children's hospital in Seattle, WA for generalized tonic-clonic seizures. He was implanted with two subdural electrode arrays for the purpose of seizure foci localization (see Figure 8). Twenty-four hour cortical recordings were performed for four days, after which the grids were explanted and epileptogenic tissue was resected. Both parents gave informed consent for their child to participate in this study in accordance with Seattle Children's Institutional Review Board and HIPAA compliance.

3.2.2 Electrode array

Due to the suspected proximity of the suspected seizure foci to primary motor cortex, two smaller grids than are normally used for clinical protocols were implanted. Each grid contained an 8x8 array of 3mm disk platinum electrodes spaced at 5mm center-to-center diameter, smaller than the clinical grids previously used Figure 10. This allowed the grid to cover a total of 12.25cm^2.

3.2.3 Biosignal recording

The superior, inferior 64 contact ECoG grid was sampled at 1200Hz using a g.USBAmp biosignal amplifier (G.Tec, Austria). Signal acquisition and cue presentation was operated using the BCI2000 software suite[48]. Signals were recorded hardware filters of 0.1Hz high-pass and 500Hz low-pass and a notch filter of 60Hz.

3.2.4 Experimental Protocol

With the grid implanted over an area of the brain predicted to be associated with hand motor cortex, we opted to perform an overt hand motor task. In young adult and adult subjects, this would entail a visual cue to appear on a computer screen instructing the patient what to perform (i.e. gross hand movement or individual digit flexion). Because the subject was young and incapable of understanding and following directions, this usual visual cue based experimental paradigm required modification.

To elicit hand movement, we chose to select three items the child showed interest in and enjoyed and presented them one at a time to the subject (Figure 9). At a visual cue to the researcher that occurred 4s after the previous, they would select one of the three object and move it into reachable range of the subject. In response to the presentation of the object, the child would reach out and grasp the object. After 4s, the object was taken back out of range of the subject's reach and consequently the

subject released the object. Each object presentation was done in such a way as that would likely elicit the same, repeatable object-specific grip by the subject.

Each of the three objects was selected to require a different, unique level of grasping coordination (Figure 8). The first object was a large, multicolor stuffed toy snake. When presented with the toy, the subject would reach out and grasp the object in a palmar, "power grip" as decribed by Landsmeer *set al*[49]. This grip involved extending all digits in a splayed fashion on approach and, upon reaching the object, partial yet incomplete closing of the hand. The next object was a vertically-oriented ball-point pen that required the subject to extend all digits in a splayed motion similar to the snake. On closing, the subject would simultaneously contract all digits around the pen, completely enclosing around the pen with the thumb resting on top of the other four digits. The last object was a 6cm by 6cm square sticker of the subject's favorite cartoon character "*Dora The Explorer*". It was presented so the subject would perform a four-finger long-prismatic grip with the thumb and fingers on opposing sides of the sticket[50].

Recording the exact position of the subject's had was proven impossible due to the small size of the subject's hand in relation to any available datagloves; no amount of stretching or modifying of the adult-sized gloves allowed any to reasonably fit his hand.

3.2.5 Analysis

Recorded signals were re-referenced using common average re-referencing:

$$\dot{V}_i(t) = V_i(t) - \frac{1}{64}\sum_{k=1}^{64} V_k(t) \qquad \textbf{3.1}$$

Where $V_i(t)$ is the raw recorded signal. Each channel was then notch filtered for 60, 120 and 180Hz line noise and band-passed for high gamma (75-200Hz) using a 4th order butterworth filter. Movement epochs were designated as 1750ms after visual cue onset to 1750ms after cue disappearance. This delay was introduced to account for the time taken during presentation and retrieval of each object.

Continuous-time power for each channel was calculated by applying the Hilbert transformation to each channel, taking the absolute value of the result to attain the amplitude, and squaring the result to continuous achieve power. Since signal power is distinctly non-Gaussian, the log power is calculated to make the results approximately Gaussian. Once in log space, the each signal was smoothed using a 250ms Gaussian window. For each object presentation e, the mean log power was calculated for every channel i:

$$\bar{P}_i(e) = \frac{1}{e_1 - e_0} \sum_{t=e_0}^{e_1} P_i(t) \quad \textbf{3.2}$$

Where e_0 and e_1 are the beginning and end samples of the presentation epoch and $P_i(t)$ is the log normalized power at sample t.

Overall Z-scores were calculated for each channel i and object o with respect to resting (inactive) epochs:

$$Z_i(o_{type}) = \frac{1}{n_{type}} \sum_{m=1}^{n_{type}} \frac{\bar{P}_i(e_m) - \mu_{rest}}{\sigma_{rest}} \quad \textbf{3.3}$$

Where $o_{type}$is one of the three objects, $n_{type}$is the number of presentations of that object, μ_{rest} is the mean of the log power epochs, and $\sigma_{rest}$is the standard deviation of log power of rest epochs. In addition, time-course z-scores were calculated based on rest:

$$Z_i(t) = \frac{P_i(t) - \mu_{rest}}{\sigma_{rest}} \quad \textbf{3.4}$$

3.3 Results

3.3.1 Spatial Distribution

Each grip type elicited a unique pattern of activity when averaged across all epochs of the same grip type (Figure 11). Activity during Dora was higher and wider spread than Pen or Snake, with one electrode maintaining an average of 4.71 standard deviations above high gamma log power during res (inter-trial intervals). Pen in turn showed a lower maximum than Dora, but presented a different average spatial pattern which was, on average, higher than Snake. Though snake did not show the broad activity that Dora or Pen did, 10 electrodes did remain above 2 standard deviations away and 5 of those averaged greater than 3.

3.3.2 Temporal Activiy

Because we were unable to record the position and timing of the subject's hand motion due to the size of his hand, temporal plots were time-locked to cue onset. Figure 12 demonstrates that even though precise time-locking was not possible due to the variations in object presentation intervals, there was still robust increase in high gamma activity during all three object grips. Onset of power increase was approximately the same in all object grips at about 2s, though the peak power occurred a different time points for each grip (Figure 13).

3.3.3 Classification

Table 1 shows the results of 10-fold cross-validation results for both K-Nearest Neighbor (KNN) and Support Vector Machine (SVM) classification. Our initial classification attempt was performed using the average epoch power for all electrodes as input, and all three object grip types as output, classified by KNN. This resulted in an average of 74.4% accuracy. Culling the input to only include electrodes with high levels of activity (13, 20, 21, 22, 29, 30, 35, 36, 37) showed a decreased classification rate of 60%, suggesting the additional variability in input aided classification.

Binary KNN classification using all electrodes showed that Pen/Snake was classified correctly 75% of epochs, Dora/Snake at 95%, and Dora/ Pen at 75%. To explore whether the classification results could be improved through the use of a different algorithm, we applied support-vector machine (SVM) classification to the binary classification. Pen/Snake was classified correctly 70% of the time, Dora/Snake 80%, and Dora/Pen at 65%. This suggests that the additional complexity added by the SVM algorithm did not aid in classification and in fact lowered classification across all types.

3.4 Discussion

During the course of the experiment, a marked change in the subject's behavior was observed. Initially during the initial few presentations the subject would reach out and grasp the object and attempt to remain holding as when the object was removed from reach. However, after repeated presentations the subject began to perform arm motions suggesting that he was offering the object he was holding back to the researcher. Further, when the object was removed from his reach, he released grip voluntarily. Though investigation of this behavioral change is beyond the scope of this study, it is indicative that the subject successfully performed the gull range of grip/release that this study hoped to elicit.

3.4.1 Unique activity levels

The spatial patterns associated with each grip suggest an interesting pattern. Activity patterns produced during the snake grasp are much lower than the others. Because the snake is plush-like and large, the precision required during grasping it is subjectively lower than the other objects and the lowered levels of activity reflect this. On the other hand, the grip motion during pen grasping requires simultaneous coordination of distal digits and thumb, suggesting a high degree of dexterity is required and possibly elevated levels of neural activity or activation of broader motor networks; an idea supported by the increased mean activity vs the gross, uncoordinated movements required to grasp the snake (see Pen, Figure 11). In contrast to the other two objects, the Dora sticker is wide in two dimensions but very thin in the third, requiring a four-finger prismatic grip with opposing thumb

pressure. The concept of a prismatic grip on an object that is as flexible as a sticker requires balancing of opposing forces on the sticker by modulating muscle contraction and activity of both digits and thumb. Initiating and maintaining this type of dexterous grip would likely require more precision and coordination, with an correlated increase in cortical activity, a suggestion supported by the wide increase in activity during these grasps.

Though the activity levels show an increase in activity level with increasing grip complexity, the spatial pattern is not uniform across grips. Indeed, Figure 14 suggests that the relative power of some channels – even neighboring ones – varies greatly by object. Neural activity recorded by electrode 21 relative to electrode 35 was nearly identical for both Pen and Snake grips, but much higher for Dora. In electrode 22 showed much higher activity relative to electrode 30 for Snake. This suggests that not only are there different levels of cortical activity for each grip type, there is also a unique spatial distribution to the observed activity for different grip types.

3.4.2 Temporal patterns

In spite of the inability to time-lock the analysis on the onset of movement, there are still surprisingly strong patterns that can be seen in the temporal activity. Additional confounding factors such as the variable reaction time of the researcher after cue was presented, varying attention levels of the subject, and lack of movement onset data would suggest that any patterns that do end up being observed are robust across trials.

Indeed, Figure 13 suggests that there is an initial burst of activity across at the onset of movement, followed by a short dip and a further increase. Unique to the pen activity is a large increase in over 25 channels during initial movement as compared to the Dora and Snake grips, both less than 10 for the first 250ms after grip onset. All three grips reach a peak of 37 active electrodes at 2520ms. However, the prolonged increase in the number of active electrodes for the remainder of the grip suggests that continuous modulation is present during the prismatic grip that is not present in the less dexterous grips.

In addition, it should be noted that classification was performed on average activity during the entire epoch, compressing the time domain of each epoch into a single value. It is likely given the unique temporal activity of each grip type that classification could be much improved by taking into account the temporal variability of each channel during classification training and testing.

3.4.3 Implications for miniaturizing

The unique nature of this subject's medical condition, clinical protocol, and implanted grids allows us to begin to explore the concept of grid miniaturization. Activity levels identified during the

Dora grip suggest that if the same area of cortex had been recorded on a standard 10mm-spaced grid, approximately four electrodes would have shown the same changes in activity (Figure 15B). This is consistent with the findings of Miller *et al.* and Scherer *et al*. that separable activity can be seen in 3 or 4 electrodes in 10mm spaced grids. By examining the total number of electrodes that show significantly increased activity, it is possible that an electrode array with electrodes spaced at 3mm center-to-center would cover nearly the entire area (gray area, Figure 15C) and show very high activity in upwards of 21 electrodes. With this target in mind, we will explore the fabrication and use of grids of this size in future studies.

The presence of varying activity levels and unique spatial patterns suggest that it is likely that designing smaller, higher-density arrays would provide more detail and insight into the underlying neuro-encoding of dexterous hand motion.

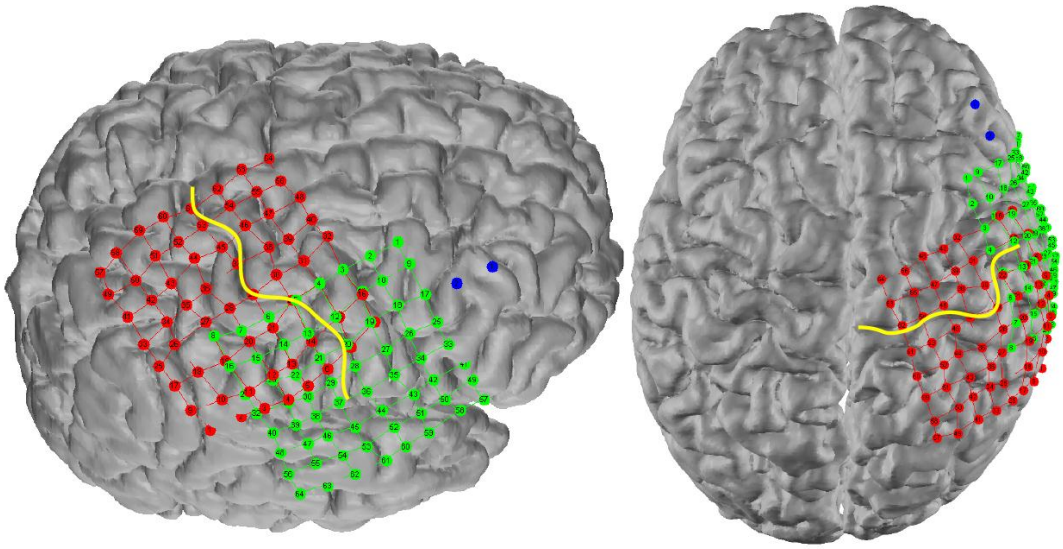

Figure 8 – Electrode locations of implanted grids. Both grids were 8x8 arrays spaced at 5mm center-to-center. The superior posterior grid (red) was the grid used recorded during the experiment. Electrode 1 was inferior posterior and electrode 8 was inferior anterior. The anterior inferior grid (green) overlapped the other grid with 24 electrodes not making contact with the cortical surface and as such was not recorded. Ground and reference electrodes were placed epidurally over dorsolateral prefrontal cortex (blue). Central sulcus is highlighted in yellow.

Figure 9 – Objects presented to the subject included a 6cm x 6cm picture of cartoon character "Dora the Explorer", a ball point pen, and a stuffed toy snake. Each was presented to the subject in such a way as to induce a 4-finger opposed prismatic grip, power grip, and gross envelopment grip, respectively.

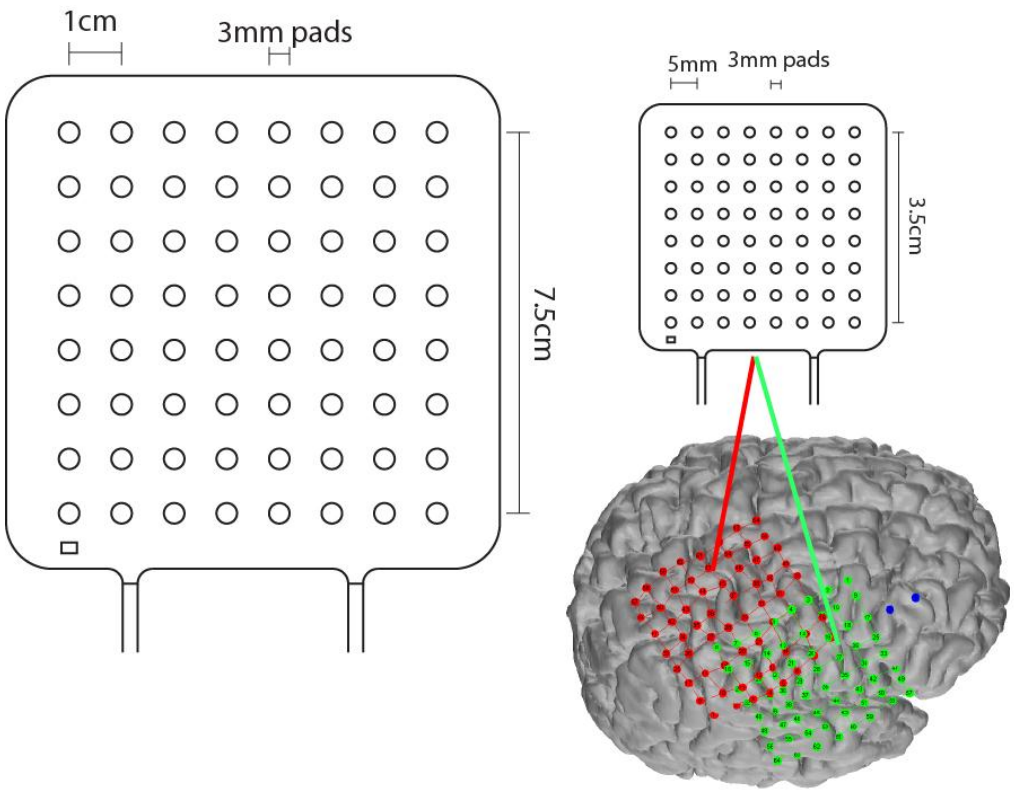

Figure 10 – Relative size of the smaller 5mm grid (top right) relative to the standard clinical grids previously used (left).

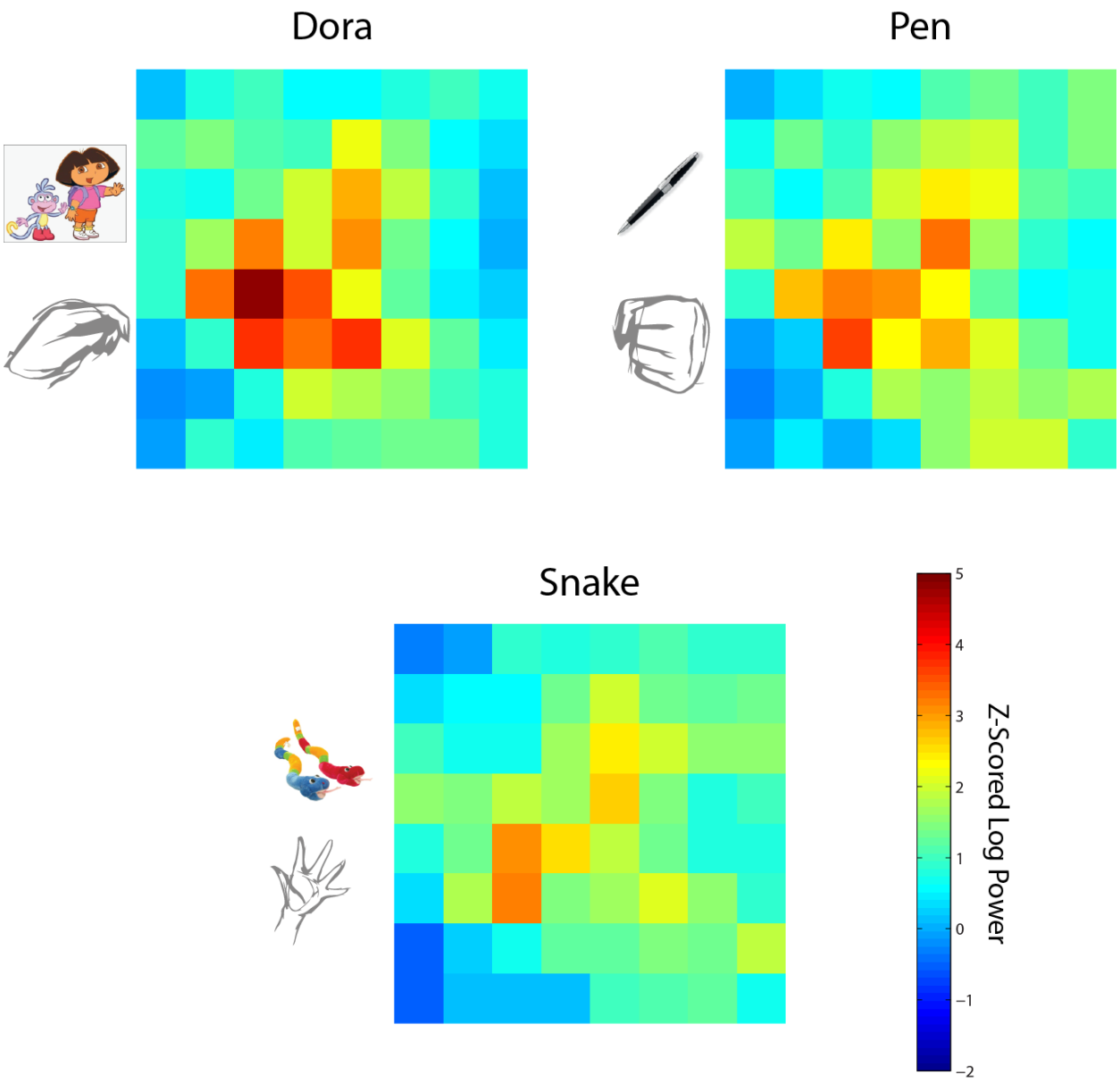

Figure 11 – Spatial patterns of activity during each grip. Electrode #1 is located in the upper left; #8 lower left. Color indicates z-scored difference in log power from rest. The maximum average z-score was in electrode 21 during the Dora grip at 4.71 standard deviations. Unique patterns of activity can be seen for each object grip.

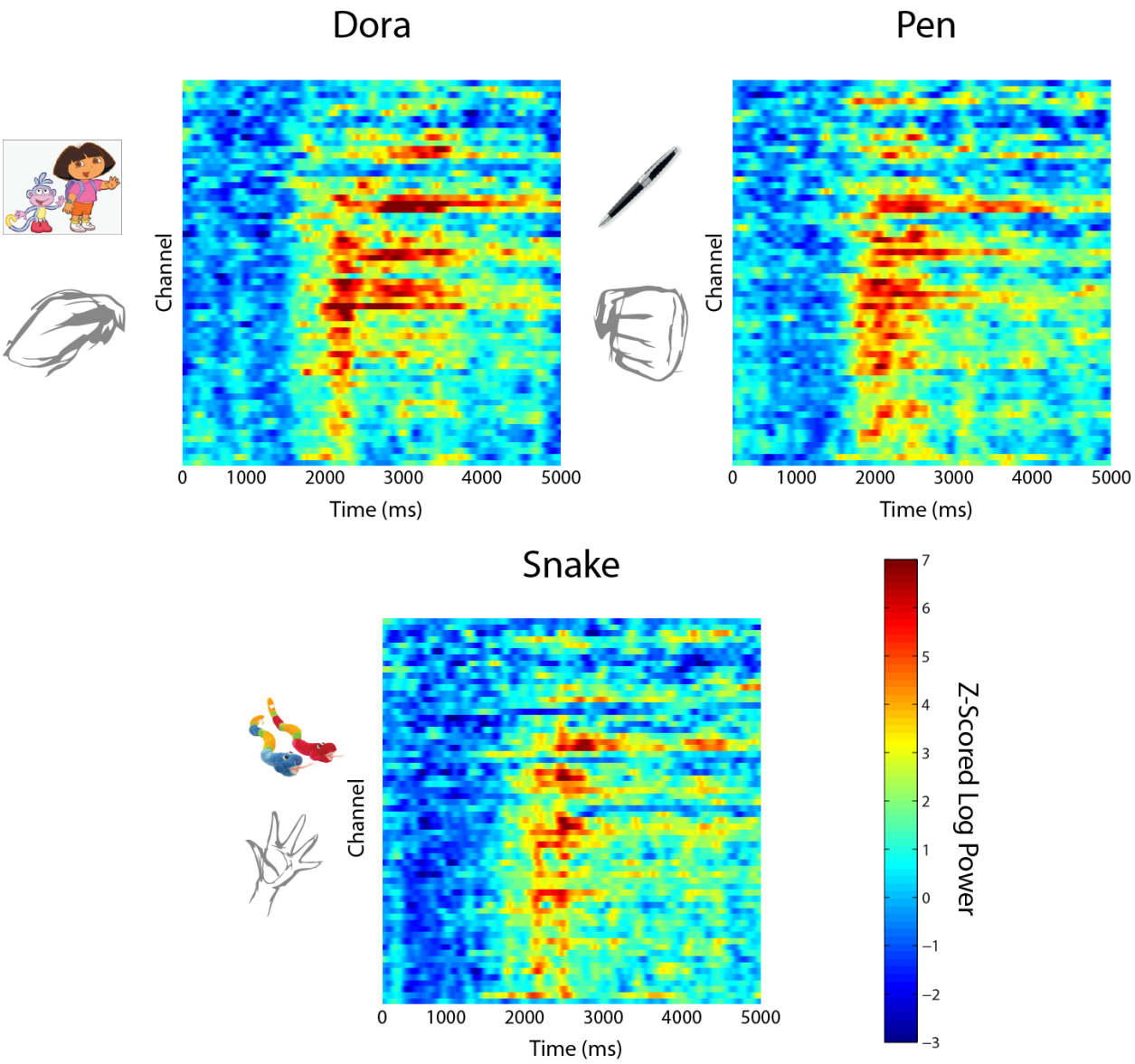

Figure 12 – Averaged time course z-score power for all 64 grid electrodes for each grip type, time-locked on visual cue. Electrode 1 is at the top of the y axis with electrode 64 at the bottom. This arrangement is a form of an "unraveled" 8x8 grid, which can be seen in the apparent periodicity traversing the channels. The visual was presented to the researcher at time 0, demonstrating that there was on average about 2000ms of delay before the subject activated motor cortex (due to object selection, presentation and reaction time). Note that the Z-Score scale shown is broader than Figure 11.

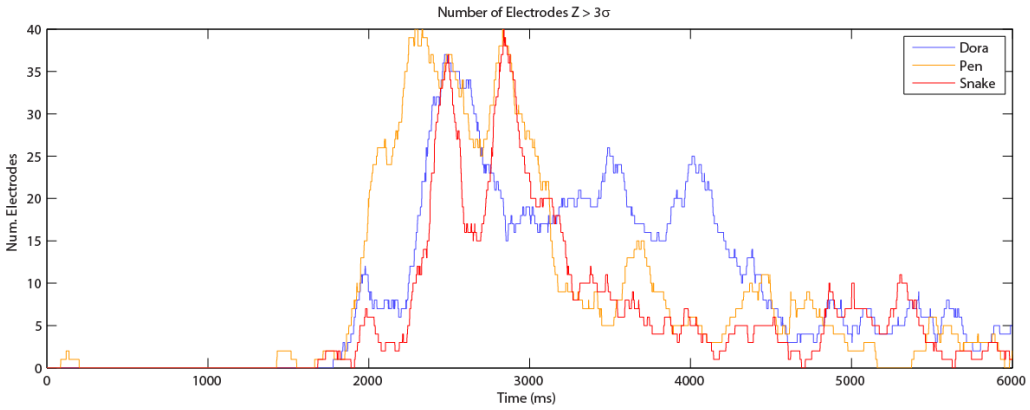

Figure 13 – Number of electrodes over time that showed z-scores greater than 3 standard deviations away from rest In spite of time-locking on cue (t=0), clear patterns can be seen during initiation, maximal peaks, and subsequent maintenance of grip position.

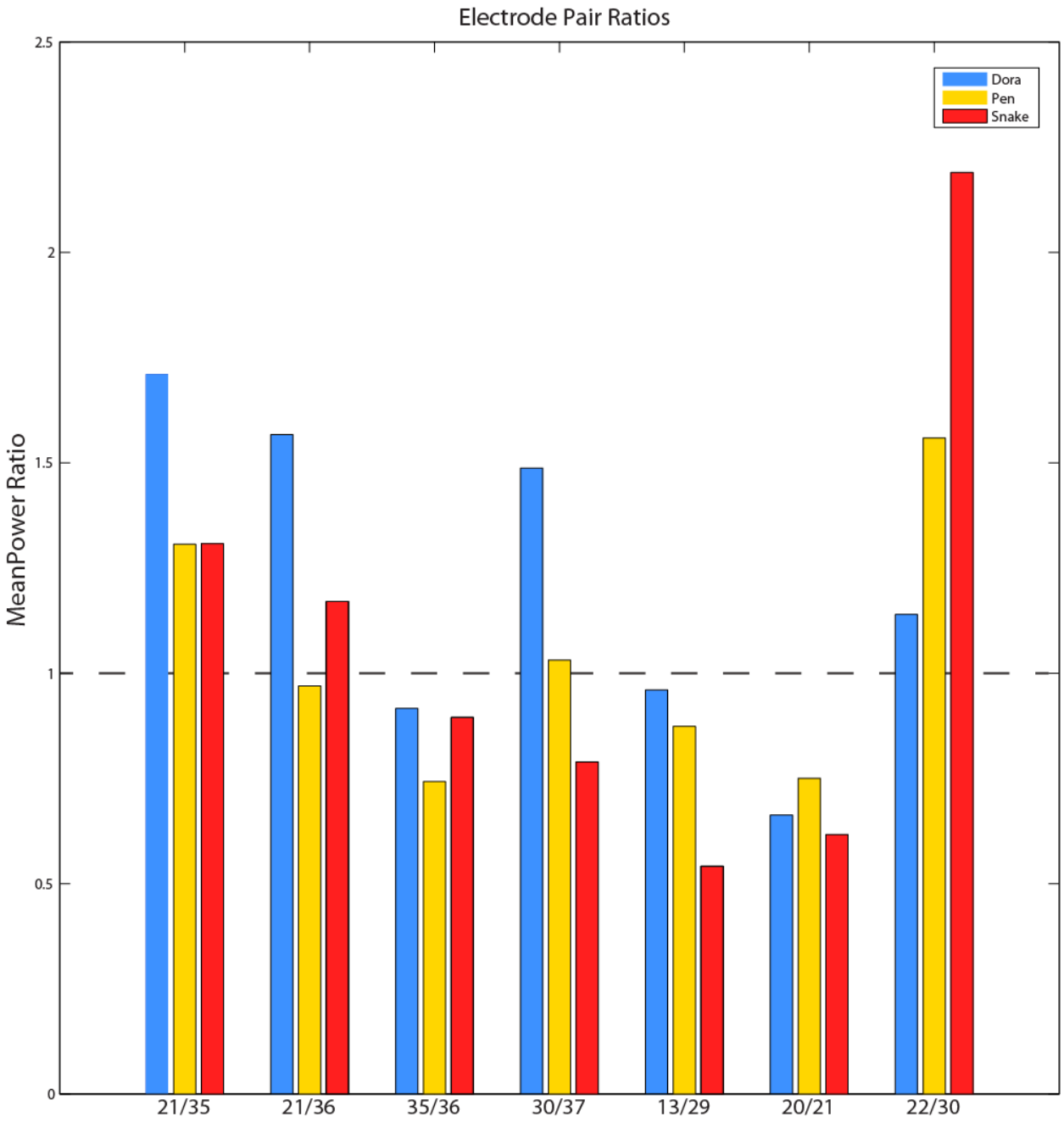

Figure 14 – Ratio of power between pairs of electrodes for each grip. Certain electrodes can show preferential relative activity for a certain grip relative to others (i.e. 21/35 for Dora), or preferential relative suppression (13/29 for Snake).

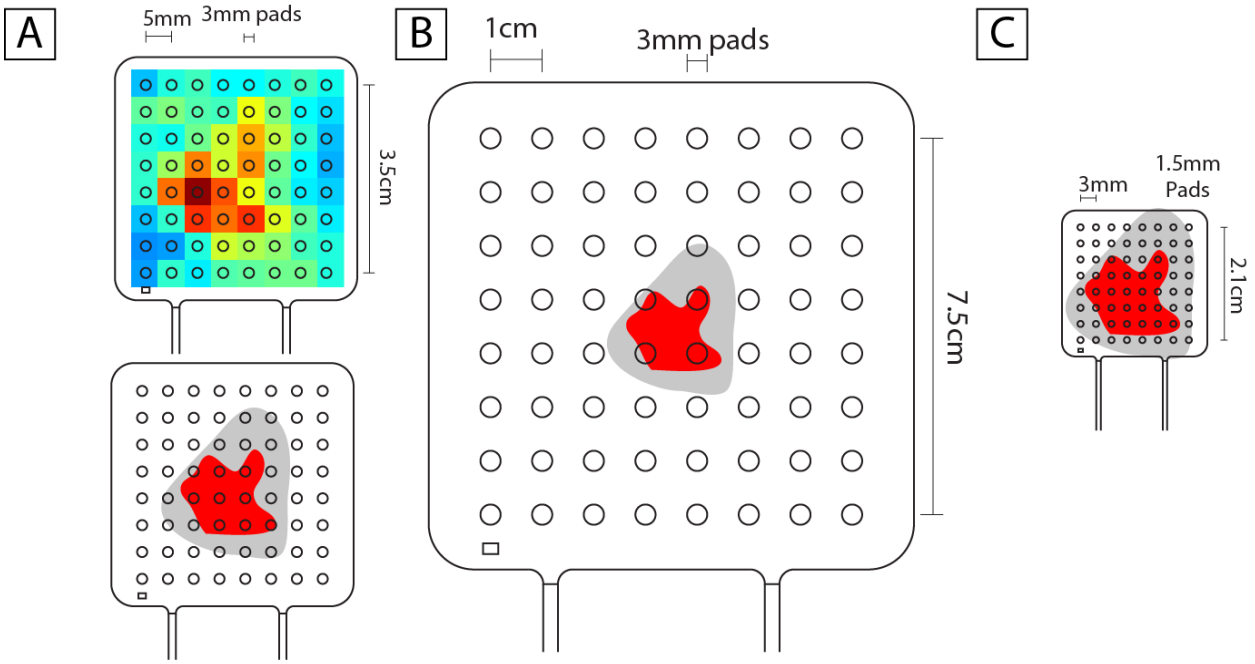

Figure 15 – Estimated activity ranges. Nine electrodes showed very high levels of activity (A, lower, red) during the Dora prismatic grip. If the same cortical shape were to be recorded on a standard clinical grid (B), this would correspond to approximately 4 electrodes, or 1cm^2, consistent with Miller *et al.* and Scherer *et al.*'s findings. C) Same coverage based on a 3mm–spaced grid, corresponding to a coverage of about 21 electrodes in the primary activation areas (red) and nearly all in the secondary activation areas (gray).

Classification Type	Channels	Objects	Accuracy
KNN	All	Dora, Pen, Snake	74.4%
KNN	13, 20, 21, 22, 29, 30, 35, 36, 37	Dora, Pen, Snake	60%
KNN	All	Pen, Snake	75%
KNN	All	Dora, Snake	95%
KNN	All	Dora, Pen	75%
SVM	All	Pen, Snake	70%
SVM	All	Dora, Snake	80%
SVM	All	Dora, Pen	65%

Table 1 – 10-fold cross-validation classification results for K-Nearest Neighbor and Support Vector Machine (SVM)

4 Chapter 4 – Spatial Acuity of High-Resolution ECoG

4.1 Motivation

In order to decode information the complexities of human motion, it is necessary to identify and separate the relevant signal from the background noise level of the brain. The ideal signal-to-noise ratio recordings come from single-unit arrays. These arrays have inter-electrode spacing of upwards of 400um allowing the electrodes to record individual action potential spikes from single neurons[51]. However, these systems are significantly limited in the area of cortex they can cover. Even with an electrode array with 256 of these electrodes spaced at 16x16, this would cover less than half of a square centimeter. It has been demonstrated the areas associated with motor cortex can be as large as 22cm^2[52], and while it is accepted that areas of motor cortex can be specialized to control individual muscle regions, limbs, etc, the area that is likely associated with hand motor cortex is likely much larger than what single unit grids can cover. Missing areas of the cortex activated by volitional movement during experiments can lead to lowered decoding ability.

In contrast to single units ECoG arrays can cover larger areas of cortex by design, as they have been developed mainly for identification and localization of seizure foci. However, their inter-electrode spacing only allows for few electrodes to cover the regions of interest. We propose that in order to attack this problem, a new form of ECoG grid needs to be developed: a high resolution (<5mm inter-electrode spacing), wide coverage (>2cm^2) array of surface electrodes. Though in actually not containing any measurements less than 1mm, we call this type of array "micro-ECoG" in reference to its significantly smaller size relative to standard ECoG grid.

A good initial test to see whether micro-ECoG arrays can provide the spatial fidelity and signal-to-noise ratio required to study the dynamics of hand movement would be to apply such arrays to an area of the brain that is known to be spatially laid out over the cortex. In this chapter we investigate the ability of miniature ECoG arrays to determine if they have the ability to identify the tonotopic organization of speech areas of the brain in addition to its ability to decode individual phonemes.

4.2 Background

A significant amount of human communication is done through speech. Language assimilation begins at an early stage in human development and is reinforced throughout the lifetime. However, the exact representation of this speech is yet unknown[53,54]. One of the initial forays into the area of speech representation in human cortex was the use of tonotopic maps[55–57]. Further investigation by Diesch & Luce illustrated that tonotopic organization is insufficient to explain specific phoneme representation.

They showed that the N100m component responded differently when exposed to two-formant vowels and their decomposed formants separately and could not find sufficient evidence to suggest that the vowel source locations were linear combinations[58].

Diesch and Luce then investigated whether vowel formants F_1 and F_2 can interact at one or more early stages of the auditory pathway[59]. Neurons in the auditory pathway demonstrated the ability to respond to narrow info[58]rmation bands, effectively band-passing the auditory information to lower auditory areas. Investigating the possibility of early formant interactions in gerbils, Ohl *et. Al* found interactions as far away as 2000Hz and as close as 500Hz[60]. Wang *et. Al* approached the possibility of formant interactions from a spatial perspective in marmosets. They observed distributed neuronal discharge patterns in the marmosets' primary auditory cortexes from behaviorally relevant, species-specific vocalizations[61]. Due to the limitations in techniques available on humans at the time, it was not possible to get the same spatial resolution in humans. Diesch proposed to use Euclidean distances between from evoked magnetic field measurements and found that the distance between the vowels 'I' and 'u' was further than the distance between vowels 'a' and 'e' in more than 60% of trials[62]. In 2003, Eulitz et al investigated magnetoencaphalography (MEG) evoked N100m responses due to auditory queues. Like the results observed by Diech, they determined that the acoustic vowel sounds generated by 'a' and 'i' were more spatially separated in comparison with the similar sounding vowels 'e' and 'i'.

In this paper we present a look at direct cortical surface potentials acquired via an electrocorticography (ECoG) microarray. This microarray allowed us to look at frontal processing regions with a much greater spatial resolution than currently used ECoG grids (10mm spatial resolution). Surface potential changes were recorded during overt pronunciation of language-base phonemes at high spatial resolution to determine if core language phoneme pronunciation can be separated and classified.

4.3 Methods

4.3.1 Subject

Because this study was an exploratory study using a new device and a new IRB protocol, there was only a single subject in this study. The subject that participated in the experiment was a 46 year old left-handed, female, epileptic patient who was diagnosed with intractable epilepsy. She was implanted with a 64 contact (8x8) subdural electrocorticography array and an 8 contact (8x1) single strip array for the clinical purpose of seizure foci identification. The larger array was placed superiorly over the central sulcus, covering primary sensorimotor cortex, while the strip was placed anteriorly over prefrontal

cortex. This left an area of cortex uncovered by the clinically relevant grids that included Broca's area, an area commonly associated with speech generation[63].

4.3.2 Microgrid

During the clinical array implantations, an additional experimental ECoG array manufacturedby Ad-Tech (Racine, WA) was placed over Broca's area over left inferior frontal cortex (Figure 16). This experimental grid contained 1.5mm diameter platinum electrodes spaced at 3mm center-to-center. Placement of this grid did not interfere with clinical mapping, as the seizure focus was determined to be in frontal cortex, significantly dorsal and anterior to the location of the miniaturized experimental ECoG array. The density of electrodes in this array is significantly higher than previously used ECoG grids that have used inter-electrode spacing of 10mm[25,64–66].

4.3.3 Recording

Leads from the experimental array were connected to four 16-channel g.USBAmp biosignal amplifiers (manufactured by g.tec, Austria). Each amplifier bank was synchronized to sample at 1000Hz and referenced to a clinical sub-dural reference that was also used as ground. After being converted to a digital signal in the ADC, each sample was recorded and saved by the software suite BCI2000[24,25,48].

4.3.4 Task

The subject was presented with a visual cue displayed on a monitor at the bedside. The visual cue was there was the visual depiction of one of four phonemes: /Ba/, /Wa/, /Ra/ or /La/. During the stimuli presentation, the patient was instructed to repeat the phoneme 3 times within the 2 second cue period. Each experimental run consisted of 2 paired phonemes (/Ba/-/Wa/, or /Ra/-/La/). Each cue was repeated 30 times for each phoneme, presented in random order. After the cue was presented for 2 seconds, there was a subsequent 2 second pause.

4.3.5 Signal Processing

The electrode recording was transformed from the original 64 input array into 112 pairs of nearest-neighbor pairwise difference changels, resulting in 112 "virtual" electrodes. This re-referencing was performed so that any fluctuations in potential found were as local as possible, minimizing both common-mode input and noise. Signal processing was performed offline after data collection in the Matlab analysis environment. Data recordigns were notch filtered at 60, 120, and 180Hz to eliminate the presence of line noise using a 3rd order Butterworth filter. We computed the Fast Fourrier Transform (FFT) for each 2 second cue interval and each 2 second rest interval. The data from these

epochs were transformed using overlapping 256ms windows (equivalent to 256 samples) with 100ms step sizes between them. In addition, a Hann window was imposed on each data window to attensute edge effects. Each spectrum from each phoneme cue and rest period was averaged by the mean spectrum throughout the trial for each virtual electrode. More information on the technique can be found in previously published papers[24,2526].

4.3.6 Feature Selection

The mean power was calculated in each electrode in 6 discrete frequency ranges: low alpha (7-12 Hz), high alpha (10-13Hz), beta (14-25Hz), low gamma (26-35Hz), gamma(36-70Hz), and high gamma (70-150Hz). The high gamma values were used to select the ten best channels, by r2 value, for discriminating /Ba/ vs /Wa/ and /Ra/ vs /La/, independently. Interestingly, these channels were different for each pair, suggesting that the miniature array is capturing the level of "phonemotopy"[62], a finding which was strongly supported by classification result.

4.3.7 Classification

We performed binary classification between paired phonemes, using the 6 frequency ranges, in 10 different channels at a time. The ten channels used can be seen in Figure 17c, in green for /Ba/ vs /Wa/ and red for /Ra/ vs /La/. Classification was performed by using a linear support vector machine with 4-fold nested cross-validation[67].

4.4 Results and Discussion

Using the ten red electrodes shown in Figure 17c, /Ra/ and /La/ could be discriminated with 75% accuracy, but /Ba/ and /Wa/ could only be discriminated with 48% accuracy, or slightly worse than chance. Conversely using the ten green electrodes /Ba/ and /Wa/ could be discriminated with 70%, yet Ra and La were correctly identified 47% of the time. This demonstrates that specific phonemes can be classified and discriminated using a high resolution array and that discrete sub regions – as small as 3mm away from each other – have preferential phonemotopic representation in Broca's area. It should be noted that the orientation of the grid in Figure 17 is flipped about the horizontal axis when compared to the x-ray image in Figure 16.

Figure 17b shows differentiation between phonemes /Ra/ and /La/ clustered towards the center of the grid while electrodes showing statistical differences between /Ba/ and /Wa/ are spatially distant towards the bottom of the grid in Figure 17b. This observation has two implications. It is possible that phonemes are represented in distinct spatial locations on the cortex. Discrete phonemes have, until

now, been too spatially close to differentiate using common 10mm-spaced grid resolutions, and far too low to below the resolution threshold of electroencephalography (EEG). Using high spatial resolution ECoG grids, we have shown that there is separable information within the cortical potential at electrode spacing resolutions of 3mm.

In addition, the close proximity of some of the pairs of green and electrodes suggests that there is mutually independent information being collected and recorded at neighboring electrodes. Having electrodes as close as 3mm yet containing independent signals would allow many more electrodes to sample the same amount of cortical space. This increases the dimensionality of the recorded neural signal, which may provide for greatly increased decoding and classification ability when applied to brain-computer interface systems. It should be noted that because this was a new type of experimental array, the entire array was designed and arranged by hand, possibly limiting the accuracy of electrode position. Future arrays would likely be arranged by industrialized processes and thus provide an even more uniform center-to-center distance.

Our results indicate that the best chance for decoding unknown, highly complex interactions of networks of neurons – such as those in primary motor cortex that drive volitional hand movement – would be to use this type of high resolution ECoG array.

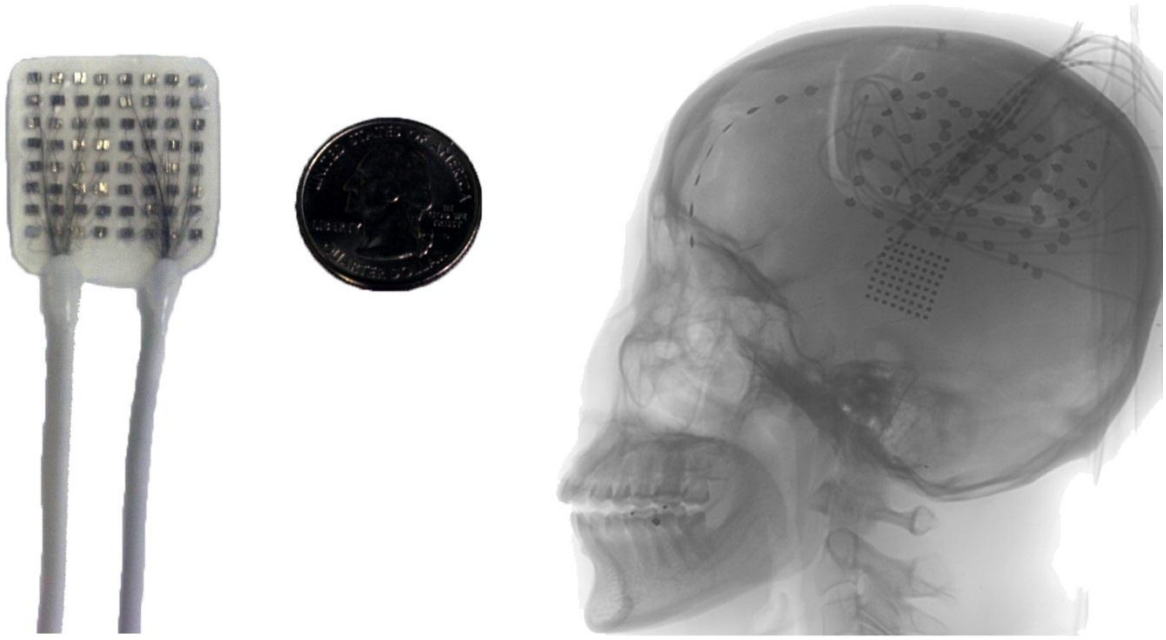

Figure 16 - Left – The miniature ECoG array can be seen on the left, with a quarter to demonstrate the scale. The electrodes were spaced 3mm apart from center to center. Right – The subject's x-ray demonstrates the clinical array (larger electrodes, spaced 10mm) and, over Broca's area, the microgrid with a spacing of 3mm. The higher spatial resolution of the grid allows each electrode to average over a smaller number of neurons, allowing more distinct potential recordings from smaller populations of neurons.

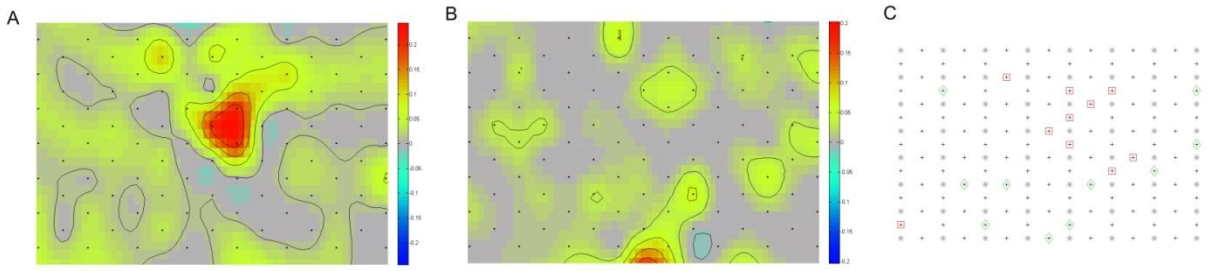

Figure 17 – A) Topographic signed r-squared cross-correlation maps showing significant differences for phonemes /Ra/ and /La/ within the center of the grid. Spatial resolutions as small as a single virtual electrode (created by pairwise re-referencing) show significant correlations. B) Topographic signed r-squared cross-correlation map for /Ba/ vs. /Wa/, showing significant differences towards the bottom of the grid, spatially separate from the significant electrodes in /Ra/ vs. /Wa/. C) Each plus represents the virtual electrode generated by pairwise re-referencing the electrodes(shown as circles). The 10 virtual electrodes that were used for classification for /Ra/ vs. /Wa/ are marked as red squares, with the virtual electrodes used for classifying /Ba/ vs. /Wa/ outlined by green diamonds.

5 Chapter 5 – Synergistic Components of Grip

5.1 Motivation

It is a simple matter for humans to reach out, grasp, and pick up an object. While little conscious thought may be given to the task, the control dynamics and kinematics behind the motion planning, musculoskeletal activation and force production are far from simple. The mechanics of grasping in humans varies depending on the object being manipulated. During reach-to-grasp movements, there is first a continuous opening of the fingers and thumb sufficient to encompass the object, followed by a gradual closing of the grip around the object until contact is made. Studies have observed that this pattern is robust when grabbing objects, with maximum aperture size occurring 60-70% of the way through the complete motion[68,69]. However, other tasks such as typing on a keyboard, writing with a pen or holding a ball in the palm of your hand can not be described using simple aperture metrics.

Any model applied universally to human grasping motions must take into account the observation that objects can be grasped and held in several different ways, with the final grip position directed by interactions between both motor and visual pathways. Modeling the multiple degrees of freedom in the human hand requires exploring how individual finger joints move in concert with one another in a coordinated fashion. Because little conscious attention is paid to the movement of individual joint angles in the hand during dexterous activity, researchers have often presumed that the human brain directs coordinated digit movement through combinations of motor primitives encoded at the cortical level. Though studies of hand posture performed with electromyography (EMG) and motion capture provide evidence to suggest that these motor primitives exist, no experiments have been performed in humans that record synchronized cortical activity and generation of motor primitives due to ethical and safety concerns.

Many studies have provided evidence to support the hypothesis that there is a basic set of underlying hand motion synergies that are task independent. Thakur explored this in unconstrained set of hand postures via blinded haptic exploration[70]; Santello identified synergistic hand poses during tool use[71]; Kawato and Wolpert reviewed literature exploring the creation and integration of sensorimotor movement models within the central nervous system[72,73]. It is likely that the cortex does not direct individual joint angles directly; rather it operates in a lower dimensional space whose output is translated into higher order muscle forces later on in lower parts of the central and/or peripheral nervous system. Thus, performing dimensionality reduction on the high DOF metrics of hand movement may elicit the underlying descending cortical state space.

5.2 Experimental design

Though the overarching goal is to be able to estimate and reconstruct the position of the hand from cortical signals, it is not necessary to record neural activity from the brain to determine if joint angles can provide synergies. Employing healthy subjects in this study addresses two concerns: that the subjects do not have an abnormal pathology that may affect their synergy generation (as opposed to the epileptic subjects studied in cortical electrocorticography studies), and that our target population for this study is readily available and can be performed in a controlled setting.

5.2.1 Dataglove

Figure 18 shows the dataglove; a right-handed 22 degree-of-freedom (DoF) Cyberglove II (CyberGlove Systems, San Jose, CA). Each DoF records movement of the hand via an array of resistive strips that vary electrical resistance when flexed (see Figure 19). Two strips cover the joint of the thumb, and three joints cover the proximal, medial and distal joints of each remaining finger. In addition, four measurements are taken of ab/adduction between each pair of fingers, one for thumb extension/flexion, one for palm roll and two for ab/adduction and flexion and extension of the wrist, giving a total of 22 values per sample. It should be noted that the Cyberglove does not record joint angles directly, rather an 8 bit value corresponding to the resistivity of the strips. Figure 20 demonstrates that this mapping is approximately linear, and thus a direct mapping from recorded values to joint angle for the i^{th} joint can be derived as follows:

$$\theta_i = \vartheta_i \frac{x_i - \ddot{x}_{i\_min}}{\ddot{x}_{i\_max} - \ddot{x}_{i\_min}} \qquad 5.1$$

where x_i is the recorded value, $\ddot{x}_{i\_max}$ and $\ddot{x}_{i\_min}$ are the maximum and minimum recorded values during the calibration process (described below) and ϑ_i is the range in radians the joint went through during calibration.

To account for the variability is subject hand side and varying fit of the glove across subjects, we developed a calibration process to ensure that the values recorded could map directly onto joint angles. We identified 12 different poses that identified the limits $\ddot{x}_{i\_max}$ and $\ddot{x}_{i\_min}$ for all of the possible recorded values. For each pair of poses, we calculated the approximate range of motion ϑ_i in radians unique for each joint, allowing the full joint angle vector $\hat{\theta}$ to be determined.

Because the dataglove's data connection runs over a 115200 baud serial connection, the maximum recording frequency of the dataglove is approximately 135Hz. This limitation does not prove problematic in this analysis, but because the ECoG recordings in later chapters are captured at a sampling rate of an order of magnitude higher it is necessary to upsample and interpolate the recorded

glove data to match the sampling frequency of the bioamplifiers. This is done by applying piecewise cubic Hermite interpolation (PCHIP) between the recorded dataglove samples (See Figure 21). Applying PCHIP interpolation is possible due to the inherent limitations of biological systems. The dataglove is sampled at 135Hz, or approximately 7.4ms between samples. Volitional movement of musculoskeletal systems can be modeled as an approximate bell curve model and as such requires a period of acceleration and deceleration between movements [74]. The 7.4ms in between samples is simply too short for the subject to make large movements that cannot be approximated by a cubic interpolation.

5.2.2 Experimental Design

Subjects were placed in a closed room in the building which varied by subject, though all rooms were graduate student offices that contained objects typical of an office setting such as computers, coffee mugs, books, pens, etc. The subject was instructed to don the dataglove and move about the room manipulating and grasping objects in a manner they thought was appropriate for everyday use. As the subject moved about the room manipulating and lifting objects, the dataglove recorded the simultaneous positions of all 22 joint angles of the glove. No additional instruction was given so that the subjects would go about grabbing objects in a natural way, moving through a natural joint state space. Data was collected for a period of 60 seconds.

5.2.3 Synergy Generation

Principal component analysis was performed in a similar way to previous studies[75]. Data frames from the glove were combined into one 22-by-N vector. If $P_i(t) = \theta_i$ is joint angle i of the 22 possible joint angles, a vector through the 22-dimensional space is of the form $\vec{P}(t) = [P_1(t), P_2(t), P_3(t) \dots P_{22}(t)]$, with each individual point represented as $P_i(t)$. Vectors at each time point collected during the object grip data collection are used to construct the covariance matrix

$$cov = \frac{1}{\sum T(n) - 1} \sum_{n} \sum_{t=1}^{T(n)} \left(\vec{P}_n(t) - \bar{P}\right)\left(\vec{P}_n(t) - \bar{P}\right)^T \qquad \textbf{5.2}$$

$\vec{P}_n$ is the vector associated with the n th object for all time points $t = [1, T_n]$. Eigenvalues and eigenvectors associated with the 69-dimensional covariance matrix in equation **Error! Reference source not found.** will be calculated and sorted in descending order of eigenvalue e_i. Hand postures associated with each eigenvalue can be calculated as a scalar deviation from the average hand posture $\bar{P}$, resulting in hand posture $H_i = \bar{P} + \alpha E_i$ for eigenvector E_i and scalar α. The hand postures with the highest

eigenvalues contain the most variance from the mean hand pose, according to the scalar α. The linear space defined by these hand poses can be found for any combination of m eigenvectors by

$$H_{new} = \bar{P} + \alpha_1 E_1 + \alpha_2 E_2 + \cdots + \alpha_m E_m \quad \textbf{5.3}$$

To calculate a time-course contribution of recorded hand poses from each synergy, eigenvectors that account for 95% of the variance in hand posture according to normalized eigenvalues are projected onto the recorded joint angles:

$$S_n(t) = \vec{h}_n \cdot \vec{P}(t) \quad \textbf{5.4}$$

Where h_k is the eigenvector associated with the principal component n and $\vec{P}$ is the 22 by T vector $\vec{P}(t) = [P_1(t), P_2(t), P_3(t) \ldots P_{22}(t)]$. This gives a scalar representation of the contribution of synergy n at a given time point, known as the hand synergy timeseries S_n.

At any given time t, the total variance of the system is:

$$\sigma^2_{total}(t) = (P(t) - \bar{P})^T (P(t) - \bar{P}) \quad \textbf{5.5}$$

Where $\bar{P}$ is the mean hand position in joint angle space. The percent of variance captured for the first n vectors can be found by:

$$\sigma^2_n(t) = \sum_{i=1}^{n} [(P(t) - \bar{P})^T E_i]^2 \quad \textbf{5.6}$$

5.3 Results

5.3.1 Joint Correlations

Correlation measurements were calculated for the entire duration of the data collection. The distal joints of all fingers were highly correlated across all fingers with lower correlation values in the thumb. (see Figure 22). Groups of high correlations can be seen in the correlation matrix, indicating that while the distal joints themselves may be correlated (#s 5,6,7,8,9,10,12,13,14,16,17 and 18), their correlations to ab-/adduction is not as high. In contrast, correlations across ab-/adduction joints (4,11,15, 19) significantly higher than with the distal joints. A large range in correlations suggests that the synergies generated using linear principal component decomposition may well describe the system.

5.3.2 Synergies

We identified a total of 21 different possible synergies that described the total variability of joint angle observed during room exploration. In both subjects, the first 7 principal components accounted for >90% of variance and a total of 10 principal components accounted for >95% of the total variance observed (Figure 23). Neither subject demonstrated a synergy that described more than 50% of the variance.

Projecting along the synergies of subject 1 (Figure 24) shows that the first synergy identified primarily is consistent with a "power grip"[76,77], identified by the distal joints of the fingers curling in and extending in unison. In contrast, the thumb does moves much less in the first synergy than subsequent synergies, as seen in Figure 24. By adding the contribution of all 21 synergies together, we confirm that the full principal component decomposition does indeed describe the full variance observed (Figure 25).

5.3.3 Contribution over time

The contribution over time was calculated as per Thakur *et al* (Figure 26)[75]. While most of the variance is accounted for by the first synergy, subsequent synergies can be seen contributing over short durations. On average, the first 10 synergies contribute on average >95% of the variance. However, on occasion there are large drops in the contribution of the first 10 components, suggesting that there may be something about this pose.

5.3.4 Reconstruction Error

Hand pose was reconstructed over time by summing the contributions of the first n synergies. Figure 27 shows the actual hand pose at one time point in comparison to the reconstructed pose based on synergies. The mean-squared error (MSE) by reconstructing the pose from only the first principal component is significantly higher than when adding subsequent synergies (847 vs 276, 235, 226 and 221). It should be noted that while in theory reconstructing the hand's position from all 21 possible synergies should result in the original pose, this is not the case. The full-synergy MSE is 1.56, which appears to be due to floating-point inaccuracies inherent in limited-precision computers and introduced during the decomposition and reconstruction process.

5.4 Discussion

5.4.1 Cooperative movement in joints

The fact that the wrist joints were negatively correlated with distal joints of the fingers suggests that as subjects grasp and manipulate objects, there is an agonist/antagonist muscle relationship between wrist flexor muscles and distal curl muscles. This correlation also suggests that as the subjects grasped objects, they most likely approached and grasped using a palmar grasp, with the wrist flexor muscles contracting and lifting the palm of the hand.

5.4.2 Synergy Contributions

None of the synergies in either patient accounted for more than 45% of the variance, a significant difference from those observed by Thakur *et. Al*[75]. In their studies, the first principal component accounted for approximately 58% +/- 8%. This suggests that synergies identified through

joint angles may contain more mutually independent information than those found using Cartesian coordinate recordings. Further evidence of this is indicated by the cumulative eigenvalue metric observed in this study. Though both studies required the first 7 principal components to account for >90% of the variance, the first synergy – the synergy that accounted for most of the variance – was lower when PCA decomposition was performed on joint angles directly. This suggests that even though joint angle space is a mathematical subset of Cartesian space, synergies identified in joint angle space may be even better candidates for motor cortical primitives than those identified using Cartesian coordinate recordings.

Another unique difference can be seen in the normalized contribution of each synergy in Figure 28. Thakur *et al.* showed that their synergy contribution curve followed a near-perfect inverse logarithmic curve. In contrast, the normalized eigenvalues identified here show two observable "transition" points along the principal components. When considering the log normalized contribution of each synergy (Figure 28), subject 1 appears to have a significant drop in contribution between eigenvectors 8 and 9, whereas the accompanying drop in subject 2 occurs between synergies 7 and 8. A second significant deviation from logarithmic contribution occurs between synergies 12/13 and 11/12 for subjects 1 and 2, respectively. Though the number of subjects in this study is too small to come to a definitive conclusion, it suggests that further study may reveal a subset of components of grip in joint angle space that may be common across subjects.

5.4.3 Synergies as a unit of motor control

The results of this paper demonstrate two key points. First, though joint-angle space is a mathematical subset of Cartesian space (i.e. a mapping from one to the other can be created if the size of each bone is known), it was not known whether biokinematically sound synergies existed in this space nor if those relationships could be identified by linear decomposition. Our results show it is possible to identify plausible synergistic movements through measuring hand pose in terms of joint angles directly. And secondly, our identifying synergistic motions during complex, free-form manipulation sets up the possible underlying components of dexterous motion at the biokinematic, musculoskeletal level. Further studies are needed to determine whether these kinematic components are generated at the level of motor cortex or solicited further down the central or peripheral nervous system. Other recent studies have begun to shed light that these movements are actually generated by primary motor cortex[78]. Even if we cannot identify the way motor cortex does encodes motion, synergy generation is inherently a form of dimensionality reduction and as such may be able to more accurately be mapped from cortical activity via regression.

Figure 18 – CybergloveII dataglove used to record joint angles

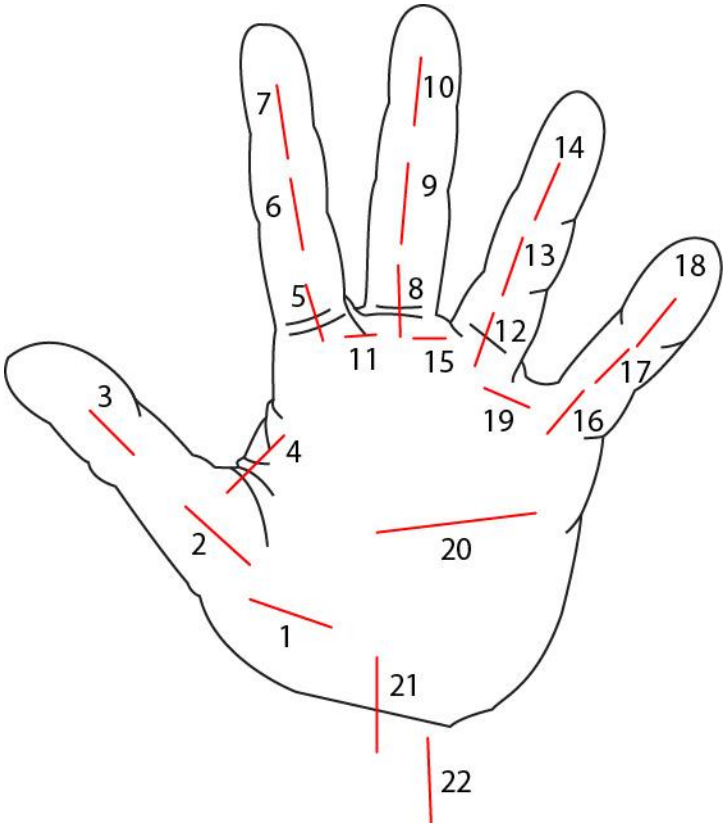

Figure 19 – Location of the 22 resistive strips. Thumb flexion is captured by 1, 2 and 3; index flexion by 5, 6, 7; middle by 8, 9, 10; ring by 12, 13, 14; and pinky by 16, 17, and 18. Ab/adduction measurements between thumb and index are captured by 4; index and middle by 11; middle and ring by 15; and ring and pinky by 19. Palm roll is measured by 20. Wrist dorsiflexion and ab/adduction are measured by 21 and 22 respectively.

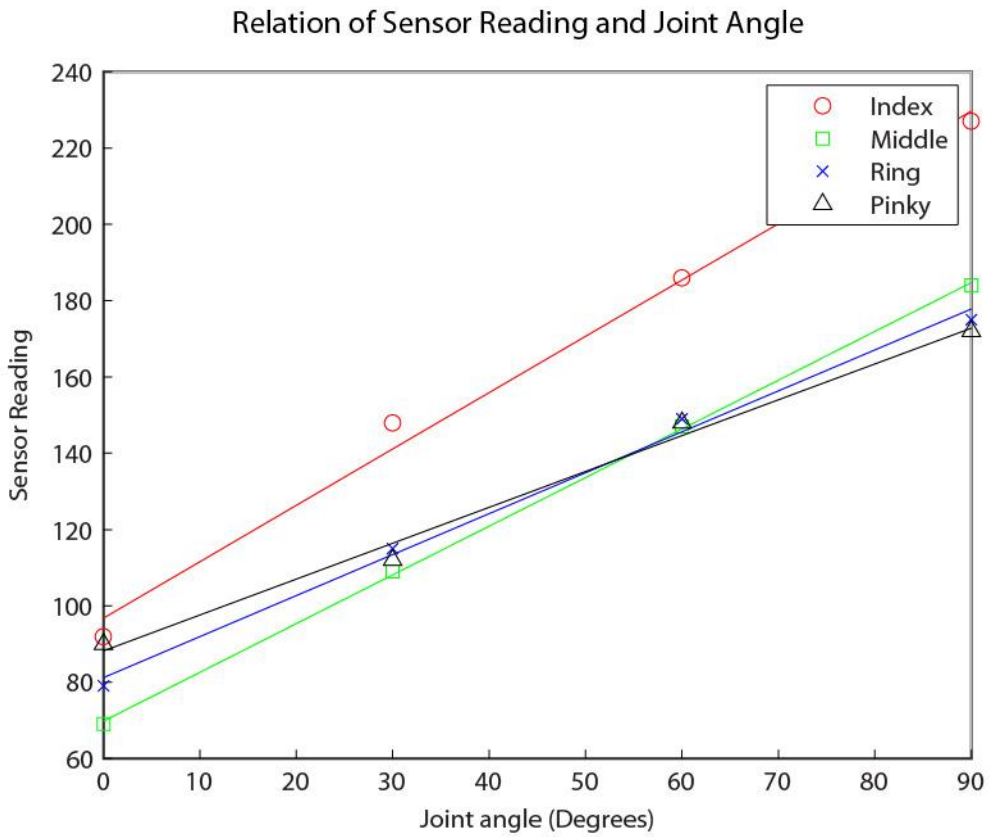

Figure 20 – Mapping between joint angle and sensor reading. Measurements were taken at joint angles of 0, 30, 60, and 90 degrees. For all fingers, the mapping is linear, indicating a linear mapping between sensor readings and joint angles can be obtained.

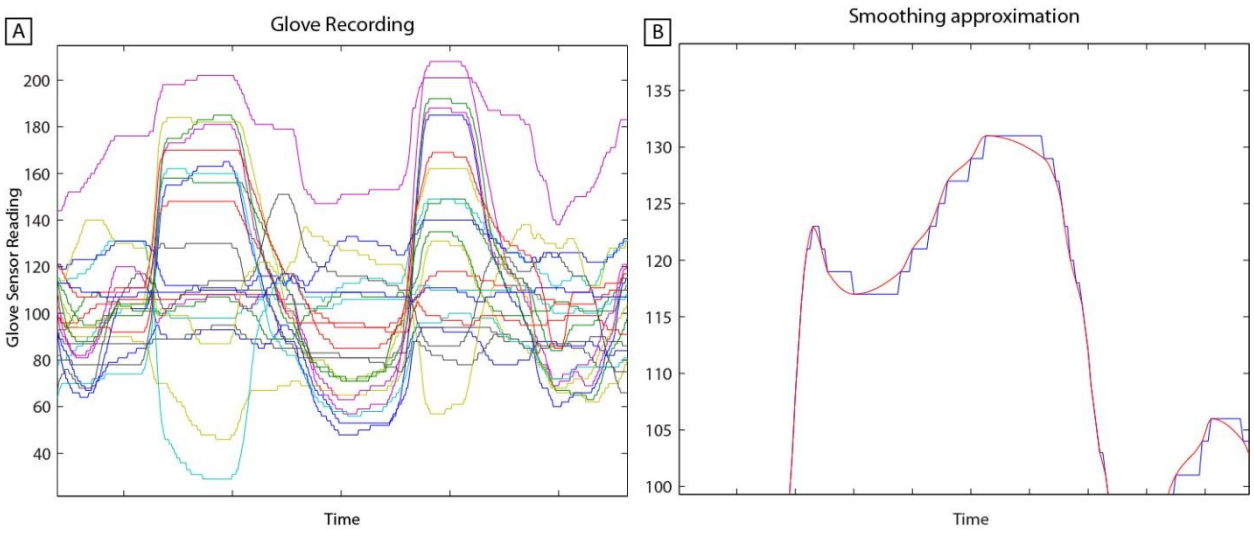

Figure 21 – Sample recordings on the left. A) Values for each sensor. Note how each sensor does not return to the same value during periods of rest. B) The blue trace shows the recorded values from the dataglove. Due to the low sampling rate of the dataglove, the data is smoothed using cubic Hermite interpolation (red trace).

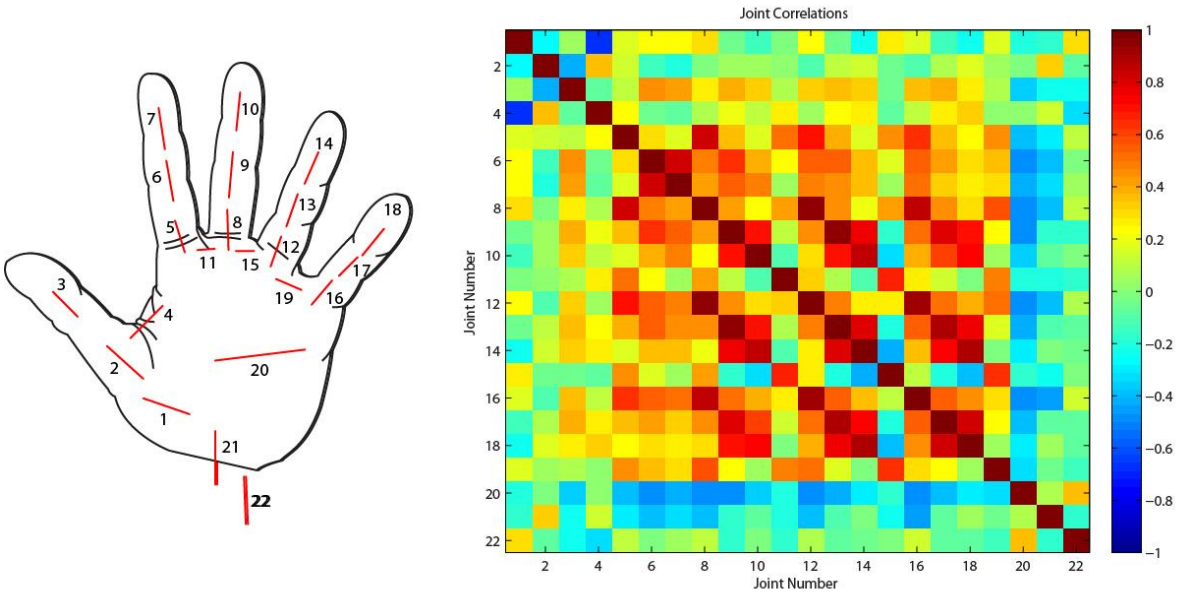

Figure 22 – Cross-joint correlations. Groupings can be observed for each finger and high correlations can be seen across all fingers except thumb. Wrist flexion shows a negative correlation with fingers, indicating that palmar grip was used most often during exploration.

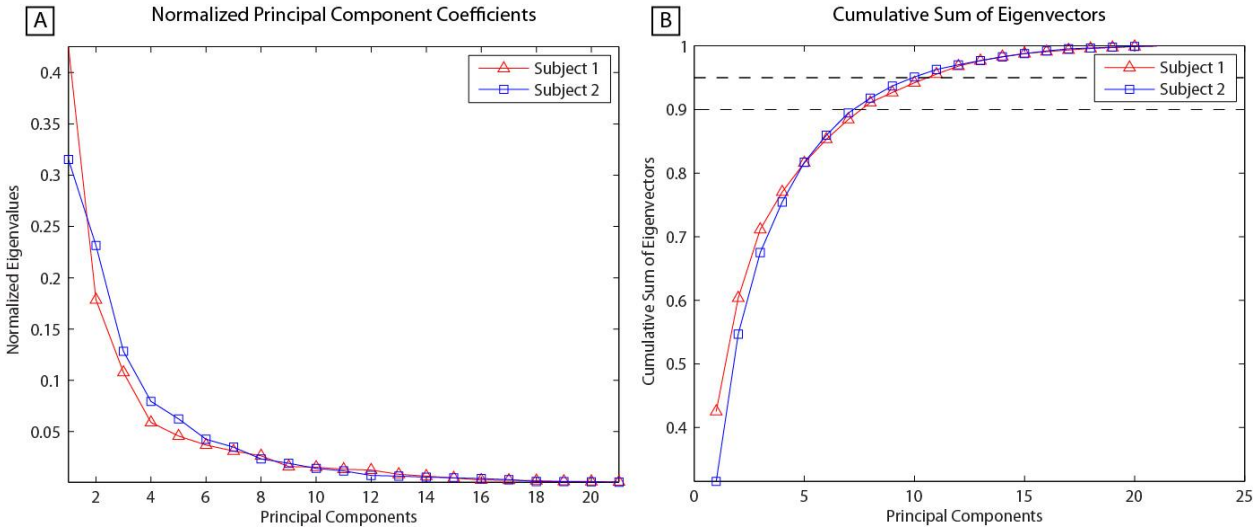

Figure 23 – Contributions of each principal synergy identified from each subject. A) Normalized eigenvectors showing the total contribution of each synergy to the variance seen. B) Cumulative sum of all normalized eigenvectors. For both subjects, 7 principal components cover just under 90% of the data (consistent with Thakur *et al.*, and 10 components cover 95% of total variance.

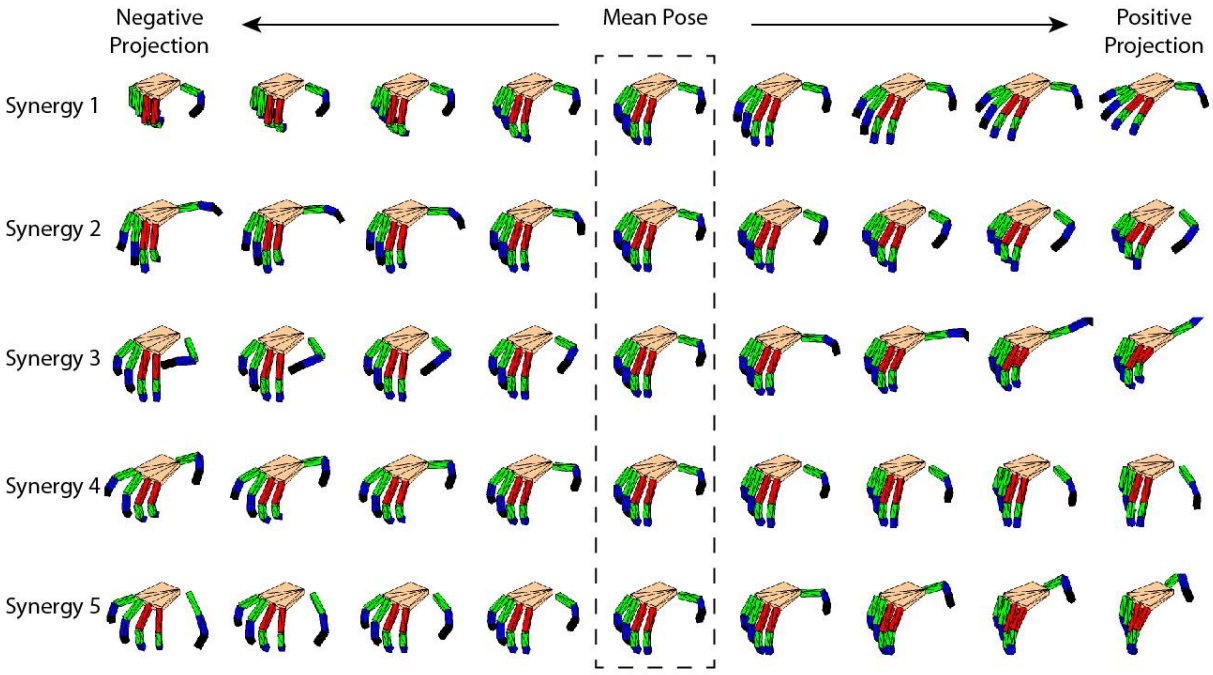

Figure 24 – Projection of the first five synergies of subject 1. The first synergy covers more than 40% of all movement observed. The majority of movement along the synergy is the fingers flexing and extending in unison. The second synergy, however, shows significantly more movement in the thumb than the first. Synergy 3 shows nearly all of the movement contributed by the thumb, which ab- and adducts greatly along the synergy. Synergies 4 and 5 involve movements of all digits.

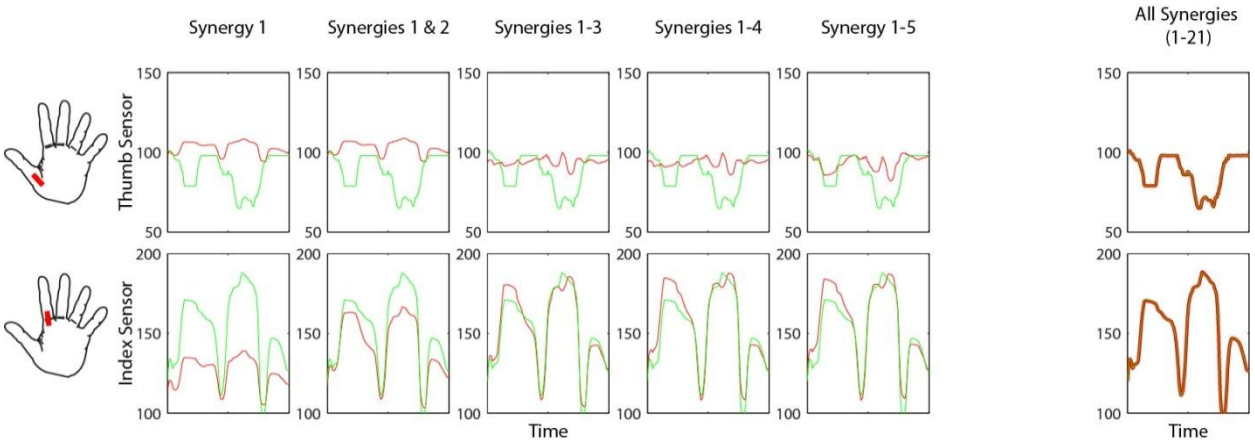

Figure 25 – Reconstruction of two joint sensors over time (thumb top row, index proximal joint bottom row). The recorded positions (green) show significant differences from the reconstructed pose (red) created by just the first principal component. However, adding subsequent synergies into the reconstruction rapidly increases the accuracy of both the thumb and index. By adding all 21 synergies together, we confirmed that the predicted traces match the recorded traces (right column) for both joints.

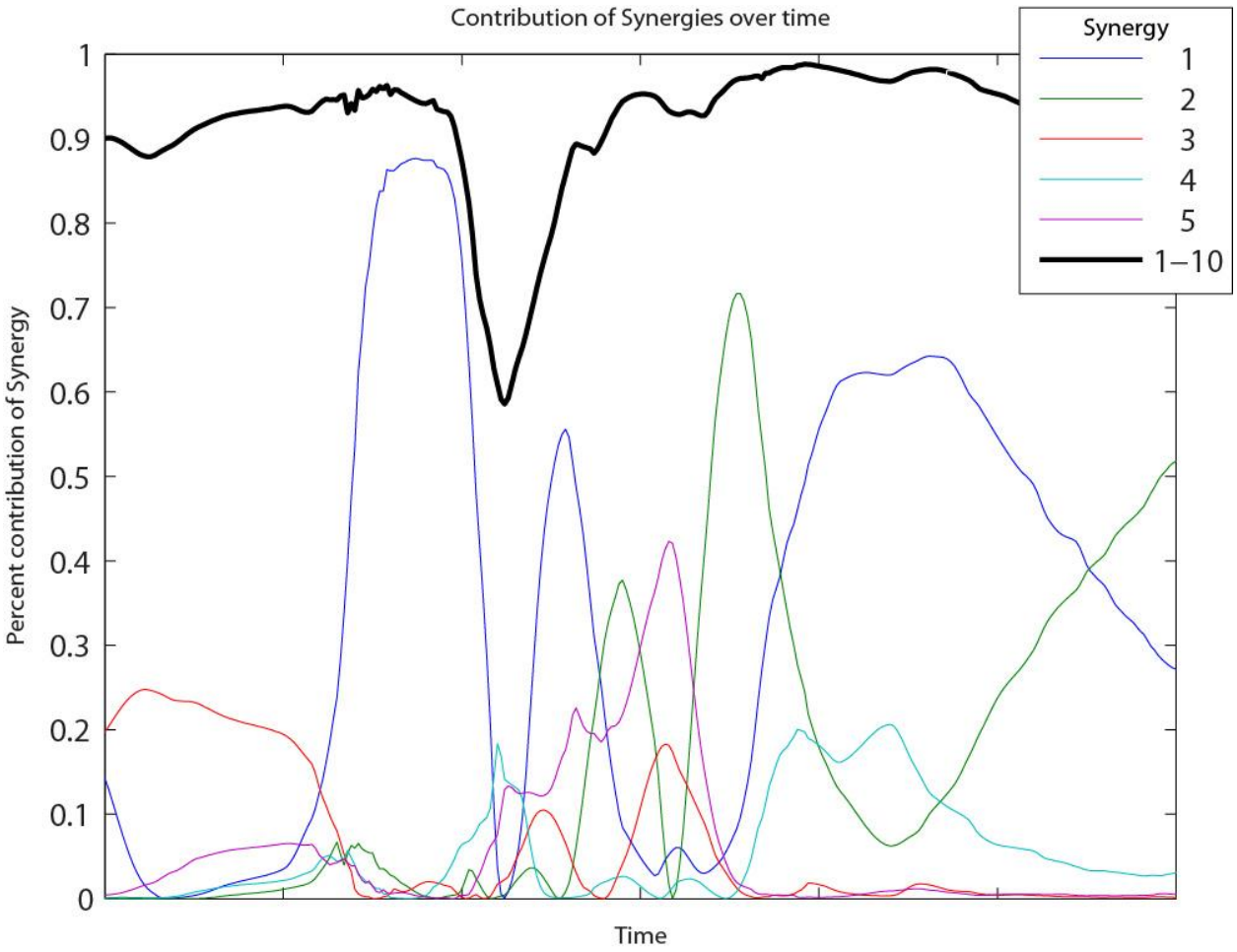

Figure 26 – Contributions over time for individual synergies. Normalized contributions to hand pose vary with time. Adding contribution of the first 10 synergies (black trace) shows that on average they capture 95% of the variance. However, at times the remaining 11 synergies can briefly contribute as much as 40% of the pose, as evidenced by the dip in the cumulative trace.

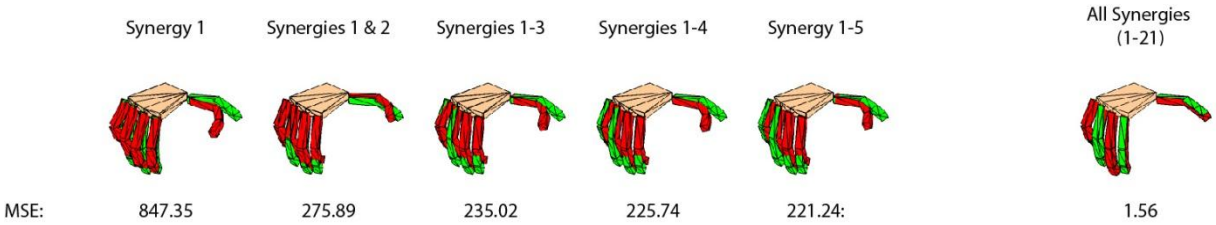

Figure 27 – Recorded hand pose (green) and reconstructed hand pose (red), and their associated mean-squared error with respect to all 22 joint angles.

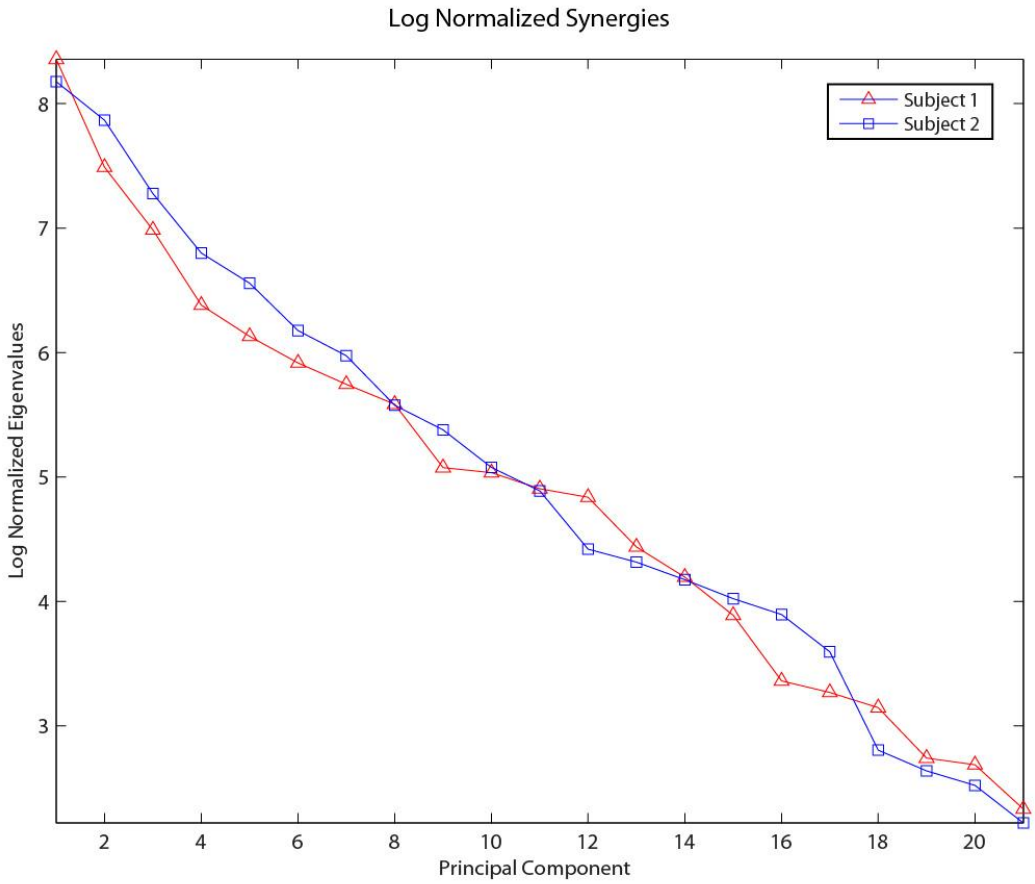

Figure 28 – Log normalized contribution of each principal component.

6 Chapter 6 – Microgrid Recordings of Primary Sensorimotor Cortex

6.1 Considerations and goals

6.1.1 Basis

The first two aims of this dissertation were designed to establish the feasibility of using micro-ECoG arrays to investigate the presence of low-dimensional cortical components of dexterous hand motion. Chapter 1 presented the foundation and previous research that laid the groundwork for this hypothesis. Chapters 2 established that though the time-course fidelity of ECoG is high and shows significant variation, robust, reliable changes in high gamma activity (75-200Hz) can be seen. These high frequency changes are indicative of a broad-band, noise-like processes that is correlated with an increase in underlying neural activity[8]. Because this signal is stable and reliable, any results that we show in the following two chapters should not be directly dismissed as transient, temporary correlations.

In the third chapter we discussed the possibility that ECoG signals may be able to provide the required spatial and signal-to-noise ratios required to decode dexterous hand movements in humans by leveraging higher resolution ECoG arrays. Though the circumstances surrounding the subject were unique relative to the standard subject pool and clinical protocol, the higher-density arrays used in that study suggest that ECoG may be able to identify these patterns. However, the resolution of the grids used in this chapter was insufficient and a new, smaller ECoG grid needed to be developed.

Targeting the established tonotopic maps of auditory cortex, in Chapter 4 we investigated the use of a grid that has 9x the spatial resolution of standard ECoG grids. Our hypothesis was that we could use a grid of this size to discriminate individual phonemes, yet had to demonstrate that despite each electrode being 67% closer than the 10mm-spaced grids, each channel was able to record mutually independent information.

6.1.2 Design of the grid

The primary consideration during the final design of the microgrid we developed for these experiments was inter-electrode spacing. However, in practice the first decision that had to be made was the choice of either platinum disk contacts or microwires. As the conductance of each electrode is directly proportional to the surface area of the contact, the microwires were likely to be problematic at 100µm in diameter. In addition, we had previously shown that disk electrodes could be reliably spaced at 3mm and still provide spatial fidelity (see Chapter 4). Though the microwires provided the option to go to a higher spatial resolution, we were limited to 64 contacts based on the amount of ADC inputs in

our biosignal amplifiers. Without the ability to add additional electrode contacts and the requirements from Chapter 3 that identified that the grid would optimally cover 4.41mm^2, we worked with Ad-Tec (Racine, WA) to develop an 8x8 grid of 1.5mm diameter platinum electrodes spaced at 3mm center-to-center. Figure 29 shows the relative size of the microgrid relative to previously used clinical grids, and Figure 30 shows the final design and relative size of the grid.

6.1.3 Intraoperative subjects

A major change in this study from the previous studies is that the subjects were not epileptic patients. Implanting a targeted microgrid over primary hand sensorimotor cortex is impractical or impossible, as it may have interfered with the placement of the standard clinical arrays dictated by the subject's medical protocol. Instead, we opted to record from primary motor cortex during the awake craniotomies performed as part of the clinical protocol for tumor resections.

Working with these subjects has three main benefits. First, the anaesthetized subject is brought out from full unconsciousness when the craniotomy window is open as part of the standard surgical procedure. This allows us to place the grid on the cortical surface at a specific location of our choosing without impeding or disrupting any clinical recording. Secondly, it provides a controlled experimental environment not usually found in bedside recordings that is free from distraction and other confounding factors. Lastly, contrary to the epileptic patients we have previously studied the pathology of these subjects is well-known, well-documented and distant from hand sensorimotor cortex.

In spite of these advantages, there are some disadvantages that accompany these subjects. Because of the minimal risk of the craniotomy remaining open for additional time, our recording sessions were limited to a maximum of 30 minutes in total including set-up and experimenting. In addition, the craniotomy window is not necessarily over primary motor cortex and requires that the grid be slid underneath the dura out of view of the surgeon. Though not dangerous to the subject, it impedes precise visual localization of the grid (see Figure 31). The former can be mitigated through careful experimental planning. We address the latter using real-time cortical mapping that allows us to quickly identify volitional changes in high gamma associated with hand movement (see Methods: Quickmap below).

6.2 Methods

6.2.1 Subjects

Two subjects underwent surgery for tumor resection on their left temporal lobe at Harborview Medical Center, Seattle, WA. After each subject was anesthetized and the head fixed into supports, a

craniotomy was performed on the left lateral inferior area of the skull. The craniotomy window was approximately 6.5cm across. Pre-operative MRI angiograms were performed that allowed reconstruction of the cortical surface for each subject. The angiogram was then aligned with intraoperative photos, allowing the identification and localization of the craniotomy window. Stimulation mapping was performed using a clinical visual auditory repetition task. After speech areas were identified, our 64 contact microgrid was implanted subdurally and experiments subsequently performed for 25-30 minutes. After experiments concluded, the grid was removed and the surgery continued as normal.

6.2.2 Data Acquisition

Data was recorded using a bank of 4 g.USBAmp biosignal amplifiers (g.Tec, Austria), each consisting of 16 DAC channels for a total of 64 unique inputs. Potentials were sampled at 1.2kHz and band-passed in hardware from 0.5-500Hz, with a hardware notch filter present at 60Hz. Syncronization and cue presentation was done using the BCI2000 software suite[48]. Hand pose was time-locked and recorded using a Cyberglove II system (Cyberglove Systems, San Jose, CA). Due to the sampling rate difference between the Cyberglove and DAC – 135Hz vs 1.2kHz – piecewise cubic Hermite interpolation was used to estimate the glove's position between samples (see Chapter 5,Figure 21);

6.2.3 Quickmap

In an ideal situation, the subject's craniotomy window would be large enough to expose primary sensorimotor cortex. This would allow stimulation mapping of the area to directly map out areas of motor cortex that elicited hand movement. However, in the event that the craniotomy window was inferior to hand motor cortex and did not expose areas associated with hand movement – as was the case in both of the subjects we studied here – an alternative to stimulation mapping was developed we call Quickmap.

Initial placement of the grid was performed by the surgeon by sliding the grid subdurally in the direction that corresponded to the most likely area associated with superior central sulcus. After initial placement, the first iteration of Quickmap was performed. This involved recording all 64 electrodes while the subject rested for 5 seconds. After the rest period, the subject was instructed to open and close their hand to activate areas of cortex associated with gross motor movement. Recording ended after 10s and the file was processed for changes in high gamma (75-200Hz) between the rest period and hand movement. The results were visually displayed to the researcher as seen in Figure 32. If the grid showed no activity, the grid was moved to the next most likely area based on pre-operative MRI images.

If an area of the grid showed activity, the grid was carefully repositioned to be centered over the active area of cortex, and Quickmapping was performed again. This sequence was repeated until the majority of the grid showed robust increases in high gamma during movement, indicating that the grid was likely over primary hand sensorimotor cortex.

6.2.4 Experiment I: Gross Motor Movement

After the subject was brought out of deep anesthesia and Quickmap confirmed that the grid was over an area that showed increases in high gamma during hand movement, we began an experiment to identify cortical activity elicited by gross motor movement. A screen was placed comfortably within visual range of the subject and the dataglove was put on the subject's right hand. The subject was instructed to flex their outstretched hand into a fist when they saw a picture of a hand appear on the screen, and relax when it disappeared. Each cue was presented for 3s followed by 3s of rest, repeated a total of 10 times.

6.2.5 Experiment II: Finger flexion

In addition to investigating activity during gross motor movement, we designed an experiment to elicit highly stereotyped but unique movements of each digit. A white silhouette of a hand was presented to the subject. After 2 seconds, one of the five digits was colored or the index and thumb was highlighted (see Figure 33). The subject was instructed to flex the corresponding finger on their right hand. After another 2 seconds, the highlight was removed and the subject rested. This sequence was repeated 15 times for each of the 6 stimuli.

6.2.6 Cortical reconstruction

Because the craniotomy window does not expose the central sulcus, it is important to create an accurate estimation of the grid's location. Pre-operative MR angiograms are performed. A cortical surface is generated from this volume using the Freesurfer reconstruction pipeline[79]. As intra-operative CT scans are not part of the clinical procedure, grid position relative to the craniotomy window was measured from the base of the grid at the hillock of PDMS (due to the single multi-lead wire) to the edge of the dural opening. Taking into account the direction of the visible wire in intraoperative photos and aligning the photo's vasculature to that of the MR angiogram, we are able to estimate the position of the grid over the reconstructed cortical anatomy. Figure 31 shows the results of the reconstruction and estimation of cortical location.

6.2.7 Signal Analysis

Offline signal analysis was performed as per previous chapters. High gamma timeseries were calculated using a 75-200Hz band-pass 3rd order Butterworth filter and the Hilbert transform. However, contrary to previous chapters, common average re-referencing was not performed.

6.3 Results

6.3.1 Grid Noise in Subject 002

While there were no problems with the signals recorded for Subject 001, the recordings for Subject 002 exhibited noise issues in some of the channels. The power spectra of the first half of the grid (oriented superior to the second half) appeared similar to the expected power spectra when recorded from human cortex[8]. However, the second half (channels 33-64) showed a much higher noise floor and exhibited unusually large variance in cortical potentials (see Figure 34). While a small minority of the channels in this latter half of the grid showed normal power spectra, we opted to discount these channels from the recordings so as not to skew the results. In this respect, the grid from Subject 002 can be treated as an 8-by-4 array of 32 electrodes.

6.3.2 Coherence across channels

Coherence across the grid was calculated without additional re-referencing. Coherency measurements were taken at 1,2,3,4,5 and 7-away neighbor measurements. Both subjects show a strong coherence across in low frequency values (Subject 001 at 25-35Hz, 002 at 8-12 Hz), but significantly lowerd decreases in the range associated with high gamma (75-200Hz). A spike in the coherence measurements can be seen in both subjects at 60 and 120Hz due to harmonics of line noise. An upward trend in coherency is present as the signal-to-noise ratio approaches the noise floor at higher frequencies.

At 3mm – a single nearest-neighbor electrode – both subjects exhibit a coherency consistently below 0.5 in high gamma. Moving to second-nearest-neighbor, electrodes at a distance of 6mm are consistently below 0.2. These results indicate that while there is appears to be scome mutual information at 3mm spacing, the majority of the signal is accounted for by signals unique to each recording.

6.3.3 Gross grid activation – comparison with prediction

According to the estimations made in Chapter 3, with a 3mm grid over hand area we would expect to see about 21 electrodes (32%) that show large-scale increases in high-gamma activity and around 54 electrodes (84%) that show minor increases. Figure 36 demonstrates the high gamma (75-

200Hz) activity comparing movement periods to rest periods. Setting the lower threshold for both subjects at a z-score of 2 – already a significant increase with a P value of < 0.05 – we see 52 electrodes in Subject 001 and 32 electrodes in Subject 002 that show increases in high gamma (81% and 94% respectively). Z-scores for both subjects are as high as 6 standard deviations above resting potential for movement. This suggests that both grids were successfully placed over areas of cortex that are associated with volitional hand movements.

6.3.4 Finger flexion

Figure 37 shows the results of the finger flexion task for subjects 001 and 002. Every digit movement for Subject 001 shows at least three electrodes with mean z-scores above 4, and all but thumb have 9 or more. The pattern of activity of high gamma activity associated with each digit movement is clearly spatially distributed for both subjects. Subject 001 had significant thumb activity on the inferior edge of the grid (left edge in Figure 37), while index, middle, ring, and pinky progressing further superior along the grid. Subject 002 showed thumb activity in the middle of the grid, with each subsequent digit appearing along the posterior edge of the grid from inferior to superior, respectively. Pinch activity for both subjects showed surprising patterns of cortical activation. In both cases, areas of cortex that increased in activity during thumb and index appear in pinch. Areas that are associated with middle, ring and pinky finger are not coactivated to the level of index and thumb.

6.3.5 Temporal Activity

Unlike the study we performed in Chapter 3, we are not limited to time-locking analysis on cue onset. Recording the dataglove position synchronized to the cortical recordings allows precise movement and cortical time-series averaging. The Joint Angle and Channel traces in Figure 37 show that the high gamma activity is very tightly correlated to the onset of movement and at times the high gamma reaches 12 standard deviations above rest.

It is important to note that the movement executed by each subject differs. When instructed to "flex the indicated finger" before the experiment began, Subject 001 repeatedly flexed and relaxed each digit repeatedly during stimulus presentation. In contrast, Subject 002 flexed the indicated digit and maintained this flexed pose until the cue was removed. This difference can account for the difference in the duration of the high gamma increase associated with movement.

6.3.6 Joint correlation

Log(high-gamma) timeseries for each channel were correlated with to the flexion value associated with the suggested cue (Figure 38) and individual joint angle recordings (Figure 39). Spatial

patterns of correlation with flexion values followed similar patterns to those seen in the relative high gamma traces from Figure 37. Similar to the previous mappings, pinch also seemed to be simply a superposition of index and thumb movement for both subjects.

However, the spatial patterns seen in Figure 39 show a much finer pattern of spatial distribution between the proximal and medial digits of each finger, suggesting that the spatial representation of each individual joint may be at a higher resolution than whole finger flexion. Proximal joints show a much broader pattern of correlation than medial joints of the same digit. In addition, it appears that for some joint angles the correlation is inversely correlated. This may be an artifact of the way that the dataglove's resistive strips measure extension that occurs as the subject presses the distal bone against their palm during finger flexions.

6.3.7 Classification

Classification of each cue presentation period was performed on the finger flexion task. Mean power for each channel was calculated for all channels and was classified into one of 6 categories (one of five digits or pinch) using K-Nearest Neighbor classification[80]. 10-fold classification was performed for each subject. When using all recorded channels, the correct digit flexion was identified 100% of the time for Subject 001 and 73% of the time in Subject 002. Chance prediction for 6 classes is 1/6, or 17%.

As a further test of classification, the number of channels used for classification was reduced to 5 for each subject (see Figure 40). For Subject 001, five electrodes were chosen that were roughly discriminable by observation for each digit. For Subject 002, due to the smaller size of the grid all possible combinations of 5 channels were tested and the five that best predicted the outcome were identified. 10-fold classification based on five of Subject 001's 64 electrodes gave a classification accuracy of 100%, identical to the accuracy when using 100% of the grid. Classification accuracy using the 5 best electrodes for Subject 002 resulted in an increased prediction accuracy of 85%.

6.4 Discussion

6.4.1 Subject 002 Noise

The exact nature of the noise seen in Subject 002's recordings is unknown. Likely scenarios include a short in the microgrid's microwires in the exiting lead, a problematic ground or reference connection between the first two and last two biosignal amplifiers, or a misalignment of the pigtail lead connectors. In spite of the problem, however, the remaining 32 channels still provided enough discrete information to be able to classify each grip well above chance.

6.4.2 Quickmapping critical

We had originally hoped that the craniotomy windows in these intraoperative surgeries would have allowed the use of stimulation mapping to locate and enumerate primary hand motor cortex. Due to the clinical requirements in both subjects, the craniotomy ended up being far inferior to the predicted area making grid placement problematic. Since we had anticipated this scenario and developed Quickmap based on previous studies that suggested high gamma was a realistic alternative to stimulation for functional mapping[64,81–83], we precisely locate and map areas of the cortex that were correlated with volitional hand movement in rapid succession, successfully identifying the desired neuroanatomy hidden underneath the skull within 90s both times.

6.4.3 Gross movement may be built from subcomponents

The classification accuracy for both grids was surprisingly high, reaching 100% classification rates for 10-fold validation in Subject 001. This means that during the 10-fold training/testing classification runs, not a single epoch was erroneously decoded. Given the variability of any type of recorded biosignals and that ECoG signals themselves are second- or third-order metrics of neural activity, the robustness of the signal is apparent. Even in Subject 002, classification rates were well above chance; a metric that would almost certainly be higher given a fully functional grid.

Even more remarkable, however, is the classification accuracy when restricting the input to just 5 channels. Just five channels allowed for 100% accurate classification of Subject 001's movement. It should be noted that classification was performed on all movements including pinch. This means that in spite of having just five dimensions of variability, a full six states can be classified with perfect accuracy, even when one of them is a movement that is comprised of a combination of two of the other states. Figure 41 shows that significant differences in activity levels can be seen across the grid, suggesting that there is a spatial basis for cortical organization in hand sensorimotor cortex.

This latter aspect has a broader implication in the context of volitional movement. Even though the spatial patterns elicited during pinch appeared to be the superposition of the two individual finger flexions, the pinch movement could successfully be classified distinct from the individual digit movements. This suggests that complex dexterous movements could in fact be built from a combination of simpler basic building blocks; such is the idea of muscle synergies. If we were to able identify a basic set of synergistic movements, it may be possible to reconstruct more complex motions from them, such as those used during object grasping and manipulation. The following chapter will

investigate the possibility that not only do these synergies exist at the cortical level, but that they can predict the vast amount of variance in hand pose.

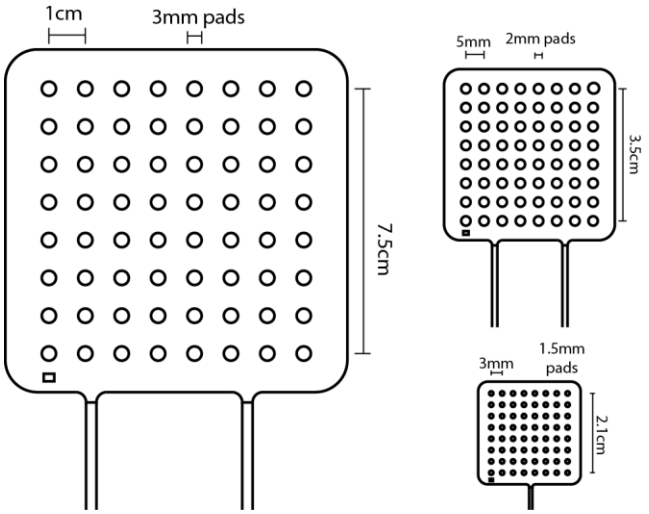

Figure 29 – Relative size of the microgrid designed for this experiment. Standard clinical grids (upper left) have 3mm platinum disks spaced at 10mm center-to-center. The electrode grid implanted into the pediatric patient – described in Chapter 3 – used the 2mm pads spaced at 5mm. The grid we developed for this study (lower-right) contained 64 1.5mm-diamater electrodes spaced at 3mm.

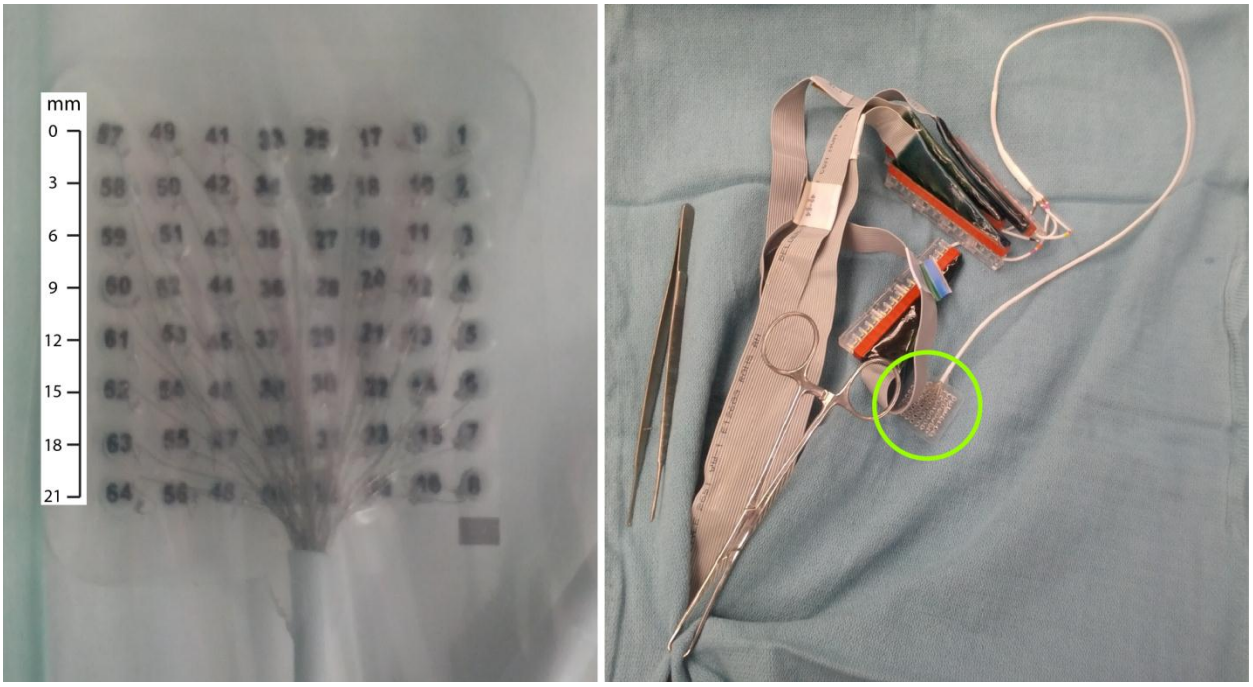

Figure 30 – Image of the microgrid that was implanted. It's scale can be seen next to a set of standard clinical forceps. All 64 contacts come out in a single wire that splits in to four 16-contact pig-tails. Each pigtail was plugged into a single biosignal amplifier.

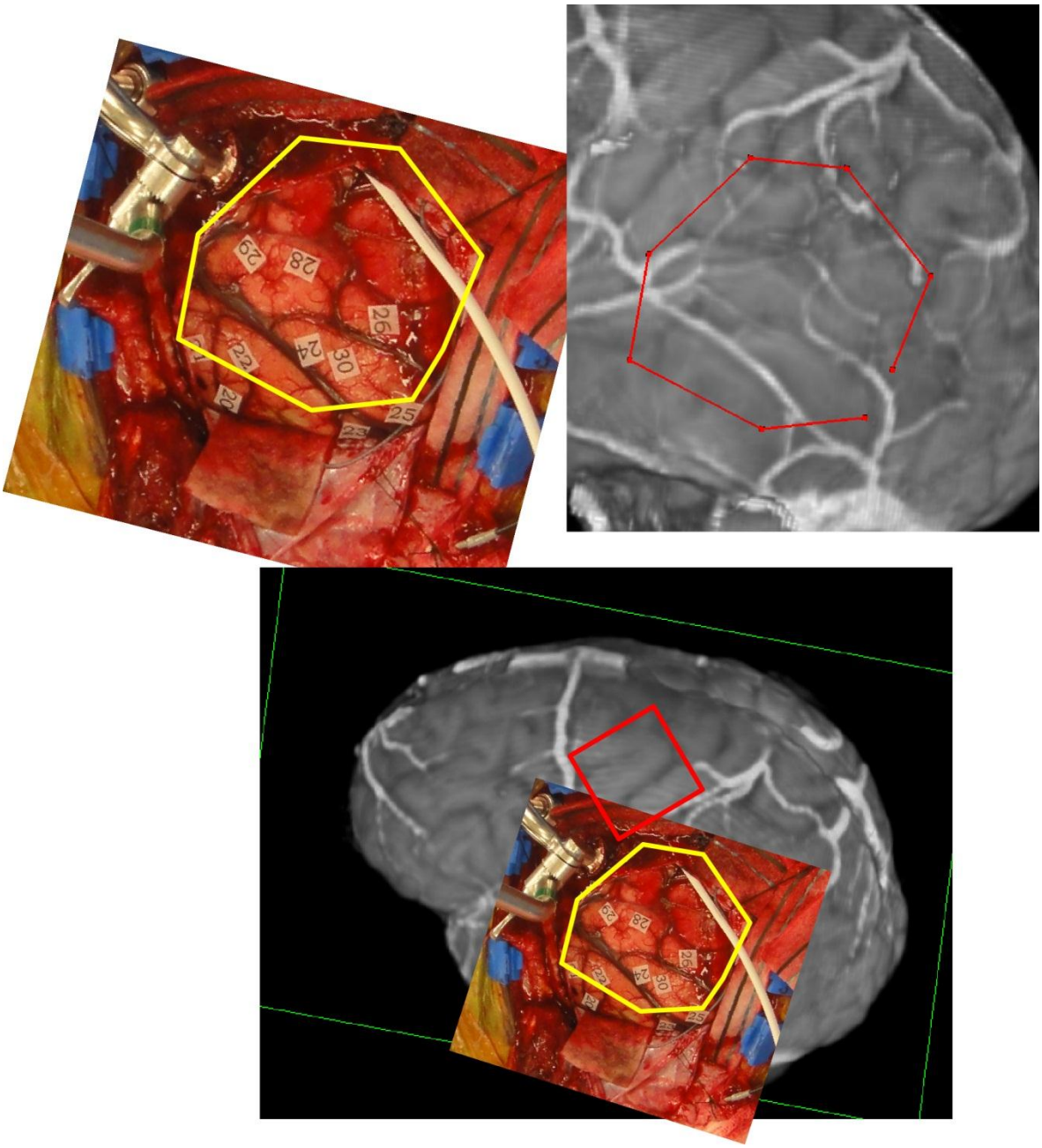

Figure 31 – Upper-left: intraoperative photo of the craniotomy of Subject 001, with artificial landmarks highlighted in yellow. The lead coming from the microgrid can be seen in white. The vasculature from the intraop photo was aligned with the vasculature in a pre-operative magnetic resonance angiogram (MRA, upper-right). Estimated artificial landmark location is highlighted in red. After alignment, 3 dimensional grid location is estimated to cover primary sensorimotor cortex (red square, lower).

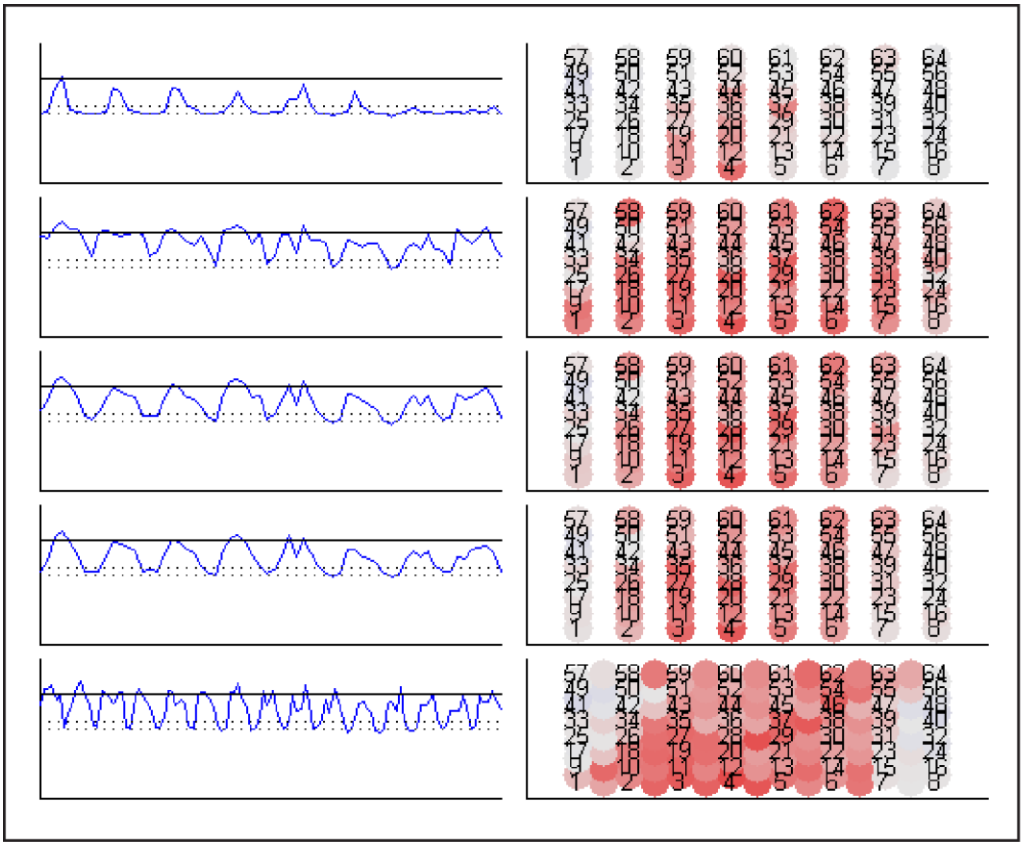

Figure 32 – Screenshot of the quickmap program used to identify whether the grid was over motor cortex. Left columns show the unrolled grid (channels 1-64) vs RSA-value. The lowest dotted line in each plot indicates zero correlation with activity, followed by RSA=.1 above it, with the solid line at 0.5 RSA. Values above .1 indicate weak positive correlation, and values approaching 0.5 indicate strong correlation. Right column shows a graphical representation of the grid, with a redder color indicating a stronger correlation. To ensure that noise did not contaminate the results, the raw signal (top row) was re-referenced four different ways to try to eliminate noise and identify signal: common average, amplifier bank, corner – reference, and pairwise referencing (2nd through bottom, respectively).

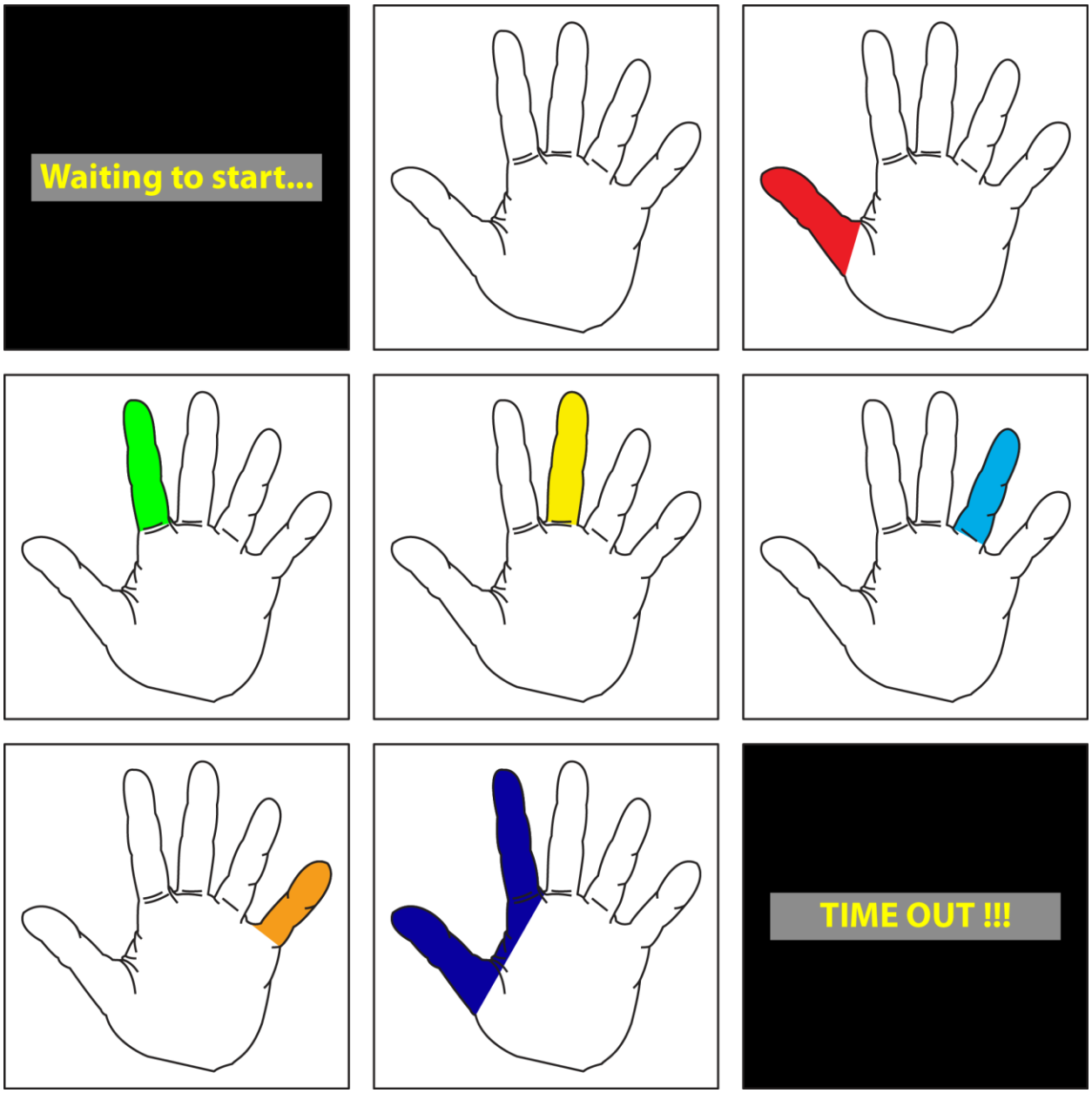

Figure 33 – Experimental instructions for finger flexion task. During rest periods, an empty silhouette of a hand was presented to the subject (top middle). Every 2s one of five digits (or index and thumb for pinch) was highlighted for 2s. Subject was instructed to flex the indicated digit during cue presentation.

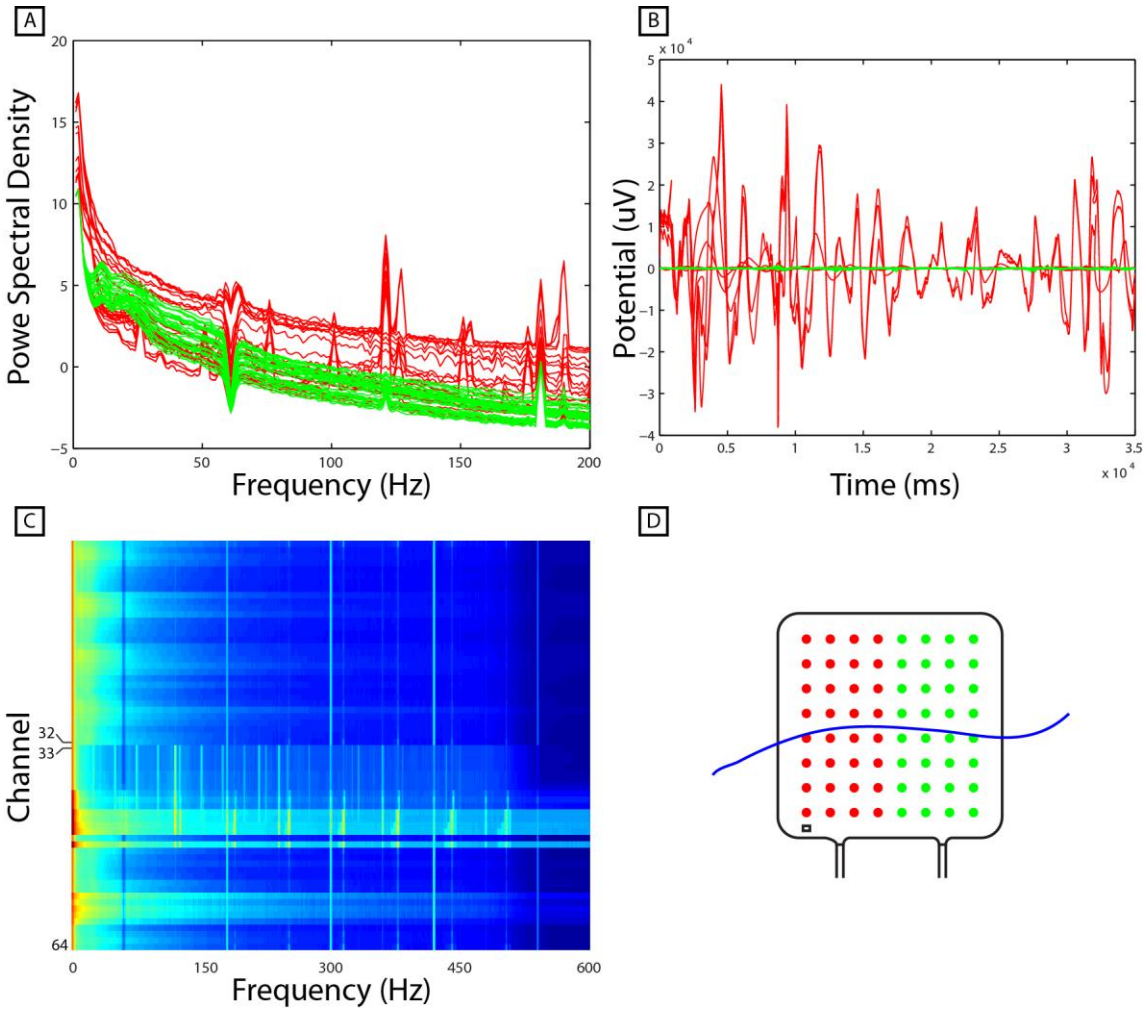

Figure 34 – Illustration of the noise issue in Subject 002. The first 32 channels (green) showed normal, expected power spectral densities commonly seen during human studies. However, channels 33-64 exhibited strange noise-like across nearly all channels with a marked decrease in signal-to=noise ratio (B). Power spectra in A are shown stacked in C, with a clear division between electrodes 32 and 33. However, the first 32 channels are estimated to have spanned both sides of central sulcus, illustrated by the blue line in D.

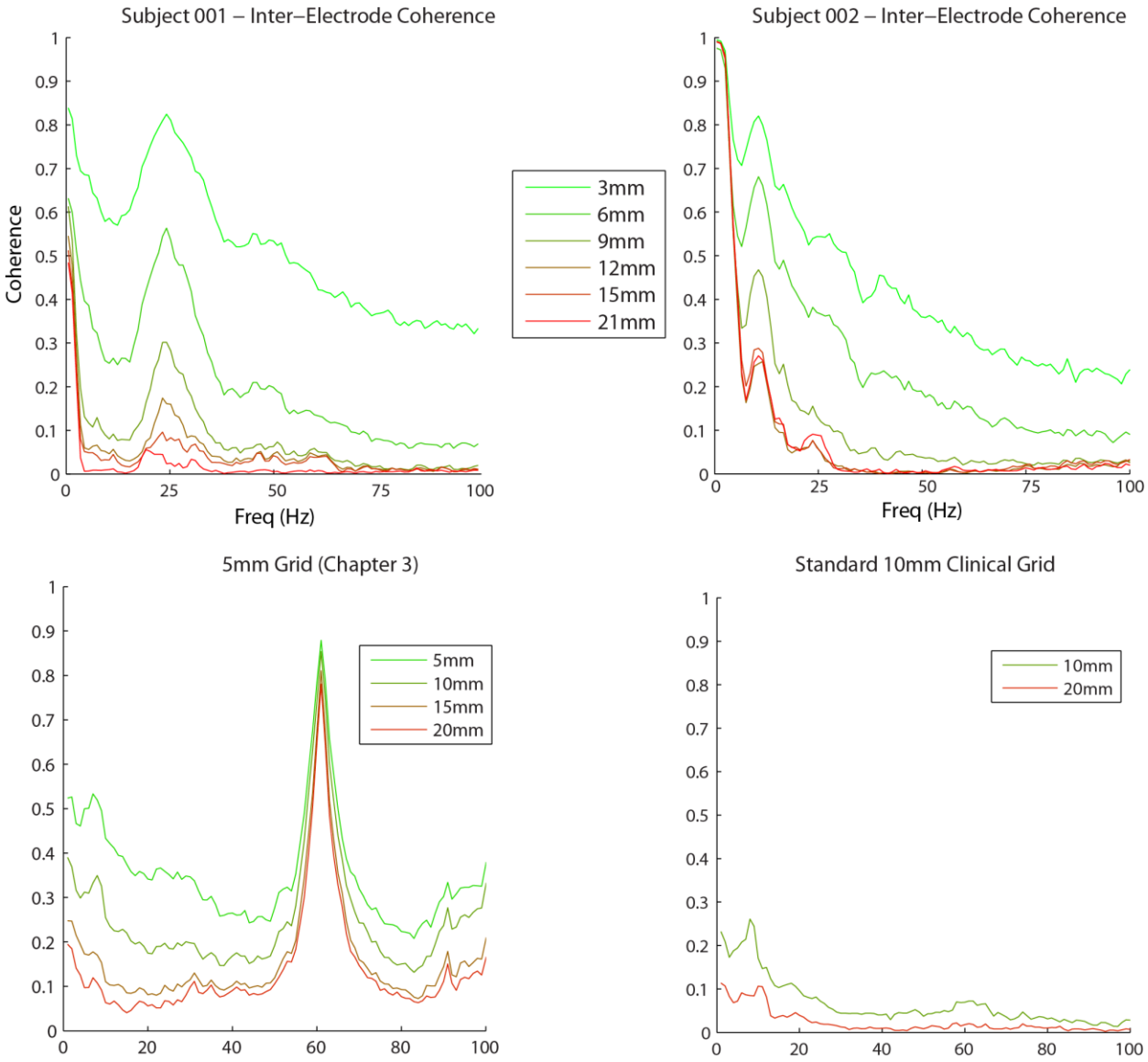

Figure 35 – Averaged coherence measurements across both subjects and comparison to the 5mm grid recorded in Chapter 3 and a sample from a standard 10mm clinical grid. High coherence in beta can be seen. However, coherence at higher frequencies was lower. There was nearly no coherence at 9mm in the broad-band high frequency range (75-200Hz), consistent with the results of the standard clinical grids.

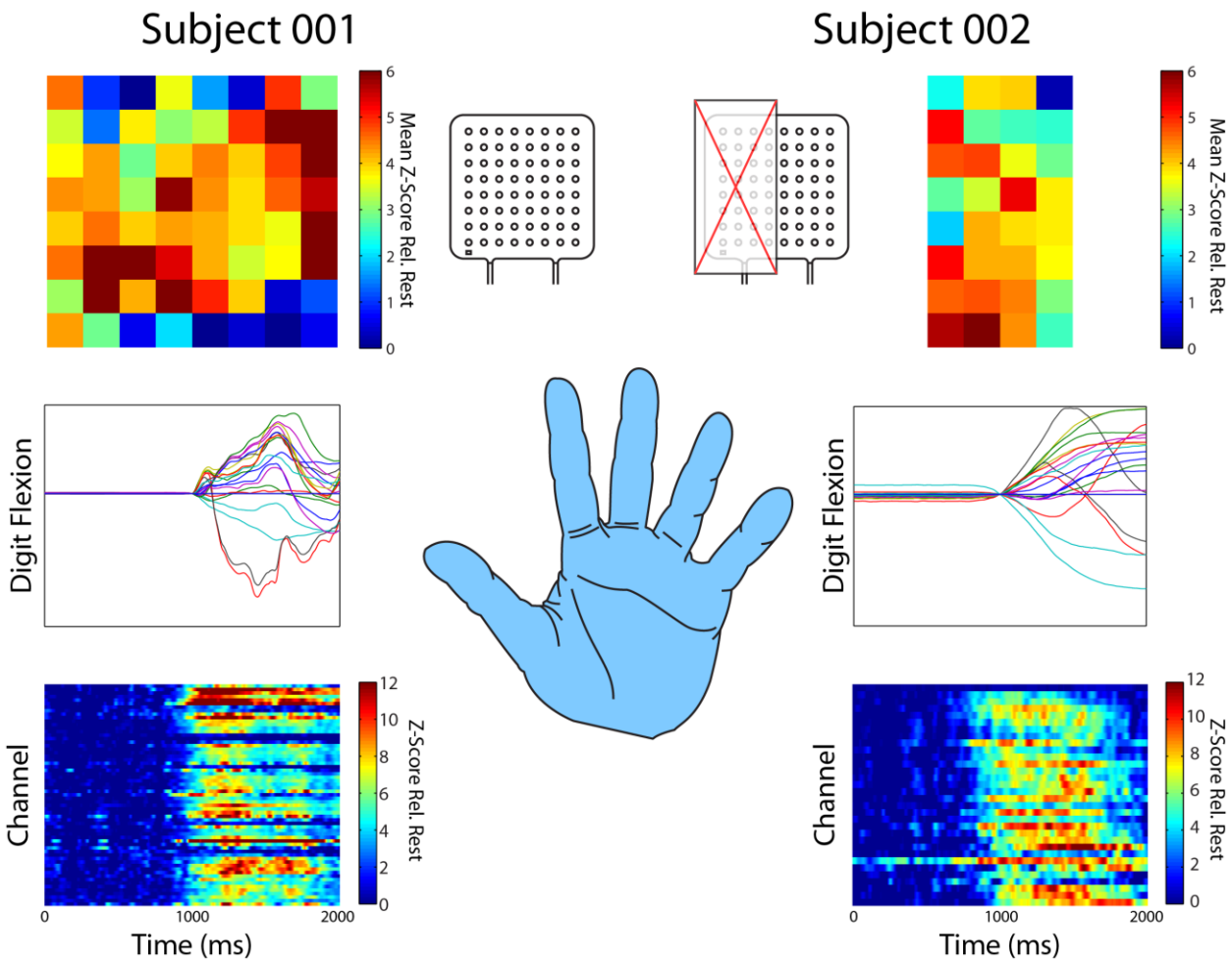

Figure 36 – Results of gross hand motor movement. Nearly every electrode in both Subject 001 and 002 showed a log high-gamma power (75-200Hz) Z-score of 2 or greater relative to the mean resting log power (top). Average joint angles are shows in the middle row, time-locked to the onset of movement. Time course signals for both subjects show about a 1s delay from cue presentation to the onset of movement (time=0)

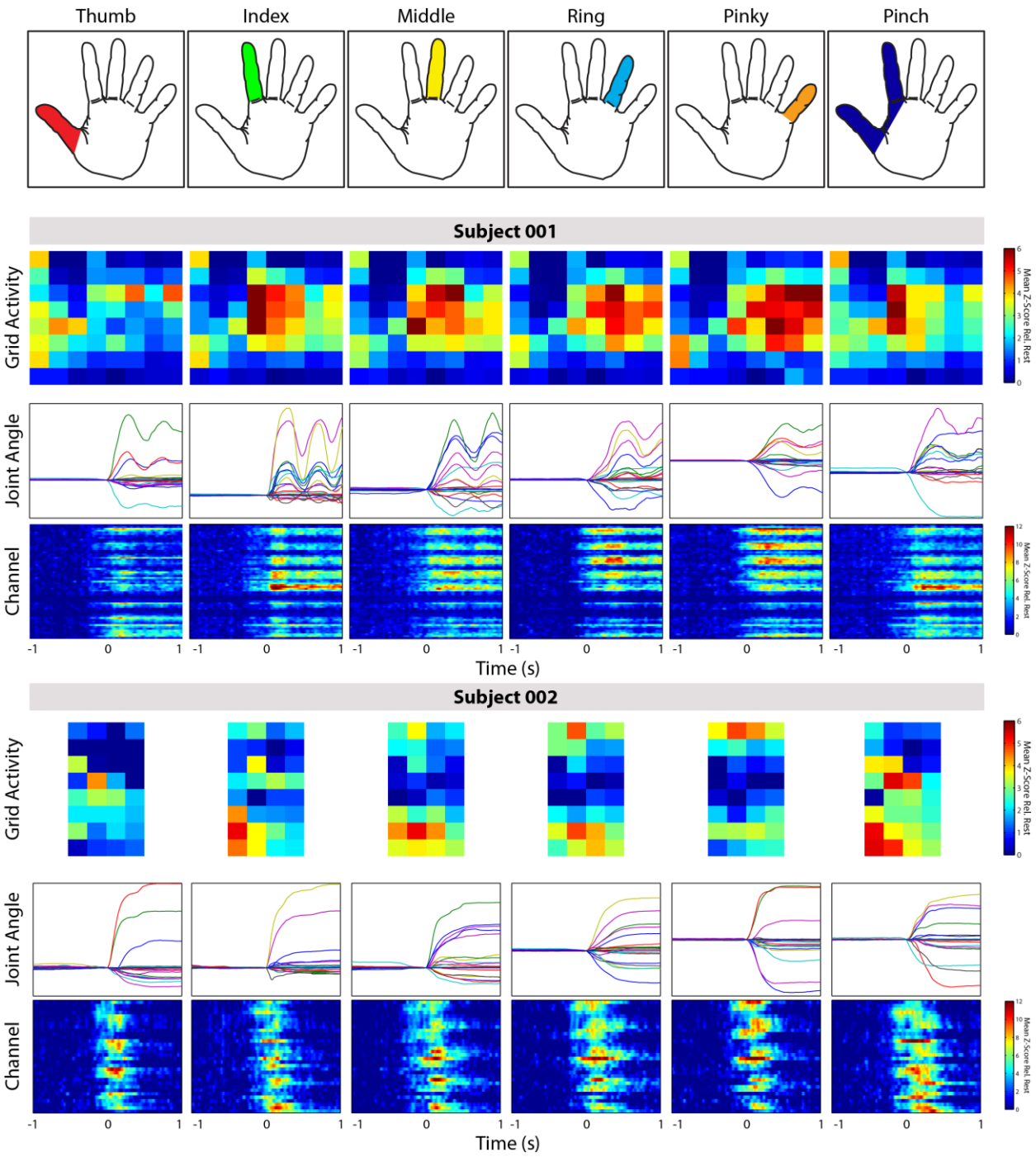

Figure 37 – Results for each individual finger flexion. Each column indicates activity associated with the stimuli in the first row. Grid activity is shows in terms of mean z-scored log power in high gamma (75-200Hz) during movement periods relative to rest, time-locked to the onset of movement. Each of 19 joint angles is shown relative to movement onset. The bottom row shows time-course z-scores for each channel; movement onset was at t=0.

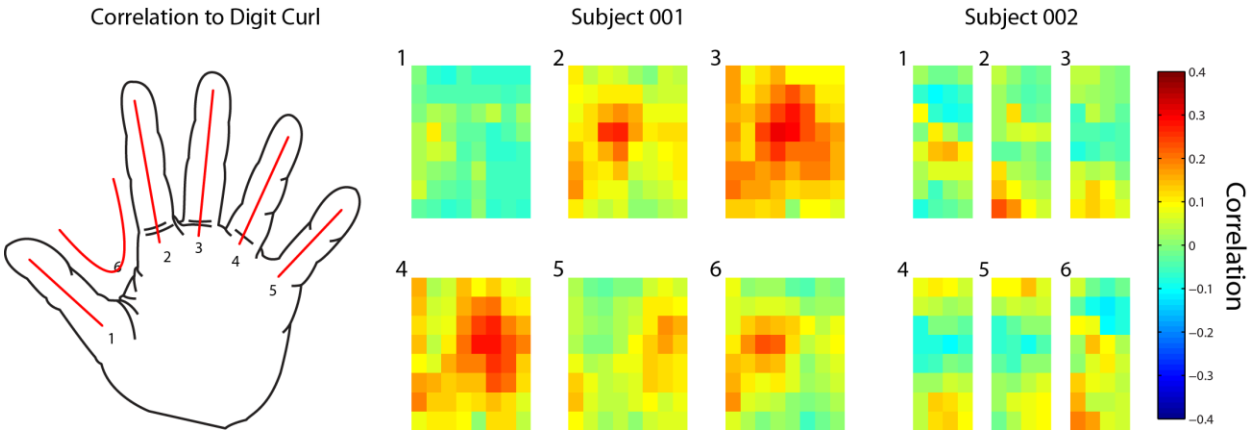

Figure 38 – High gamma signals recorded from the microgrid correlated with each digit (1-5) and pinch (6).

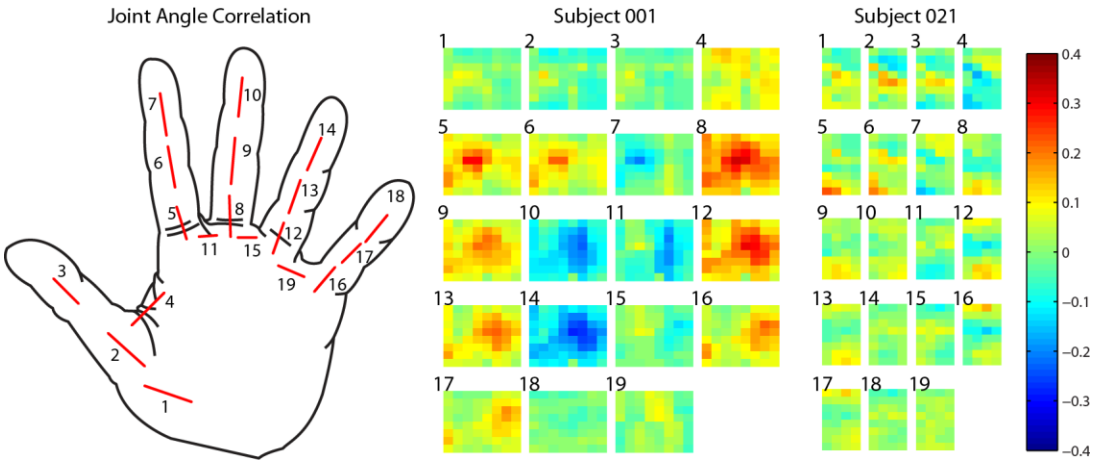

Figure 39 – Joint angle correlations with high gamma across the grid. Subject 001 shows negative correlation vales for distal joints of index and ring, likely due to the distal joint of the middle and ring fingers pressing against the palm during finger flexion.

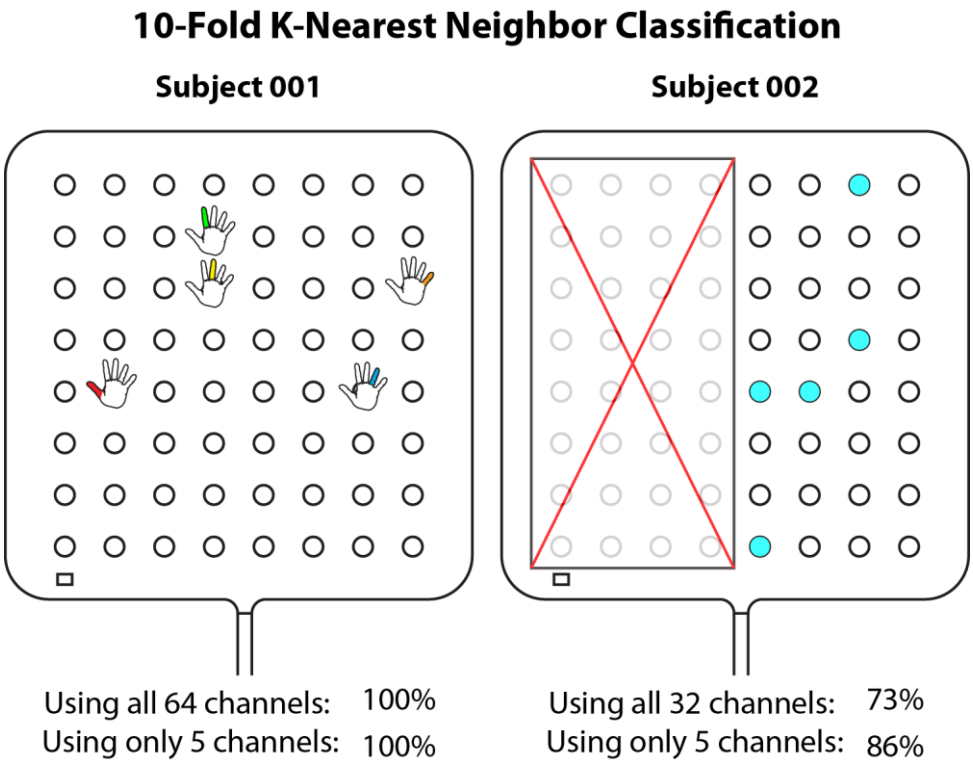

Figure 40 – Classification results for Subject 001 and 002 for finger flexion task. Using all 64 and 32 electrodes netted 100% and 73% classification for all six movement types (five digits and pinch). Using the 5 most varying electrodes for each digit for Subject 001, classification remained at 100%. An optimization routine was used to select the 5 channels used for Subject 002 resulting in 86% classification accuracy.

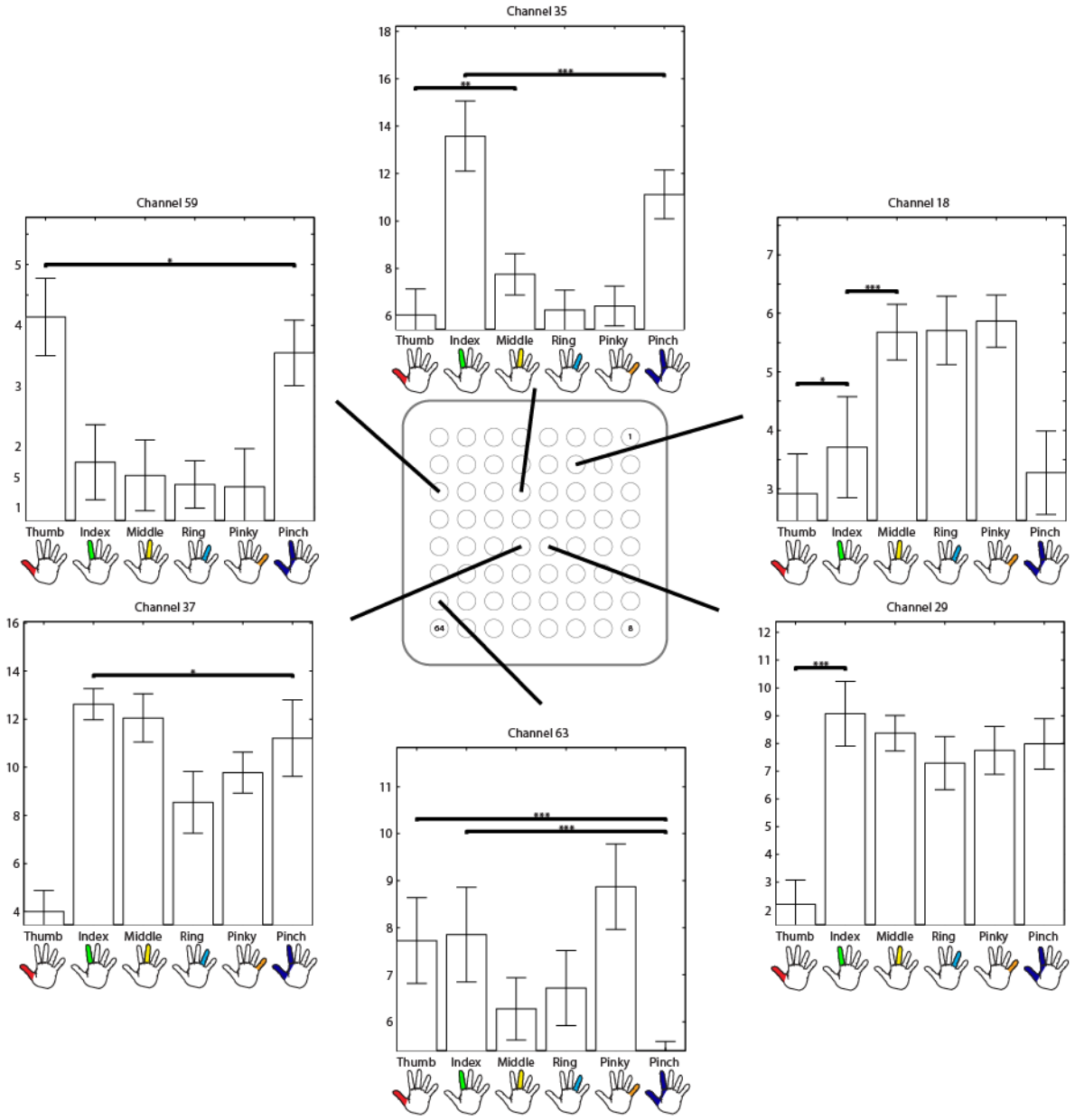

Figure 41 – Mean power +/- one std dev. for selected electrodes in Subject 001 for each motion. Comparisons marked with *, or *** are significant at p < 0.05, 0.01, and 0.001 respectively, and all non-overlapping error bars are considered significant at p < 0.001. Electrodes show broad activity (channel 29, 27) and digit specificity (ch 59, 35). Channel 63 shows unique activity for pinch in comparisons to other electrodes. It was the only electrode to show insignificant activity for pinch, whereas thumb or index finger activity was present.**

7 Chapter 7 – Reconstructing Hand Pose from Neural Signals

7.1 Further Microgrid Study

The brain takes care of many processes simultaneously: processing input, calculating internal states, goal evaluation, planning motor output and execution of movement among many others. With the large number of neurons and high interconnectivity in synaptic connections between them, many areas of the cortex are coactivated to process this input. It is important to show that our assumption that primary motor cortex is the appropriate area to look for evidence of the proposed synergies. This requires evidence that kinematic correlations exist with recordings from the outermost layer of primary motor cortex during highly stereotyped movement. Moran *et al.* observed that primates implanted with primary motor cortex electrode arrays showed highly correlated neural activity to proximal arm movements, indicating reaching information is encoded in that region[81]. Recent progress in high dimensional reconstruction of proximal primate limb movement from neural firings show highly robust activation patterns exist within motor cortex sufficient to perform accurate approximation of limb posture [11]. These findings provide evidence that while other areas of the brain may play a role in planning motor movement, accurate reconstruction of distal hand pose is possible by observation of primary motor cortex alone.

Our hypothesis suggests that though there may not be unique spatial locations of cortex that control each individual digit or synergy, spatial patterns of activity can be observed over time that, though overlapping, can be regressed to show correlation to hand dynamics. Many mathematical tools have been developed recently that can identify correlates of populations of neurons to dynamic motion, though the vast majority of these model the recordings as a vector sum of preferred directions, a type of population vector. This approach works well when there are large populations of neurons being recorded, but such situations are generally situated to single dimensional decoding in local field potential (LFP) recordings.

7.2 Methods

7.2.1 Subjects and recordings

In the previous chapter, we discussed the intraoperative setup and biosignal recordings that were performed on subjects that underwent cranial surgery for the purposes of tumor resection. Though our experimental time within the surgical theater was limited to 30 minutes, the cumulative time spent on Quickmap and the first two experiments allowed us time to run two subsequent

experiments: performing dexterous motion by repeatedly grasping objects, and performing freeform, non-stereotyped hand motions. In the case of Subject 001, electrode 32 was identified as contaminated with an unknown noise source and was discounted, leaving a total of 63 valid channels.

7.2.2 Experiment III: Object Grasping

Expanding on the previous the previous chapter's range of motion during experiments, our second bedside experiment in this aim allowed subjects to explore the joint-space commonly associated with object manipulation. With the previous intraoperative experiment providing information about cortical activity during stereotyped isolated digit movement, it is important to observe if the cortical representation of simultaneous movement of multiple digits is encoded in a unique way, or whether it is encoded simply as the superposition of areas activated with individual finger movements.

The patient was instructed to place their hand outstretched on a table in front of them with their arm relaxed and their hand in a neutral, resting position. Before the experiment begins, the researcher administering the experiment instructed the subject on how to grip one of six objects: a cellular phone, a narrow tube, a large tub, the handle of a small case, a pencil, and a piece of paper (see Figure 42). The objects selected for this study encompassed a different range of possible grip variance depending on the object: power grip (five-fingered grasp), briefcase (fingers in linked curling motion with thumb supporting), pencil (index, thumb and middle finger), planar (fingers linked with pads touching thumb pad), pinch (thumb and index precision pinch), palmar (fingers splayed, palm supporting), and angled support (similar to palmar, but with increasing finger flexion from index to pinky).

At a visual cue, the researcher selected the specified object and places it near the subject's hand. The subject then proceeded to grip the object in the manner previously specified. After two seconds, the subject released the object allowing it to be removed from both sight and reach. Though the amount of variance seen during object grasping was expected be significantly higher than that seen in the previous finger flexion experiment (described in Chapter 6), the motion is still highly stereotyped. No integration with full limb movement or coordinated body motion was present, eliciting only movement from the hand.

7.2.3 Experiment IV: Free Movement

All experiments so far were in highly controlled environments involving highly stereotyped motions, ranging from basic gross movement to precision grip. However, any results found in these

controlled environments need to be able to be reproduced under less constrained circumstances. An experiment involving free limb movement allows the patient to explore the entire state space of dexterous movement during periods of normal activity that may include – but not limited to – object manipulation, gesturing, relaxation and precision grasping.

To elicit these natural movements, the patient wore the dataglove for a period of 2 minutes after the object grasping task was complete. Subjects were instructed to perform any actions, movements and gestures they wished during this time and encouraged to do motions they expected to perform during a typical day. Motions included – but were not limited to – counting on fingers, typing on a computer keyboard, pointing, gesturing, etc. The expectation is that broader the range of motions recorded – free of rigid experimental constraint – the wider the space of natural hand movement both subjects were able to explore given their limited range of motion during the surgical procedure.

Because this experiment does not involve time-locked prompts, naïve methods of grip decomposition need to be applied (i.e. principal component analysis) that make no assumptions about the state of the glove. As no intraoperative video recording takes place and no audio recording is performed, attempting to empirically label certain periods of free movement is both impractical from an accuracy standpoint and impossible from a records standpoint.

7.2.4 Synergy Generation

"Synergies" – coordinated joint movements – were determined by applying principal component analysis to the joint covariance matrix over the course of the entire recording. The synergies are the eigenvectors produced by eigenvalue decomposition, which in turn are the joint weights for each principal component. Before applying PCA, each joint angle is normalized to a range of 0-1 and subsequently zero-meaned. As our study is designed to investigate the dynamics of the hand in the context of coordinated digit movement, only the first 19 sensors of the dataglove were used; wrist yaw, wrist pitch and palm roll were not included in analysis.

Scalar projections H_i of each synergy were generated by multiplying each synergy S by a scalar α and adding the result to the mean hand position $\bar{p}$.

$$H_i = \bar{p} + \alpha S_i \qquad \textbf{7.1}$$

7.2.5 Kalman Filtering

A Kalman filter was used to map the cortical high-gamma timeseries onto both joint angles as recorded by the dataglove, and the time-course contribution of each synergy. The design of the kalman filter is based on the study performed by Wu *et al*[84]. Our study differs from theirs in that the recordings used in their study was local field potentials, and thus the metric used in their study was a modified form of firing rate. As we cannot discern single spikes and instead rely on a second order aggregate metric of high-gamma activity, modifications to their algorithm was required.

Our algorithm is based on their *likelihood model* that relates hand kinematics to neural firing rates. A generative base model is defined as:

$$z_x = H_x x_k + q_k \quad \textbf{7.2}$$

Where k=1,2,3…M where M is the number of samples in the trial, and $H_k \in \mathbb{R}^{Cx19}$ for joint angles or $H_k \in \mathbb{R}^{Cz7}$ matrix for synergies, a matrix that linearly relates the respective glove space to the log power of high gamma. We make the same assumption that Wu *et al.* make, in that the observation noise is zero-mean and normally distributed with covariance ($q_k \sim N(0, Q_k)$, Q_k= covariance).

In addition, we leverage the *temporal prior* that models how the glove state is expected to evolve over time, based on the previous timestep:

$$x_{k+1} = A_k x_k + w_k \quad \textbf{7.3}$$

WhereA_k is the coefficient matrix $A_k \in \mathbb{R}^{Cx19}$ or $A_k \in \mathbb{R}^{Cx7}$ for joint angle and synergy, respectively, and the noise term $w_k \sim N(0, W_k)$. This equation linearly relates the previous hand position to the previous hand position at time point k.

In order to solve these equations, we apply a two-step process for each timestep: the ***time update*** step, and the ***measurement update*** step, as shown in Figure 43.

Time Update: The time update step is performed by applying two equations. First, at time t_k, the priori state estimate $\hat{x}_{k-1}$ – with the state defined as the 19x1 joint angle vector or the 7x1 synergy vector – is predicted forward in time using the state update matrix A:

$$\hat{x}_k^- = A\hat{x}_{k-1} \quad \textbf{7.4}$$

Next, the uncertainty of the Gaussian noise is incorporated into the system by covariance matrix W:

$$P_k^- = AP_{k-1}A^T + W \quad \textbf{7.5}$$

Where P_k^- is the a priori error covariance matrix at time t_{k-1}.

Measurement Update: Using the prediction $\hat{x}_k^-$ from the time update step and log high gamma activity z_k ($nx1$ vector, where n is the number of channels recorded), we modify the predicted value based on the observed cortical signals and update the posterior error covariance matrix:

$$\hat{x}_k = \hat{x}_k^- + K_k(z_k - H\hat{x}_k^-) \quad \textbf{7.6}$$

$$P_k = (I - K_k H)P_k^- \quad \textbf{7.7}$$

Where P_k is the state error covariance after observing the cortical data and K_k is the Kalman gain matrix as defined by:

$$K_k = P_k^- H^T (HP_k^- H^T + Q)^{-1} \quad \textbf{7.8}$$

Training: The State update matrix A, along with the system covariance matrix W, the extraction matrix H, and the measurement covariance matrix Q can be found by using glove training data x_t and cortical training data z_t for $t = 1,2, \dots M$, and performing least-squares regression. A closed-form solution was outlined by Wu *et al.:*

$$A = \left(\sum_{k=2}^{M} x_{t,k} x_{t,k-1}^T\right)\left(\sum_{k=2}^{M} x_{t,k-1} x_{t,k-1}^T\right)^{-1} \quad \textbf{7.9}$$

$$W = \frac{1}{M-1}\left(\sum_{k=2}^{M} x_{t,k} x_{t,k}^T - A\sum_{k=2}^{M} x_{t,k-1} x_{t,k}^T\right) \quad \textbf{7.10}$$

$$H = \left(\sum_{k=1}^{M} z_{t,k} x_{t,k}{}^T\right)\left(\sum_{k=1}^{M} x_{t,k} x_{t,k}^T\right)^{-1} \quad \textbf{7.11}$$

$$Q = \frac{1}{M}\left(\sum_{k=1}^{M} z_{t,k} z_{t,k}^T - H\sum_{k=1}^{M} x_{t,k} z_{t,k}^T\right) \quad \textbf{7.12}$$

All mean-squared error calculations were derived using 10-fold cross-validation was performed, training on 60% of data and testing on 40%.

During the Grips task, there were long periods of rest between object grasps lasting as long as 8s, during which there was very little or no movement of the glove. As these periods of stationary pose affected mean-squared error calculations significantly, training and testing of the Kalman filter was performed solely on periods of movement. During training, the neighboring samples that occurred at discontinuities between two movements were discarded as they would have introduced noise into the training matrices.

For the freeform task, the entire period was treated as a single movement. The first 60% of samples were used as training to test on the remaining 40%.

7.2.6 Pose Reconstruction

By applying the trained Kalman filter K to a testing data sample z_k, we can reconstruct the predicted pose of the hand using the first n synergies by:

$$\tilde{p}(z_k, n) = \bar{p} + \sum_{i=1}^{n} K(z_k)_i S_i \qquad \textbf{7.13}$$

Where $\bar{p}$ is the mean hand position $K(z_k)_i$ is the contribution of the ith synergy S_i as predicted by the Kalman filter. Initial starting pose and error covariance estimates have a significant impact on reconstruction error. For each grasp , the starting hand pose was assigned as the glove's position at the previous sample.

7.2.7 Reconstruction Accuracy

It is difficult to directly compare the accuracy of pose reconstruction between cortical/joint-space and cortical/synergy space, as the number of dimensions differs and will affect any resulting error measurements. To be able to compare between reconstruction techniques, the synergy contributions are projected back into joint space according to Equation 5.4. This allows a direct calculation of the mean-squared error in pose reconstruction at time k between the recorded pose p_k and the estimated pose $\tilde{p}$:

$$mse(p_k, \tilde{p}\,) = \frac{1}{19}\sum_{j=1}^{19}\left(p_{k\,j} - \tilde{p}_{k\,j}\right) \qquad \textbf{7.14}$$

For all 19 joints.

7.2.8 Uniform and Optimal lag

Previous studies have shown that a roughly 140ms delay in signal propagation between neural activation and muscle activation[84,85]. Initial Kalman training and testing was performed using time-locked samples and does not take this delay into account. To determine the effect of introducing a temporal delay between the cortex and the change in joint angles, the lag l_u was found according to

$$l_u = argmin_{l_{u\in[-300:25:300]}}\left(mse\left(p_k, \tilde{p}\left(z_{k+l_u}, n\right)\right)\right) \qquad \textbf{7.15}$$

Where p_k is the true recorded hand pose and$\tilde{p}\left(z_{k+l_u}, n\right)$ is the trained Kalman reconstruction from cortical signal z_k with all channels temporally shifted byl_u.

In addition to a uniform lag, we explored the possibility that allowing each individual channel to vary in time lag may capture the transmission of information intra-cortically. A greedy algorithm identified by Wu *et al*. was used that quickly converged after 5 iterations.

7.3 Results

7.3.1 Spatial Distribution

In contrast to the results obtained in during individual finger flexion, the spatial distribution of high gamma activity was similar between grips for both subjects (see Figure 44). For both subjects, the power grip performed during the Case grasp activated the largest area of cortex, with more than half of electrodes in Subject 001 and every electrode in Subject 002 maintaining high-gamma z-scores 3σ or more above rest.

7.3.2 Time-Course Activity

Figure 45 shows the time-course traces for the dataglove and cortical signal during each object grasp, with both subjects possessing many cortical channels that reached and sustained levels six standard deviations or more above resting high gamma. Subject 001 appeared to initially extend the fingers outward around the object before closing around the grasp. Though there is a small increase in cortical activity during the extension phase, the majority of the variance in high gamma appears after extension coincident with the subsequent closing of the grasp. In contrast, Subject 002 showed broad activity across large areas of the grid at the initial onset of movement. At the end of the grasp, the cortical activity in both subjects returned to rest levels.

7.3.3 High-Gamma Onset

A histogram of the onset of high gamma relative to detected glove movement during object grasping is shown in Figure 46. High gamma onset was classified as one-third of the maximum positive derivative of high gamma before movement; in short, one third of the peak rate of increase of high gamma. For both subjects, the mean varied from -260ms to -80ms (negative values imply the cortical signal leads glove motion) though the mean varied between objects. For all objects for both subjects, the majority of electrodes showed high gamma increase onset leading the glove motion.

7.3.4 Classification

Grip classification was performed using 10-fold cross-validation with k-nearest-neighbor mapping, using mean log high gamma from all channels as the feature set. Classification for Subject 001 was 50%, while Subject 002 was 43.4%, both significantly above the chance level of 16.6% at $p < 0.001$.

7.3.5 Synergies

A total of 18 synergies were generated for each subject, with the first 6 accounting for 90% of observed variance and 9 contributing 95% of variance. Figure 47 shows that there is no significant difference between the amount of variance the synergies contribute between Grips and Freeform movement.

Figure 48 shows the projection of the first five synergies for both patients. Inter-subject variation is low for synergies 1-4, with the fifth synergy beginning to show difference. The first synergy, accounting for the majority of the variance, involves a synchronized flexion/extension for all joints of all the fingers, with the thumb remaining nearly stationary. This is consistent with the first synergy shown in Chapter 5, Figure 24. It is important to note that the PCA decomposition assigns arbitrary signs to the synergy projection. Inverting the sign on the 4^{th} synergy for either subject shows a close match.

7.3.6 Optimal lag and synergy count

While 18 synergies were generated, it is important to determine whether all of them are required for correct reconstruction, or whether only a subset of the synergies are required to generate an appropriate hand pose. We varied the number of cumulative synergies used during reconstruction in addition to uniformly lagging/leading the brain signal by -350ms to 350ms in steps of 25ms. Figure 49 shows that the lowest MSE for Subject 001's pose reconstruction occurred at -75ms using 7 synergies. Adding further synergies appears to add spurious noise to the pose estimate. For Subject 002, lowest MSE occurred at -225ms, using only 2 synergies. However, the first two synergies for Subject 002 did not involve significant thumb motion, which only began in the third synergy. Because of this, we restricted optimality for Subject 002 to the lowest MSE with three or more synergies contributing to the reconstruction. With this assumption, the next lowest MSE occurred at -150ms using 7 synergies. As a total of 7 synergies provided the lowest error in reconstruction for both subjects when using a uniform lag, subsequent reconstruction results used the first 7 synergies for reconstruction.

7.3.7 Cortical contribution to each synergy

The state update matrix A in Equation 7.3 implies that, during gripping motions, the glove moves in a predictable, linear manner. The extraction matrix H is an NxM matrix that subsequently relates the importance of each electrode (the "measurement" in a Kalman filter) to modifying this linear relationship, where N is the number of channels and M is the number of outputs (i.e. 7 synergies or 19 joint angles). Each row of the extraction matrix H can be interpreted as the spatial distribution of

activity that contributes to that specific synergy. Spatial maps associated with each of the 7 synergies can be seen in Figure 50.

7.3.8 Per-electrode delays

The mean-squared error for time-locked cortical recordings was 147 and 174 for Subjects 001 and 002, respectively (see Figure 51). Allowing the cortical signals to uniformly vary dropped the error measurements to 138 and 162, though not a significant drop. However, allowing the channels to individually vary lowered the average MSE during reconstruction down to 113 and 139, a significant drop at $P<0.05$ for both subjects. Spatially arranging the lagged values according to electrode position (Figure 52) did not produce any observable spatial arrangement.

7.3.9 Reconstruction: Joint Angle vs. Synergies

Overall: Using uniform lags, reconstruction was performed by decoding joint angles directly and decoding the first 7 synergies and reconstructing hand pose. For Subject 001, the mean-squared error was 138 for synergies vs 172 for joint angles, suggesting that decoding synergies directly can produce a more accurate hand pose (see Figure 53). Similarly in Subject 002, the mean-squared error for synergies was 162 vs 193 for joint angles. An example of the joint angles reconstructed by synergies for a single Jar grip is shown in Figure 54 as reconstructed using the Kalman filter based on cortical data.

Object-specific Performance: Though reconstruction accuracy varied according to each object, in nearly every case the decoding performance of synergies outperformed joint angle decoding (see Figure 55). The only grasp that was better predicted by joint angles was Subject 001's grasp of Paper. All other object grips were more accurately reconstructed by mapping cortical data on to the first 7 synergies.

7.3.10 Grasp classification from reconstruction

In addition to classifying grasps based on the mean high gamma activity during the entire grasp as seen in section 7.3.4, we attempted classification using the timeseries generated predicted by the kalman filter operating on the neural data. Due to the intra-object variation in grasping, an average MSE statistic was calculated by taking the difference between the reconstructed joint trajectories and each grasp of each type (i.e. average MSE difference between predicted motion and all 9 "Jar" grasps). The reconstruction was subsequently classified as the object type with the lowest MSE. However, this classification technique was not able to produce correct results above chance for any temporal lag applied to the kalman filter

It is likely that though the Kalman filter reconstructions can track the recorded joint angles closely, its accuracy is insufficient to discriminate between the grips with statistical certainty. In addition, the intra-object grasps were not uniform in length and required clipping of the end of the trial, likely impacting the results. Ideally, future experiments would be designed to control for the temporal variation observed during subsequent grasps of the same object. Set periods of time for approach, hold, and release would help ensure that the predictions for different grasps were more uniform.

7.3.11 Freeform

The first 5 synergies generated during free motion are shown in Figure 56, with their respective contributions to variance shown as dotted lines in Figure 47. The first principal component is very similar to those observed during the Grips task and in the study in Chapter 5. However, subsequent synergies are much different, with none of the following five appearing in the grips task.

Attempts at reconstruction of freeform pose from synergies identified during show that reconstruction using the first synergy produced the best results, at a lag of 0ms for Subject 001 and -100ms for Subject 002. In both cases, adding additional synergies appeared to add noise and increased the mean squared error.

7.4 DISCUSSION

7.4.1 Spatial contribution of synergies

The spatial distribution of the first synergy is somewhat surprising. In both subjects, the coefficients of the extraction matrix for the first synergy suggest that this synergy – coordinated and simultaneous curl of all finger joints from distal to proximal – can be predicted almost entirely by the state update matrix. This suggests that the relationship is linear and may be directly related to widespread cortical activity in sensorimotor cortex.

In contrast, subsequent synergies show distinct spatial variations and patterns. If it is the case that the brain encodes motion as a subset of synergistic muscle activations, there appears to be distinct spatial weighting of cortical activity associated with motion. What is unique about these cortical patterns is that they differ greatly from the spatial activity when averaging across the entire grip as seen in Figure 44, where each object was selected to elicit one of the established forms of grasping (i.e. pyramidal vs power grip).

The simplest interpretation is that the brain does not have unique encodings for grasping different objects, a result that is likewise unexpected based on numerous grasp studies that have identified robust grasp types across multiple subjects (e.g. four-finger pyramidal, precision pinch,

palmar). A more interesting observation would be that while humans may grasp and manipulate objects in robust ways, the underlying cortical activity does not encode these types of grips directly. Rather, the cortex may build these common grips out of combinations of linear subcomponents applied in a repeatable way.

7.4.2 Grips vs Freeform

There are two important questions with regard to the freeform study. First, are the synergies that we identified during the grips experiment also present during free motion? The motions the subjects performed during the grips experiment were dexterous in terms of the ability to manipulate and hold objects, yet highly stereotyped in that they performed the same motions repeatedly. On the other hand, the motions produced during freeform motion were expected to be highly dexterous and non-stereotyped. If the synergies observed in the grip were again observed in free motion, this would strongly suggest that the synergies identified were the true underlying building blocks of motion. However, comparing the synergies generated by Grips in Figure 48 and Freeform in Figure 56 appears to show significant differences beyond the first synergy – not enough to reconstruct the additional intricacies during grip.

The second question is whether the mapping identified in the grips data can reconstruct the freeform better than the inverse. Before that can be explored however, it is sensible to identify if the same number of synergies – in the case of both subjects, 7 synergies - provides the most accurate reconstruction for freeform. Exploring the error as a function of uniform lag and number of synergies produces an unusual result. Figure 57 shows that, for both subjects, the lowest error in reconstructing freeform data from synergies identified during the first 60% of freeform motion occurred using the first synergy. Adding additional synergies decreased the reconstruction accuracy.

The fact that additional synergies introduce noise into the system means that a comparison between the grip types is impractical, given that the number of synergies that best reconstructs freeform grips is just the first principal component of grip. Attempting to reconstruct hand pose using one principal component would only produce projections along that axis, not capturing movements that deviate from the projection at all.

This has important implications for future studies and the broader goal of driving a closed-loop prosthetic device directly from cortical signals. Researchers and engineers must consider the intended outputs of the desired mapping. If the goal is to recreate grasping motions, it appears there may be a set of synergies that are common among subjects and that these should be a target of any cortical

mapping. However, if the end goal is to cover the full variance of human hand motion it is important that the training dataset used when creating the mapping is not based on grasping but instead based on a broader range of motion more characteristic of everyday motions.

7.4.3 Dimensionality reduction as error minimization

Even if the cortex does not encode dexterous hand motion using these synergies, the fact that the reconstructions were better with a subset of synergies as opposed to all synergies suggests that dimensionality reduction is a viable form of error reduction. It is plausible that the cortex employs a similar form of dimensionality reduction to improve the accuracy of single movements while attempting to minimize positional error, and musculoskeletal studies in mammals have shown that motor units synapse on multiple muscle fibers[88,89].

From an engineering perspective, this evidence shows that dimensionality reduction could prove useful during on-line control of a prosthetic limb. Instead of requiring the user to maintain control over the 20+ degrees of freedom of a manipulator directly, the user would only be required to control 7 degrees of freedom; a much lower cognitive load and less prone to decoding error. Additional ease and utility in control can be achieved by leveraging the kinematics identified during the kalman filter. As the first synergy coefficients in Figure 50 show, there is not much cortical specificity required to initiate the gross grasping motion. Manipulators driven this way could initiate a grasping motion based on broad increases in cortical activity in M1 and proceed to follow the kinematic approximation given by the state update matrix in the Kalman filter and continually modified by the second, third, and later cortical-specific synergies. In this manner, the subject would begin a grasp and only modify the grasp's trajectory, a reasonable approach to control strategy.

7.4.4 Alternative error estimates

One final consideration is the metric used for error. In all reconstruction studies, we used the mean-squared error of each individual joint angle relative to the actual recorded position of the glove. This allowed us to compare mappings from cortex to joint angles and cortex to synergies using the same metric. However, there is a drawback to using this metric. As the distal tip of each digit is dependent on the previous joints, errors in reconstruction of each joint angle compound the error in end effector position. In other words, small errors at the proximal joint are compounded by small errors at the medial joint which in turn compound small errors in the distal joint. This compounding effect, though small overall, can cause large deviations in the Cartesian location of the end of the finger.

Instead, a different error measurement could be used; a metric that is based not on joint angle, but on end effector position. This would negate the compounding error problem by optimizing for precise distal tip positioning, possibly generating poses that are more physically relevant to grip. This metric is not without its own problems however. If during object grasping the subjects were to use a surface other than the distal pad to grasp the object – for instance using the medial knuckle as the object's contact point – this measurement may produce hand poses that are less fit for object grasping. As such, we believe that evaluation of mean-squared error for mapping fitness is a reasonable approach.

7.4.5 Motor vs Sensory

Because both grids were implanted under the dura and moved beyond the cranial window, it is impossible to definitively say where the grid was located. As significant high-gamma activity levels were correlated with hand motion, it is reasonable to say that the grid were located over cortex associated with volitional hand sensorimotor cortex. It is entirely possible that the grids were over sensory cortex or spanning central sulcus and including both sensory and primary motor cortex. The spatial maps of temporal delays in Figure 52 show no definitive spatial arrangement, though primate studies by Fetz and Soso suggest that areas pre- and post-central sulcus can coactivate before the onset of movement[86,87].

Irrespective of whether the grids were directly over primary motor cortex, our results suggest that it is possible to create a mapping between cortical activity and synergistic hand movement that closely reproduces the actual recorded hand pose.

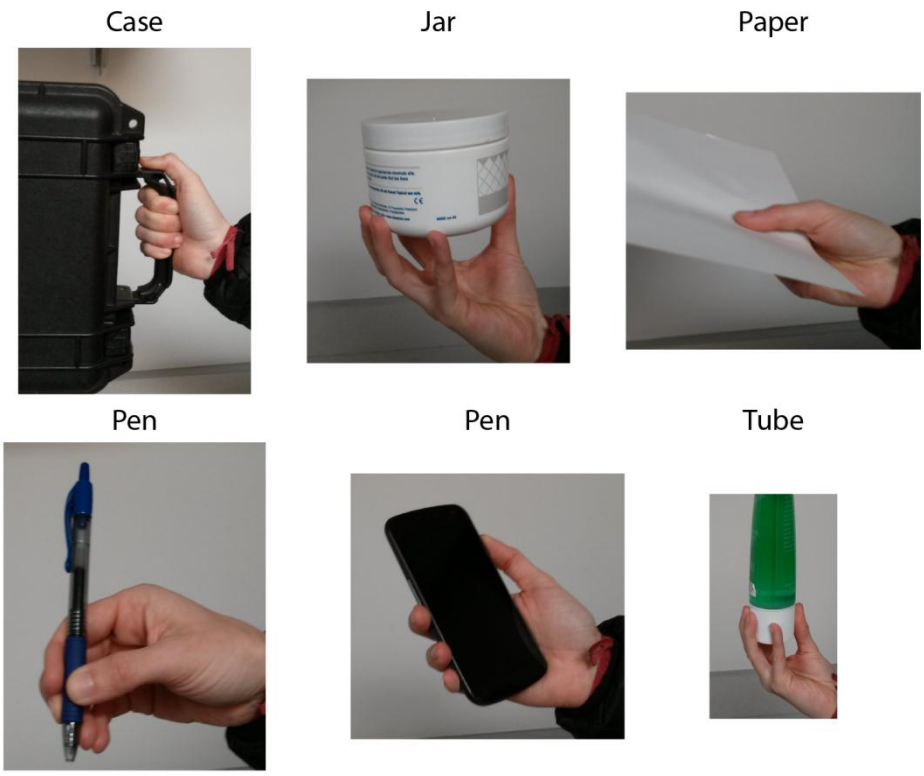

Figure 42 – Objects used during the grip task, and the suggested hand poses the subject was to take.

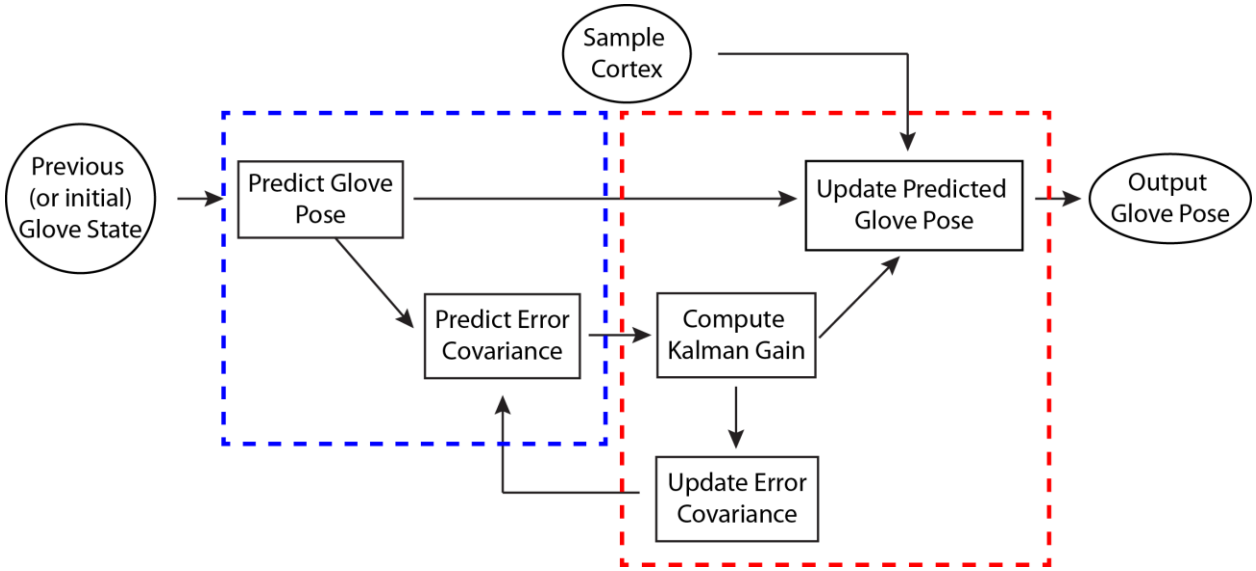

Figure 43 – Flow diagram of a step in the Kalman filter. The time update (blue) is performed on the glove state, and modified by the measurement update (red) giving the final glove pose output.

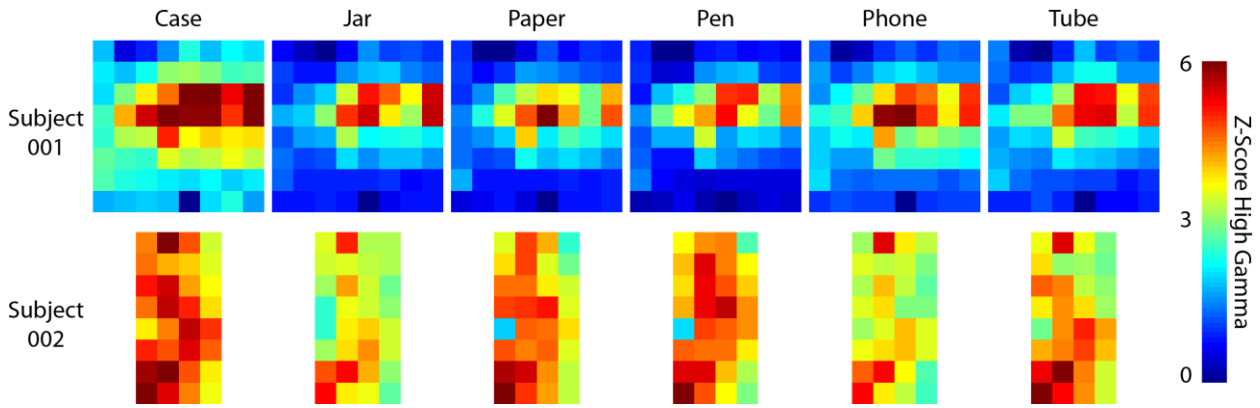

Figure 44 – High-gamma activity maps during each grip, z-scored to mean activity during rest. In both subject, the Jar required the broadest activity of cortex.

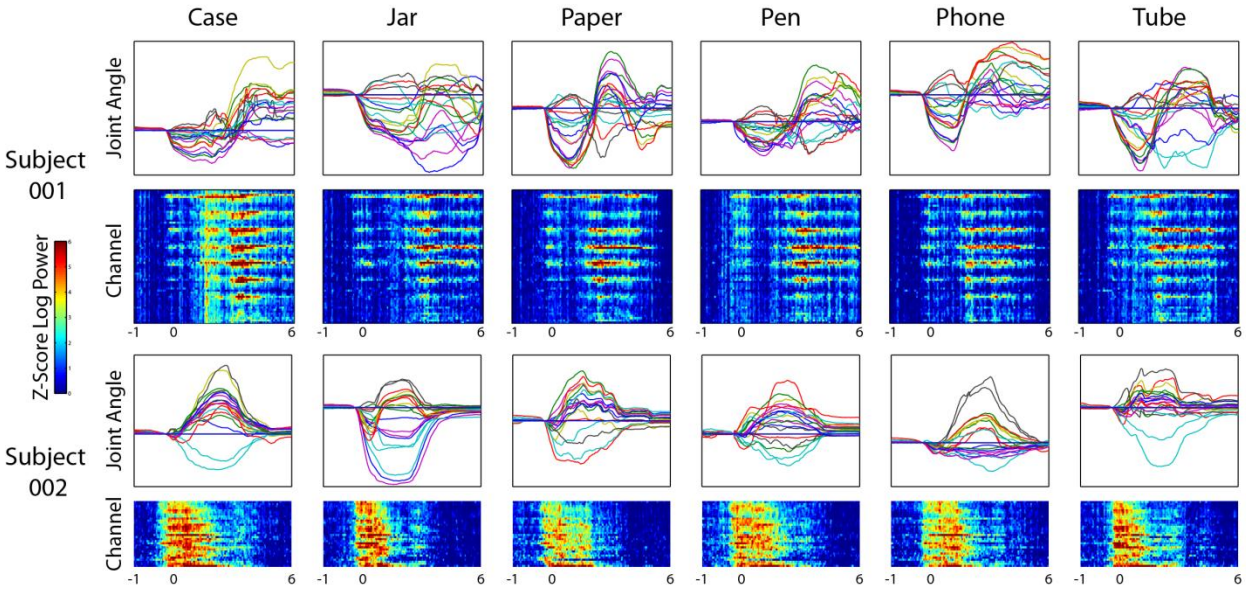

Figure 45 – Time course glove flexion (top row) and high gamma activity (bottom row), for each object for both subjects. Subject 001 initially extends their fingers (below start position on graph), followed by flexing to grasp the object. In contrast, Subject 002 maintained a flexed pose between grips and only performed a single movement to grasp each object.

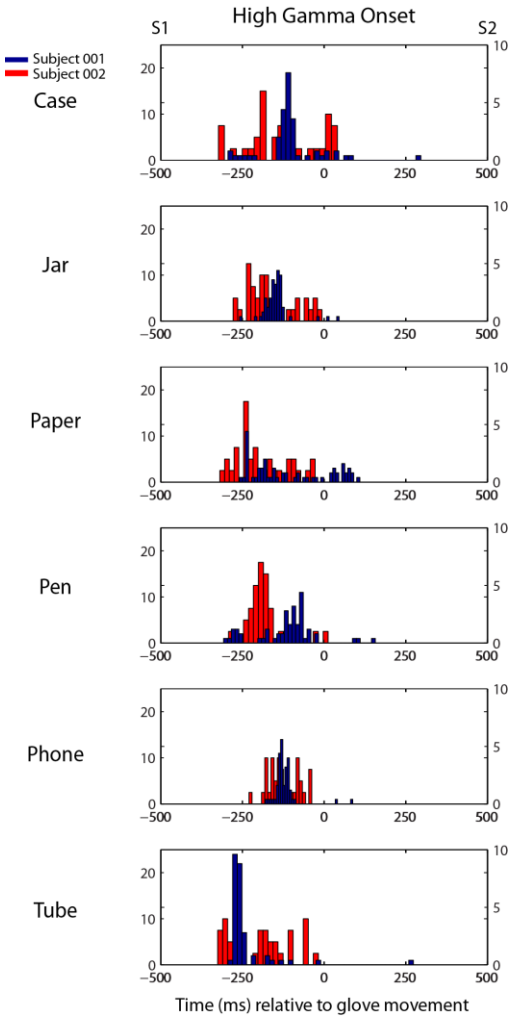

Figure 46 – Time onset of high gamma increase relative to detection of glove movement (t=0). Left vertical axis is for Subject 001 (blue) and right for Subject 002 (red).

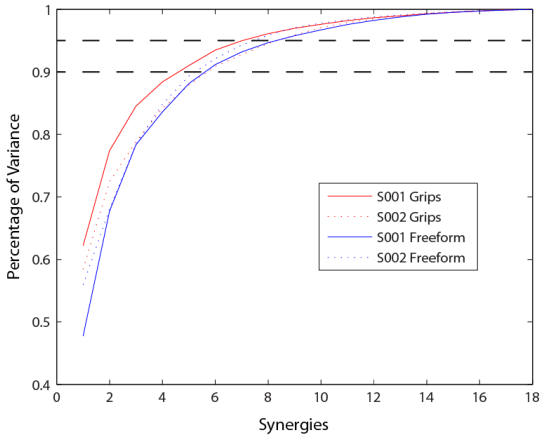

Figure 47 – Synergy contributions to variance. For all conditions, it takes 6 synergies to account for 90% of the total variance, and a minimum of 9 to account for 95%.

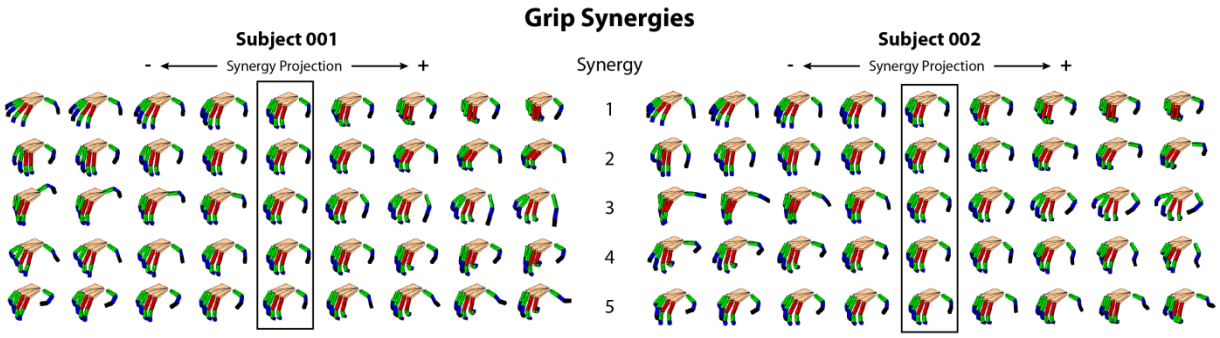

Figure 48 – Projection along the first five synergies for both subjects, with the mean hand pose boxed in the middle. The first four synergies match very closely, beginning to differ at the 4th. Note that due to the use of PCA during synergy generation was performed, the projection weight for the fourth synergy is inverted.

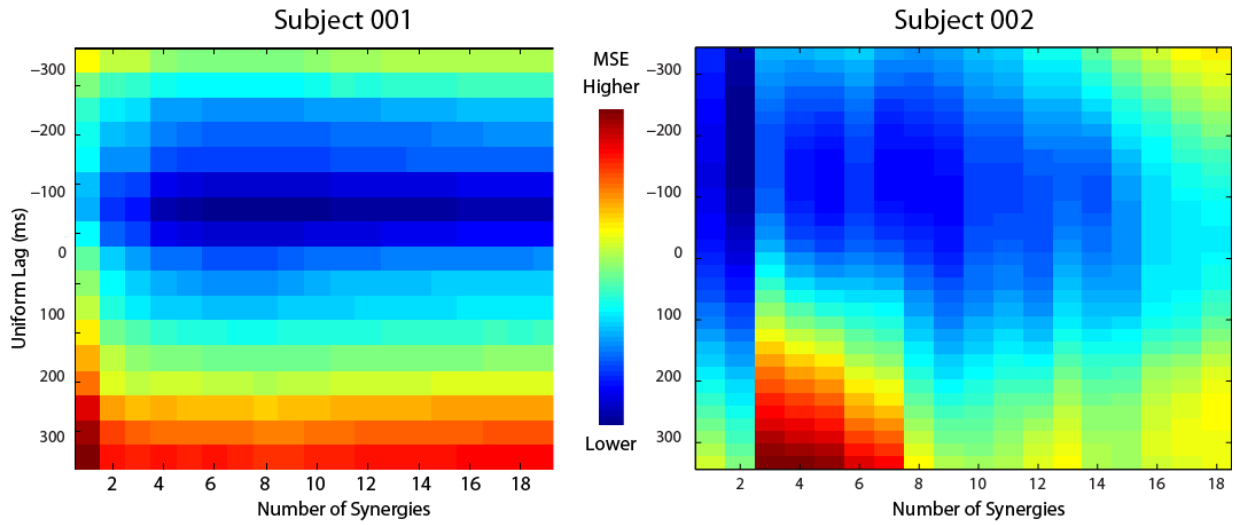

Figure 49 – Plot of mean-squared error of reconstruction as a function of uniform brain lag/lead and number of synergies used for reconstruction. In Subject 001, the lowest mean-squared error occurred at the 7th synergy at -75ms (mapping brain activity 75ms before glove motion). In Subject 002, the lowest mean square error occurred at the 2nd synergy at -200ms. However, as the first two synergies did not cover for thumb motion, additional synergies were explored, with the next lowest MSE at the 7th synergy at -125ms.

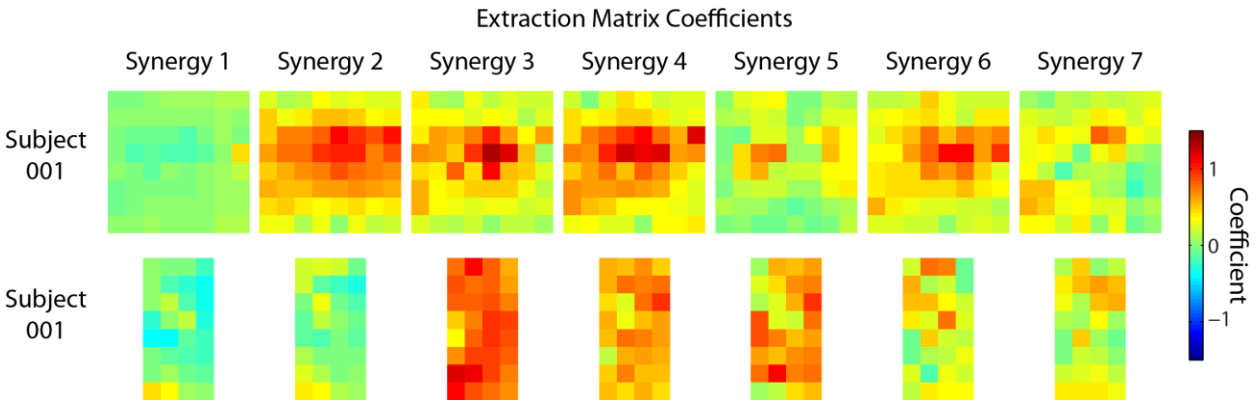

Figure 50 – Cortical weights for each of the top 7 synergies as defined by the extraction matrix used during Kalman Filter training. Weight can be interpreted as the importance of each electrode in modifying the glove's position as predicted by the state update matrix

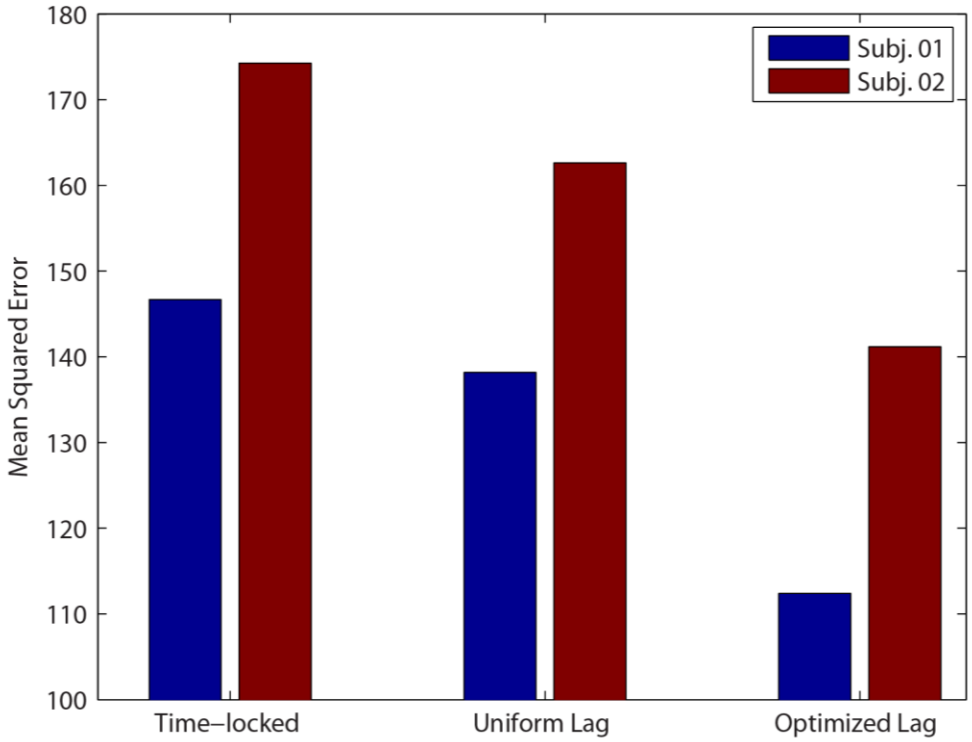

Figure 51 – Mean-Squared error as a function of reconstructed cortical data leading glove activity. Tests were performed at zero-lag (Time-Locked), uniform lag across all channels (Uniform Lag) and electrode-specific lag (Optimized Lag). Optimized lag values produced significantly better reconstructions than time-locked or uniform.

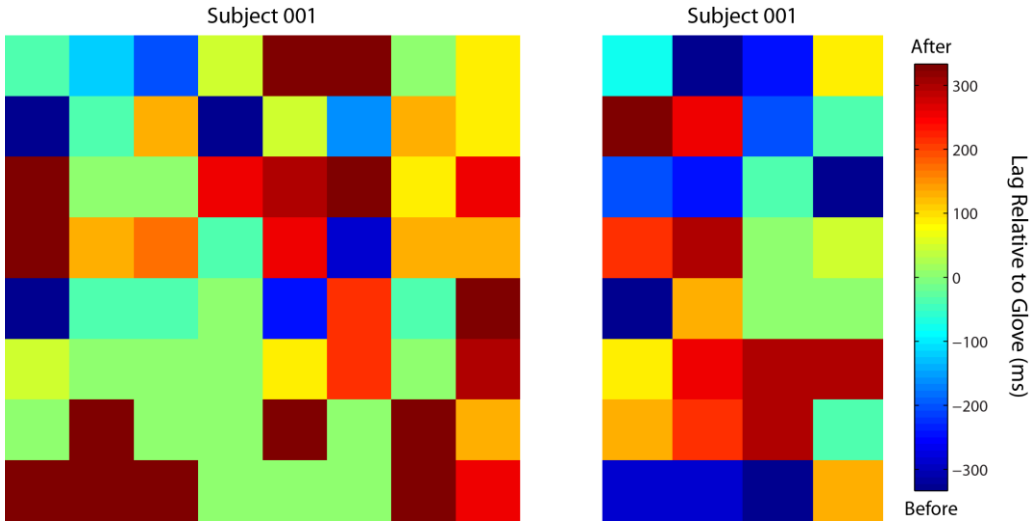

Figure 52 – Optimized lag values for both subjects, showing no significant spatial organization of lagged values.

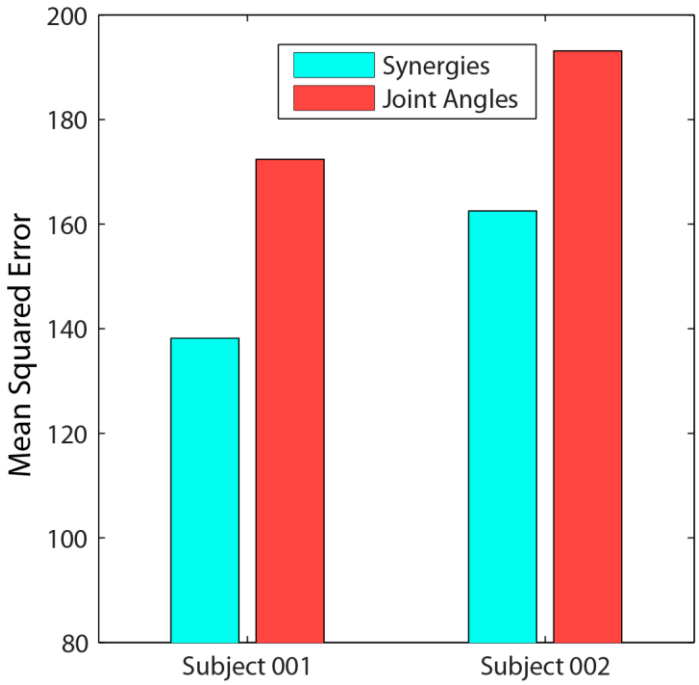

Figure 53 – Mean-squared error in glove position estimation when mapping brain data to either joint angles directly, or to the first 7 synergies.

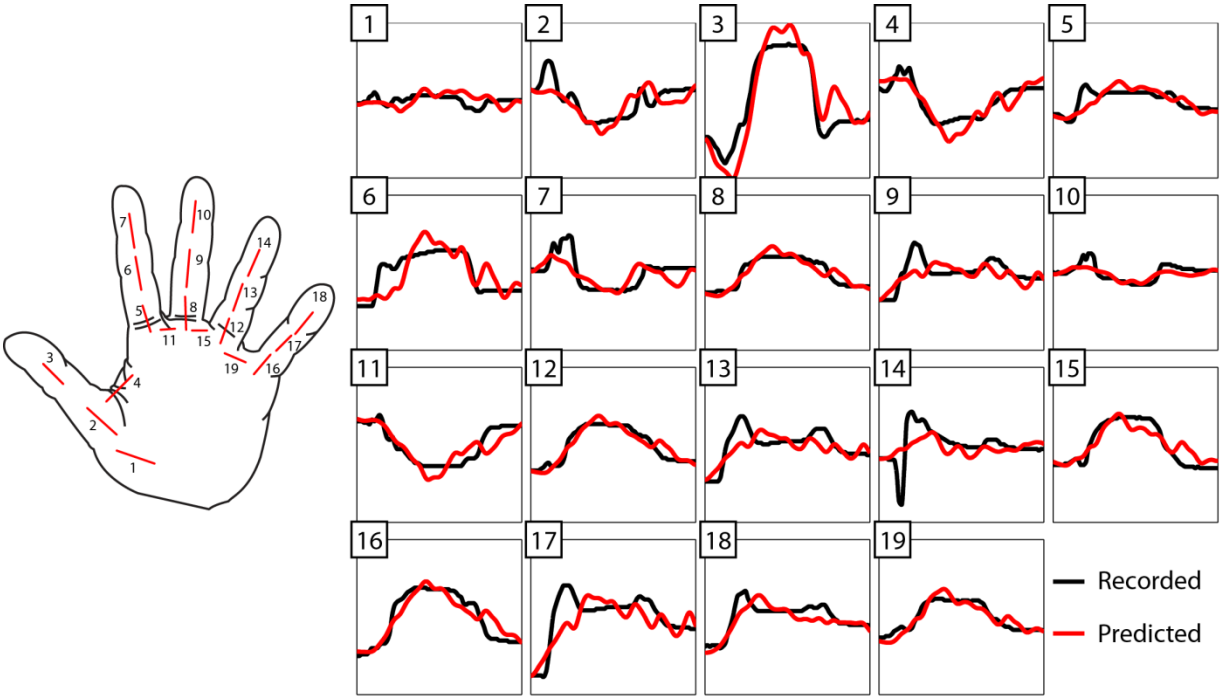

Figure 54 – Reconstruction of Subject 001's hand pose based on high-gamma (75-200Hz) cortical data to the first 7 synergies using a Kalman filter. Each trace represents the joint angle over time for recorded (black) and predicted (red) hand position during a single Jar grip.

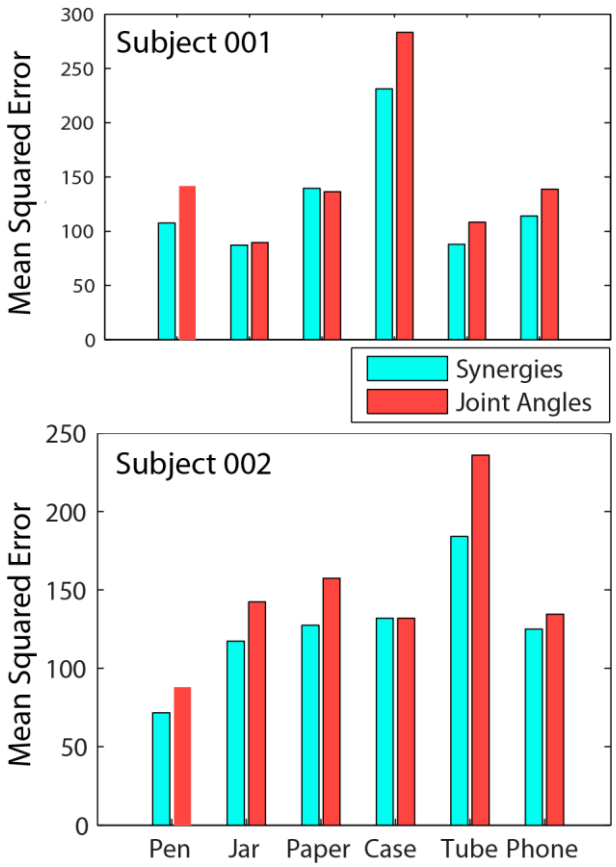

Figure 55 – Reconstruction error for each grip type, comparing reconstruction of mapping to joint angles directly or the top 7 synergies.

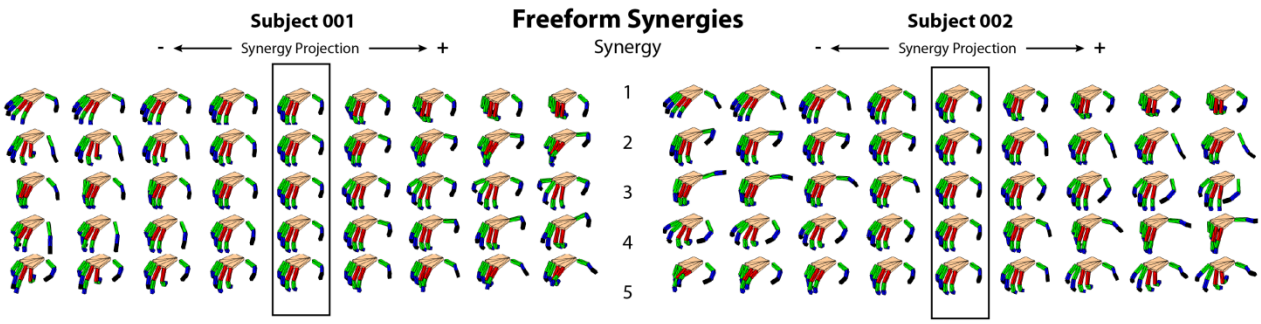

Figure 56 – Synergies identified during free movement. Synergy 1 is similar to the first synergy identified in Grips. Subsequent synergies differ significantly between subjects and do not appear in the first 5 in the grips experiment.

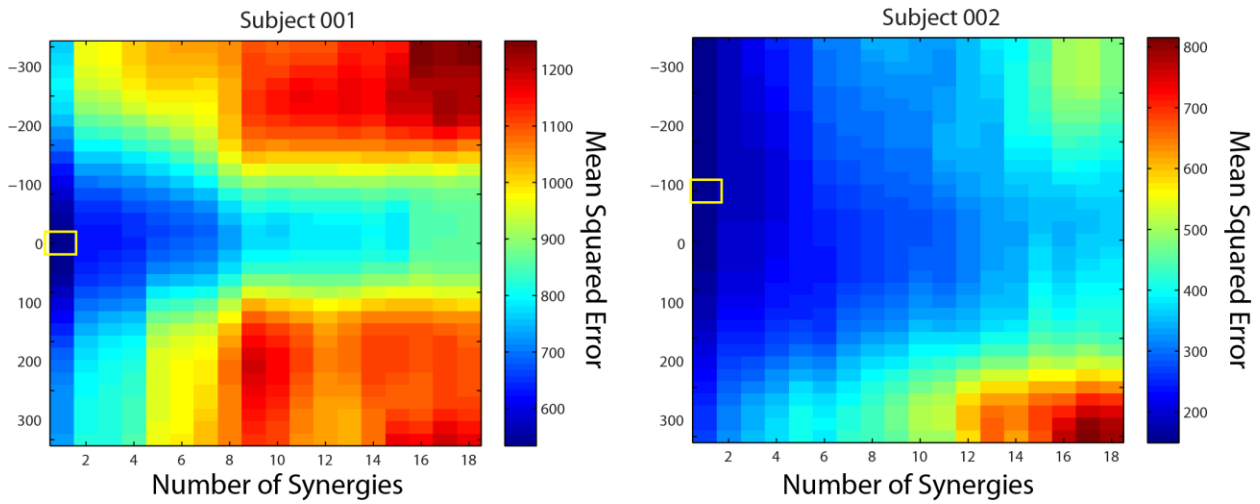

Figure 57 – MSE as a function of synergy count and lag during free movement. In both subjects, the lowest error occurs for the first synergy, with additional synergies decreasing reconstruction accuracy.

8 References

1. Williams, R. W. & Herrup, K. The control of neuron number. *Annual review of neuroscience* **11**, 423–453 (1988).

2. Herculano-Houzel, S. The human brain in numbers: a linearly scaled-up primate brain. *Frontiers in Human Neuroscience* **3**, (2009).

3. Lange, W. Cell number and cell density in the cerebellar cortex of man and some other mammals. *Cell and tissue research* **157**, 115–24 (1975).

4. SHARIFF, G. A. Cell counts in the primate cerebral cortex. *The Journal of comparative neurology* **98**, 381–400 (1953).

5. Friston, K. J., Mechelli, A., Turner, R. & Price, C. J. Nonlinear responses in fMRI: the Balloon model, Volterra kernels, and other hemodynamics. *NeuroImage* **12**, 466–477 (2000).

6. Valdes, P. *et al.* The statistical identification of nonlinear brain dynamics: A progress report. *Nova Science Publishing* 278–284 (1999).

7. Breakspear, M. *et al.* A unifying explanation of primary generalized seizures through nonlinear brain modeling and bifurcation analysis. *Cerebral Cortex* **16**, 1296–1313 (2006).

8. Miller, K. J., Sorensen, L. B., Ojemann, J. G. & den Nijs, M. Power-law scaling in the brain surface electric potential. *PLoS computational biology* **5**, e1000609 (2009).

9. Peter, R. Synaptic density in human frontal cortex—developmental changes and effects of aging. *Brain research* **163**, 195–205 (1979).

10. Perlovsky, L. I. Conundrum of combinatorial complexity. *Pattern Analysis and Machine Intelligence, IEEE Transactions on* **20**, 666–670 (1998).

11. Buonomano, D. V & Merzenich, M. M. Cortical plasticity: from synapses to maps. *Annual review of neuroscience* **21**, 149–186 (1998).

12. Koch, C. & Segev, I. The role of single neurons in information processing. *nature neuroscience* **3**, 1171–1177 (2000).

13. Koch, C. Computation and the single neuron. *Nature* **385**, 207–210 (1997).

14. Zhao, L. & Yang, Y. PSO-based single multiplicative neuron model for time series prediction. *Expert Systems with Applications* **36**, 2805–2812 (2009).

15. Hirsch, J. A. & Martinez, L. M. Laminar processing in the visual cortical column. *Current opinion in neurobiology* **16**, 377 (2006).

16. Shadlen, M. N. & Newsome, W. T. Noise, neural codes and cortical organization. *Current opinion in neurobiology* **4**, 569–579 (1994).

17. Clark, D. A., Mitra, P. P. & Wang, S. S.-H. Scalable architecture in mammalian brains. *Nature* **411**, 189–192 (2001).

18. Finlay, B. L. & Darlington, R. B. Linked regularities in the development and evolution of mammalian brains. *Science* (1995).

19. Barton, R. A. & Harvey, P. H. Mosaic evolution of brain structure in mammals. *Nature* **405**, 1055–1057 (2000).

20. Schalk, G. Brain–computer symbiosis. *Journal of neural engineering* **5**, P1 (2008).

21. Wolpaw, J. Brain–computer interfaces for communication and control. *Clinical Neurophysiology* **113**, 767–791 (2002).

22. Wolpaw, J. R. & McFarland, D. J. Control of a two-dimensional movement signal by a noninvasive brain-computer interface in humans. *Proceedings of the National Academy of Sciences of the United States of America* **101**, 17849–17854 (2004).

23. Miller, K. J. *et al.* Cortical spectral changes during actual and imagined motor movement, and the augmentation of spectral change with feedback. *Society for Neuroscience Abstracts Online* (2007).

24. Leuthardt, E. C., Miller, K. J., Schalk, G., Rao, R. P. N. & Ojemann, J. G. Electrocorticography-based brain computer interface--the Seattle experience. *IEEE transactions on neural systems and rehabilitation engineering : a publication of the IEEE Engineering in Medicine and Biology Society* **14**, 194–8 (2006).

25. Leuthardt, E. C., Schalk, G., Wolpaw, J. R., Ojemann, J. G. & Moran, D. W. A brain-computer interface using electrocorticographic signals in humans. *Journal of neural engineering* **1**, 63–71 (2004).

26. Miller, K. J. *et al.* Correlation in paired one-dimensional, closed loop, overt, motor controlled BCI. *Journal of Technical University of Graz, Special Issue: Brain Computer Interfaces* (2007).

27. Wolpaw, J. R., McFarland, D. J., Neat, G. W. & Forneris, C. A. An EEG-based brain-computer interface for cursor control. *Electroencephalography and clinical neurophysiology* **78**, 252–259 (1991).

28. Pfurtscheller, G. *et al.* Current trends in Graz brain-computer interface (BCI) research. *Rehabilitation Engineering, IEEE Transactions on* **8**, 216–219 (2000).

29. Hochberg, L. R. *et al.* Neuronal ensemble control of prosthetic devices by a human with tetraplegia. *Nature* **442**, 164–71 (2006).

30. Guger, C. *et al.* Rapid prototyping of an EEG-based brain-computer interface (BCI). *Neural Systems and Rehabilitation Engineering, IEEE Transactions on* **9**, 49–58 (2001).

31. Pfurtscheller, G., Neuper, C., Schlogl, A. & Lugger, K. Separability of EEG signals recorded during right and left motor imagery using adaptive autoregressive parameters. *Rehabilitation Engineering, IEEE Transactions on* **6**, 316–325 (1998).

32. Schalk, G. *et al.* Two-dimensional movement control using electrocorticographic signals in humans. *Journal of neural engineering* **5**, 75–84 (2008).

33. Kostov, A. & Polak, M. Parallel man-machine training in development of EEG-based cursor control. *Rehabilitation Engineering, IEEE Transactions on* **8**, 203–205 (2000).

34. Shenoy, P., Krauledat, M., Blankertz, B., Rao, R. P. N. & Müller, K.-R. Towards adaptive classification for BCI. *Journal of neural engineering* **3**, R13 (2006).

35. Serruya, M. D., Hatsopoulos, N. G., Paninski, L., Fellows, M. R. & Donoghue, J. P. Brain-machine interface: Instant neural control of a movement signal. *Nature* **416**, 141–142 (2002).

36. Taylor, D. M., Tillery, S. I. H. & Schwartz, A. B. Direct cortical control of 3D neuroprosthetic devices. *Science (New York, N.Y.)* **296**, 1829–32 (2002).

37. Carmena, J. M. *et al.* Learning to control a brain–machine interface for reaching and grasping by primates. *PLoS biology* **1**, e42 (2003).

38. Fetz, E. E. Real-time control of a robotic arm by neuronal ensembles. *Nature neuroscience* **2**, 583–4 (1999).

39. Wessberg, J. *et al.* Real-time prediction of hand trajectory by ensembles of cortical neurons in primates. *Nature* **408**, 361–5 (2000).

40. Velliste, M., Perel, S., Spalding, M. C., Whitford, A. S. & Schwartz, A. B. Cortical control of a prosthetic arm for self-feeding. *Nature* **453**, 1098–101 (2008).

41. Miller, K. J. *et al.* Cortical electrode localization from X-rays and simple mapping for electrocorticographic research: The “Location on Cortex”(LOC) package for MATLAB. *Journal of neuroscience methods* **162**, 303–308 (2007).

42. Neuper, C., Müller, G. R., Kübler, A., Birbaumer, N. & Pfurtscheller, G. Clinical application of an EEG-based brain–computer interface: a case study in a patient with severe motor impairment. *Clinical neurophysiology* **114**, 399–409 (2003).

43. Marple Jr, S. L. & Carey, W. M. Digital spectral analysis with applications. *The Journal of the Acoustical Society of America* **86**, 2043 (1989).

44. Felton, E. A., Wilson, J. A., Williams, J. C. & Garell, P. C. Electrocorticographically controlled brain-computer interfaces using motor and sensory imagery in patients with temporary subdural electrode implants. *Journal of neurosurgery* **106**, 495–500 (2007).

45. Wilson, J. A., Felton, E. A., Garell, P. C., Schalk, G. & Williams, J. C. ECoG factors underlying multimodal control of a brain-computer interface. *Neural Systems and Rehabilitation Engineering, IEEE Transactions on* **14**, 246–250 (2006).

46. Miller, K. J., Zanos, S., Fetz, E. E., Den Nijs, M. & Ojemann, J. G. Decoupling the cortical power spectrum reveals real-time representation of individual finger movements in humans. *The Journal of Neuroscience* **29**, 3132–3137 (2009).

47. Scherer, R. *et al.* Temporal dynamics of high-frequency (>75Hz) power increase in electrocorticographic brain signals during cue-guided movement of individual digits. *Temporal dynamics of high-frequency (>75Hz) power increase in electrocorticographic brain signals during cue-guided movement of individual digits* (2010).

48. Schalk, G., McFarland, D. J., Hinterberger, T., Birbaumer, N. & Wolpaw, J. R. BCI2000: a general-purpose brain-computer interface (BCI) system. *IEEE transactions on bio-medical engineering* **51**, 1034–43 (2004).

49. Landsmeer, J. M. F. Power grip and precision handling. *Annals of the rheumatic diseases* **21**, 164–170 (1962).

50. Cutkosky, M. R. & Howe, R. D. Human grasp choice and robotic grasp analysis. *Dextrous robot hands* 5–31 (1990).

51. Maynard, E. M., Nordhausen, C. T. & Normann, R. A. The Utah intracortical electrode array: A recording structure for potential brain-computer interfaces. *Electroencephalography and clinical Neurophysiology* **102**, 228–239 (1997).

52. Liepert, J., Tegenthoff, M. & Malin, J.-P. Changes of cortical motor area size during immobilization. *Electroencephalography and Clinical Neurophysiology/Electromyography and Motor Control* **97**, 382–386 (1995).

53. Sussman, H. Phonemic representation: A twenty-first century challenge. *Brain and language* **71**, 237–240 (2000).

54. Eggermont, J. J. Between sound and perception: reviewing the search for a neural code. *Hearing research* **157**, 1–42 (2001).

55. Langner, G., Sams, M., Heil, P. & Schulze, H. Frequency and periodicity are represented in orthogonal maps in the human auditory cortex: evidence from magnetoencephalography. *Journal of Comparative Physiology A: Neuroethology, Sensory, Neural, and Behavioral Physiology* **181**, 665–676 (1997).

56. Pantev, C. *et al.* Specific tonotopic organizations of different areas of the human auditory cortex revealed by simultaneous magnetic and electric recordings. *Electroencephalography and clinical neurophysiology* **94**, 26–40 (1995).

57. Wessinger, C. M. *et al.* Hierarchical organization of the human auditory cortex revealed by functional magnetic resonance imaging. *Journal of Cognitive Neuroscience* **13**, 1–7 (2001).

58. Diesch, E. & Luce, T. Magnetic fields elicited by tones and vowel formants reveal tonotopy and nonlinear summation of cortical activation. *Psychophysiology* **34**, 501–510 (1997).

59. Diesch, E. & Luce, T. Topographic and temporal indices of vowel spectral envelope extraction in the human auditory cortex. *Journal of cognitive neuroscience* **12**, 878–893 (2000).

60. Ohl, F. W. & Scheich, H. Orderly cortical representation of vowels based on formant interaction. *Proceedings of the National Academy of Sciences* **94**, 9440–9444 (1997).

61. Wang, X., Merzenich, M. M., Beitel, R. & Schreiner, C. E. Representation of a species-specific vocalization in the primary auditory cortex of the common marmoset: temporal and spectral characteristics. *Journal of Neurophysiology* **74**, 2685–2706 (1995).

62. Diesch, E., Eulitz, C., Hampson, S. & Ross, B. The neurotopography of vowels as mirrored by evoked magnetic field measurements. *Brain and language* **53**, 143–168 (1996).

63. Towle, V. L. *et al.* ECoG gamma activity during a language task: differentiating expressive and receptive speech areas. *Brain* **131**, 2013–2027 (2008).

64. Miller, K. J. *et al.* Real-time functional brain mapping using electrocorticography. *NeuroImage* **37**, 504–7 (2007).

65. Miller, K. J. *et al.* Spectral changes in cortical surface potentials during motor movement. *The Journal of neuroscience* **27**, 2424–2432 (2007).

66. Miller, K. J., Rao, R. P. N. & Ojemann, J. G. The Behavioral Split in the Gamma Band. *Neural Engineering, 2007. CNE'07. 3rd International IEEE/EMBS Conference on* 465–468 (2007).

67. Vapnik, V. *The nature of statistical learning theory*. (springer: 1999).

68. Jeannerod, M. Intersegmental coordination during reaching at natural vision objects. *Attention and performance IX* **9**, 153–168 (1981).

69. Jeannerod, M. The timing of natural prehension movements. *Journal of motor behavior* (1984).

70. Acharya, S., Fifer, M. S., Benz, H. L., Crone, N. E. & Thakor, N. V Electrocorticographic amplitude predicts finger positions during slow grasping motions of the hand. *Journal of neural engineering* **7**, 046002 (2010).

71. Santello, M., Flanders, M. & Soechting, J. F. Postural hand synergies for tool use. *The Journal of Neuroscience* **18**, 10105–10115 (1998).

72. Kawato, M. Internal models for motor control and trajectory planning. *Current opinion in neurobiology* **9**, 718–727 (1999).

73. Kawato, M. & Wolpert, D. Internal models for motor control. *Sensory Guidance of Movement* **218**, 291–307 (1998).

74. Schöner, G. A dynamic theory of coordination of discrete movement. *Biological Cybernetics* **63**, 257–270 LA – English (1990).

75. Thakur, P. H., Bastian, A. J. & Hsiao, S. S. Multidigit movement synergies of the human hand in an unconstrained haptic exploration task. *The Journal of neuroscience : the official journal of the Society for Neuroscience* **28**, 1271–81 (2008).

76. Ehrsson, H. H. *et al.* Cortical activity in precision-versus power-grip tasks: an fMRI study. *Journal of Neurophysiology* **83**, 528–536 (2000).

77. Muir, R. B. & Lemon, R. N. Corticospinal neurons with a special role in precision grip. *Brain research* **261**, 312–316 (1983).

78. Saleh, M., Takahashi, K. & Hatsopoulos, N. G. Encoding of Coordinated Reach and Grasp Trajectories in Primary Motor Cortex. *Journal of Neuroscience* **32**, 1220–1232 (2012).

79. Fischl, B. FreeSurfer. *NeuroImage* (2012).

80. Cover, T. & Hart, P. Nearest neighbor pattern classification. *Information Theory, IEEE Transactions on* **13**, 21–27 (1967).

81. Wray, C. D. *et al.* Multimodality localization of the sensorimotor cortex in pediatric patients undergoing epilepsy surgery. *Journal of Neurosurgery: Pediatrics* **10**, 1–6 (2012).

82. Leuthardt, E. C. *et al.* Electrocorticographic frequency alteration mapping: a clinical technique for mapping the motor cortex. *Neurosurgery* **60**, 260–271 (2007).

83. Sinai, A. *et al.* Electrocorticographic high gamma activity versus electrical cortical stimulation mapping of naming. *Brain* **128**, 1556–1570 (2005).

84. Wu, W., Gao, Y., Bienenstock, E., Donoghue, J. P. & Black, M. J. Bayesian population decoding of motor cortical activity using a Kalman filter. *Neural computation* **18**, 80–118 (2006).

85. Moran, D. W. & Schwartz, A. B. Motor cortical activity during drawing movements: population representation during spiral tracing. *Journal of neurophysiology* **82**, 2693–2704 (1999).

86. Fetz, E. E., Finocchio, D. V, Baker, M. A. & Soso, M. J. Sensory and motor responses of precentral cortex cells during comparable passive and active joint movements. *Journal of neurophysiology* **43**, 1070–1089 (1980).

87. Soso, M. J. & Fetz, E. E. Responses of identified cells in postcentral cortex of awake monkeys during comparable active and passive joint movements. *Journal of neurophysiology* **43**, 1090–1110 (1980).

88. Betz, W. J., Caldwell, J. H. & Ribchester, R. R. The size of motor units during post-natal development of rat lumbrical muscle. *The Journal of physiology* **297**, 463–478 (1979).

89. Hall, Z. W. & Sanes, J. R. Synaptic structure and development: the neuromuscular junction. *Cell* **72**, 99 (1993).